ANL-7267

ANL-7267

MASTER

Argonne National Laboratory

REACTOR DEVELOPMENT PROGRAM

PROGRESS REPORT

OCTOBER 1966

DISCLAIMER

LEGAL NOTICE

Printed in USA. Price $3.00 . Available from the Clearinghouse for Federal Scientific and Technical Information, National Bureau of Standards, U. S. Department of Commerce, Springfield, Virginia 22151

ANL-7267
Reactor Technology
(TID-4500)
AEC Research and
Development Report

ARGONNE NATIONAL LABORATORY
9700 South Cass Avenue
Argonne, Illinois 60439

REACTOR DEVELOPMENT PROGRAM PROGRESS REPORT

October 1966

Albert V. Crewe, Laboratory Director
Stephen Lawroski, Associate Laboratory Director

Division	Director
Chemical Engineering	R. C. Vogel
Idaho	M. Novick
Metallurgy	M. V. Nevitt
Reactor Engineering	L. J. Koch
Reactor Physics	R. Avery
Remote Control	R. C. Goertz

Report coordinated by
R. M. Adams and A. Glassner

Issued November 22, 1966

Operated for the U. S. Atomic Energy Commission
by
The University of Chicago
and
Argonne Universities Association
(Contract W-31-109-eng-38)

FOREWORD

The Reactor Development Program Progress Report, issued monthly, is intended to be a means of reporting those items of significant technical progress which have occurred in both the specific reactor projects and the general engineering research and development programs. The report is organized in a way which, it is hoped, gives the clearest, most logical overall view of progress. The budget classification is followed only in broad outline, and no attempt is made to report separately on each sub-activity number. Further, since the intent is to report only items of significant progress, not all activities are reported each month. In order to issue this report as soon as possible after the end of the month editorial work must necessarily be limited. Also, since this is an informal progress report, the results and data presented should be understood to be preliminary and subject to change unless otherwise stated.

The issuance of these reports is not intended to constitute publication in any sense of the word. Final results either will be submitted for publication in regular professional journals or will be published in the form of ANL topical reports.

The last six reports issued in this series are:

April 1966	ANL-7204
May 1966	ANL-7219
June 1966	ANL-7230
July 1966	ANL-7245
August 1966	ANL-7249
September 1966	ANL-7255

REACTOR DEVELOPMENT PROGRAM

Highlights of Project Activities for October 1966

EBWR Plutonium Recycle Program

Measurements of the uniform temperature coefficient of reactivity of the fully loaded core with eight spike assemblies in the first shim zone between room temperature and 360°F have been made with boric acid concentrations near 6 g/gal. The temperature coefficient is positive at low temperatures, becomes very small as the temperature is raised, and apparently becomes negative before 360°F is reached.

EBR-II

With planned modifications and maintenance completed during the recent scheduled shutdown, Run No. 22, projected for 1000 MWD, was begun on October 21. Almost half of this run was completed at month's end.

ZPPR

Thirty-two of 54 total piling foundation holes have been completed. The floor slab and foundation for the vault-workroom and service floor of the support wing have been poured.

ZPR-3

Detailed reports of measurements made during the last four months on Assembly 48, a large, clean, plutonium-fueled core, were compiled and presented at the ANL-sponsored Conference on Fast Critical Experiments and Their Analysis. A summary is presented.

AARR

The AARR Title I report was submitted to the AEC for approval on October 7, 1966.

The AARR core design has been changed to a HFIR type, and all research and development work on the stainless steel cermet fuel has been terminated.

TABLE OF CONTENTS

TABLE OF CONTENTS

TABLE OF CONTENTS

I. PLUTONIUM UTILIZATION

A. Research and Development

1. Transfer Functions for Plutonium-loaded EBWR

The stability, at high power, of EBWR loaded with a plutonium core can be predicted from measurements made at low power. The reactor transfer function is being measured at selected power levels and stability predictions will be made prior to operation at full power.

A theoretical zero-power transfer function curve with the following parameters is found to give a good fit to the experimentally determined transfer function:

Prompt neutron lifetime	5.8×10^{-5} sec
Percent fission composition	$U^{235} = 48$
	$U^{238} = 9$
	$Pu^{239} = 42$
	$Pu^{240} = 1$
Effective Beta	$= 5.5 \times 10^{-3}$

Transfer functions were run at power levels of approximately 4 and 9 MW(th).

A preliminary extrapolation curve to determine the power at which instability would occur was made. The predicted power level was over 40 MW, but a fairly wide margin of error is possible due to the distance of the extrapolation and the closeness of the points.

Transfer function measurements at 15 MW are being made.

2. Temperature Coefficients of Reactivity

Measurements of the uniform temperature coefficient of reactivity of the fully loaded core with eight spike assemblies in the first shim zone between room temperature and 360°F have been made with boric acid concentrations near 6 g/gal. The temperature coefficient was obtained from the multiplication constant as a function of temperature with five control rods withdrawn and four control rods inserted normalized to a boric acid concentration of 6.25 g/gal. As can be seen from Table I, the temperature coefficient which was positive at low temperatures became very small as the temperature is raised and apparently reversed sign to become negative before 360°F is reached. During the experiment the startup heater was used to heat the system. When the temperature was raised from 360°F to the operating value of 489°F by nuclear heat, the temperature coefficient was definitely negative, since the flux quickly leveled after each incremental withdrawal of a control rod.

TABLE I. Temperature Coefficient of EBWR with Five Control Rods Withdrawn

Temp (°F)	H_3BO_3 (g/gal)	Critical Ht of #4 Rod (in.)	k, #4 Rod Withdrawn	k for 6.25 g H_3BO_3/gal	$\Delta k/\Delta T$ (%Δk/°F)
64.5 ± 1	5.71 ± 0.03	28.994	1.00131 ± 0.00016	0.99456 ± 0.00052	
					0.00435 ± 0.00083
152.5 ± 1	6.02 ± 0.02	29.910	1.00115 ± 0.00014	0.99843 ± 0.00039	
					0.00430 ± 0.00105
246.0 ± 1	6.16 ± 0.04	21.882	1.00357 ± 0.00025	1.00245 ± 0.00075	
					0.00236 ± 0.00148
321.0 ± 2	6.14 ± 0.04	15.533	1.00559 ± 0.00032	1.00422 ± 0.00082	
					-0.00212 ± 0.00320
362.0 ± 2	6.35 ± 0.04	27.591	1.00210 ± 0.00021	1.00335 ± 0.00071	

The reactor is currently being brought up to operating power. The power is being raised in steps of approximately 5 MW. After each rise in power, pile-oscillator measurements are made of the reactor transfer function to investigate the stability of the reactor as a function of power (see Sect. I.A.1).

II. LIQUID-METAL FAST BREEDER REACTORS

A. EBR-II

1. Operations

Upon completion of modifications, shutdown cooler tests, and fuel-handling operations, the primary sodium system was cooled to 350°F. The steam and secondary systems were then heated and the secondary system filled with sodium. The combined systems were then returned to the normal standby temperature of 700°F in preparation for final fuel handling prior to reactor operation.

While the primary system was at 350°F, the oscillator-drive assembly was installed. During the heatup the oscillator-gripper jaws were moved periodically to free the drive shaft of any internal sodium and/or residual sodium oxide from previous test operation. Mechanical and electrical checkout was conducted. Test operation was satisfactory.

The reactor was made critical on October 19 to provide a check on reactivity, to calibrate two new control rods, and the oscillator rod. One additional enriched, blanket-type subassembly was added to provide sufficient reactivity for the scheduled 1000 MWdt run.

Reactor power operation for Run No. 22 was started on October 21. The reactivity defect measured during the power increase to 45 MW was 68 Ih, which is in substantial agreement with values previously obtained.

Calibration of the oscillator rod indicated a reactivity change of 21.6 Ih total, peak-to-peak. Rotation of the oscillator has been accomplished manually except for a short period of drive-motor operation during final installation checkout.

The main turbine has been reassembled and returned to normal operation. A manufacturer's representative was on hand for surveillance during the initial period of operation.

Aside from minor adjustments required on the overspeed trip and initial pressure regulator, the machine has operated satisfactorily.

At month's end the reactor had completed 460 MWdt of the scheduled 1000-MWd run.

a. Experimental Irradiations. The status of all experimental irradiations at the start of Run No. 22 was the same as at the end of September and is shown below with accumulated exposure data at month's end.

Subassembly	Date Loaded	Capsule Content and Number of Capsules ( )	Experimenter	Accumulated Exposure (MWd)	Goal Exposure (MWd)
XG02	7/16/65	UO_2-20 w/o PuO_2 (1) Stainless Dummies (18)	GE	7839	13,600
XG03	7/16/65	UO_2-20 w/o PuO_2 (2) Stainless Dummies (17)	GE	7839	19,450
XG04	7/16/65	UO_2-20 w/o PuO_2 (2) Stainless Dummies (17)	GE	7839	39,000
XG05	9/3/65	UO_2-20 w/o PuO_2 (9) U-15 w/o Pu-10 w/o Zr (1) U-15 w/o Pu-10 w/o Ti (1) UC-20 w/o PuC (3) Structural (5)	GE ANL ANL ANL GE	6952	10,300
XG06	9/3/65	UO_2-20 w/o PuO_2 (12) U-15 w/o Pu-10 w/o Zr (1) U-15 w/o Pu-10 w/o Ti (1) Structural (5)	GE ANL ANL GE	7412	20,600
XA07	10/27/65	U-14 w/o Pu-11 w/o Zr (16) Structural (3)	ANL ANL	6675	18,600
XA08	12/13/65	UC-20 w/o PuC (8) Structural (11)	ANL	5590	19,800
XA09	3/24/66	UC-20 w/o PuC (3) UO_2-20 w/o PuO_2 (2) 304 SS-30 v/o PuO_2 (1) 304 SS-20 v/o PuO_2 (1) UC-20 w/o PuC (3) Structural (4) Structural (3) Structural (2)	ANL ANL PNWL PNWL UNC PNWL ANL GE	4770	5,130
XO10	3/24/66	UO_2-20 w/o PuO_2 (4) Structural (11) Structural (4)	GE ANL PNWL	4770	19,600
XO11	5/9/66	UO_2-20 w/o PuO_2 (7) UO_2-20 w/o PuO_2 (9) 304 SS-30 v/o PuO_2 (1) 304 SS-20 v/o PuO_2 (1) 304 SS-20 v/o UO_2 (1)	ANL GE PNWL PNWL PNWL	3189	8,300
XO12	8/10/66	UO_2-20 w/o PuO_2 (19)	NUMEC	1070	20,600
XO14	7/17/66	Structural (17) Graphite (1) Graphite (1)	PNWL NRL GE	1769	*
U-1550X	5/6/65	Alpha Monitor	ANL	8710	9,120**
U-1551X	5/6/65	Alpha Monitor	ANL	8710	9,120

*Maximum attainable before core has reached terminal size.
**Minimum acceptable.

Ten (PuU)C fuel capsules of United Nuclear Corp. were received and underwent satisfactory nondestructive testing inspection at Illinois, then were shipped to Idaho for future loading into MK-A-type irradiation subassemblies. Two UO_2-PuO_2 (Group-7) capsules from GE were received at Illinois and are undergoing nondestructive inspection.

Six special subassemblies containing neutron-flux-measuring wires are being constructed. All drawings have been completed and fabrication of the hardware has been started.

Comparison calibration tests have been made on the prototype Mark-A Irradiation Subassembly to determine the effect of removing the inlet filter tube. The lower adapter with 0.314-in. upper-inlet holes was used. In Row 4 the flow increased from 55.5 to 68.5 gpm, a factor of 1.235. In Row 1 and 2 it increased from 68 to 88 gpm, a factor of 1.293.

b. Rotating Plug Seals. Improved vacuum-cleaning equipment, incorporating a large mechanical vacuum pump, was assembled for trial use, and an alloy-melting and -charging apparatus was fabricated and tested for adding makeup alloy to the seal troughs. Also, condenser tube cleaning brushes were procured for use in further trough-cleaning operations. These brushes are longer than those used in September and they entrap more oxide material.

Two days of vacuum cleaning with the new equipment was found to be unproductive in removing oxide material. Borescope examination of the alloy surface showed little black oxide material. However, the brush technique continued to recover some oxide-like material from the trough wall, the dip ring surface, and the body of the alloy, even though the amount of alloy removed with the oxide was greater than in previous cleaning operations (presumably because of the lesser amount of oxide in the troughs after the extensive cleaning in September). The brush-cleaning operation was continued until a "point of diminishing returns" was reached in which the amount of molten alloy removed by the brush considerably exceeded the amount of oxide material. The material removed during this cleaning operation appears to be well over 50% metal (not including the unoxidized metallic component of the oxide).

About 32 lb of material was removed from the small plug trough, lowering the alloy level from 8 to $7\frac{3}{4}$ in. From the large plug trough, 130 lb of material was removed, lowering the alloy level from $6\frac{3}{4}$ to $5\frac{3}{4}$ in.

A borescope was used to inspect each trough through the new access hole at several points around the circumference. The stainless steel trough walls, thermocouple wells, and dip ring surfaces appeared to be in good condition. They had a greyish "temper film" color. There was no evidence of gross corrosive attack.

The level in the small plug trough was increased to 9 in. by the addition of 127 lb of new alloy. Increasing the level in the large plug trough to $8\frac{3}{8}$ in. required the addition of 350 lb of new alloy. Subsequent checks of alloy levels in the inner annuli (primary argon sides) showed that the level in the small plug trough was $8\frac{3}{4}$ in. and that in the large plug trough was $8\frac{1}{8}$ in.

Samples of alloy were taken from the inner and outer annuli of both seal troughs on October 6, prior to the last cleaning operations and the addition of new makeup alloy. Sample descriptions and available analytical results are tabulated below:

Sample Description	Constituent		
	Bi (%)	Na (ppm)	Fe (ppm)
(1) Alloy from large plug (LP) trough outer annulus, taken near alloy surface ($6\frac{1}{2}$ in. above bottom of trough)	59.3	1500	46
(2) Alloy from LP trough outer annulus, taken near trough bottom (2 in. above bottom)	59.0	1750	30
(3) Alloy from LP trough inner annulus, taken $6\frac{1}{2}$ in. above bottom of trough	59.0	1800	60
(4) Alloy from LP trough inner annulus, taken 2 in. above bottom of trough	58.4	2000	64
(5) Alloy from small plug (SP) trough outer annulus, taken near alloy surface (7 in. from bottom of trough)	57.8	900	26
(6) Alloy from SP trough outer annulus, taken near trough bottom (2 in. above bottom)	57.6	800	23
(7) Alloy from SP trough inner annulus, taken 6 in. from bottom of trough	57.0	900	23

Unable to sample near bottom of inner annulus because of configuration of trough and access hole.

The foregoing analyses for bismuth content indicate that the alloy remaining in the trough after extensive cleaning operations was still close to the nominal eutectic composition (58 w/o Bi, 42 w/o Sn). Similar analyses of samples taken last May had previously confirmed the eutectic composition of the alloy in the trough.

The analyses for sodium are significantly lower than those made on the samples taken in May. The latter were in the neighborhood of 2500 ppm. This reduction may indicate the effects of prolonged residence in molten condition and agitation of the alloy during the cleaning operations, bringing sodium-bearing alloy into contact with the oxygen-containing atmosphere above the outer trough annulus. The analysis method for sodium content of the alloy is simple and straightforward. It is unlikely that the reported sodium concentration differences are due to analytical variations.

c. Maintenance and Modifications. The most important of numerous maintenance and modification items completed during the scheduled shutdown are as follows:

(i) turbine overhaul;

(ii) oscillator installation;

(iii) cleaning of and Cerrotru additions to rotating shield plug seal trough;

(iv) installation of motor operator for main steam line stop valve;

(v) installation of the improved Secondary Sodium Trace Heating System;

(vi) revision of instrumentation which provides reactor shutdown for abnormal primary bulk sodium and fuel channel outlet temperatures;

(vii) modification of reactor building isolation system to provide partial isolation condition;

(viii) steam system components, such as the main condenser, feedwater heater No. 2, blowdown after-cooler, turbine oil coolers, and cooling tower, were cleaned and inspected;

(ix) the secondary sodium recirculation pumps were interlocked to trip automatically if the system drain valves were opened.

2. Reactor Improvements

a. Oscillator System, Mark II. The complete oscillator system including control and interlock circuitry has been installed in the EBR-II reactor. The No. 1 oscillator rod (OSC-1) containing two capsules of boron carbide (see Progress Report for September 1966, ANL-7255, pp. 8-9) was inserted into the #8 control-rod location; the drive unit and controls were connected. A checkout of the system was performed, and the oscillator was run at various speeds to verify its proper operation prior to reactor start-up. These tests were satisfactory.

b. Irradiation Subassemblies. Status of the various models of irradiation subassemblies is as follows:

Mark B--Fabrication of the hardware necessary for assembly of the B-7, B-19, B-37, and B-61 types is complete. The first subassemblies are expected to be completed in October 1966.

Mark C--Fabrication of parts for a prototype Mark-C-37 subassembly has been started. All required detail drawings have been released to Central Shops, and the necessary material is on hand to complete the prototype. On completion, the prototype will undergo extensive hydraulic flow tests and evaluation to verify the preliminary calculations of coolant flow characteristics.

Mark D--The Mark-D-type irradiation subassembly design concepts are under study for preparation of preliminary sketches. This subassembly is intended to provide a means of preheating the coolant flow to higher temperatures upstream of the irradiation samples, so as to broaden the spectrum of temperatures available for experiments in the EBR-II reactor.

c. Control Rod, Model IHE. The drawings have been completed for the Increased Holddown Effect modification to the standard control rod (see Progress Report for July 1966, ANL-7245, p. 26). A prototype of the IHE model is being fabricated from a reworked, standard-type control rod for use in hydraulic tests which will be performed to check the calculated reduction of lifting effect. The tests will measure the actual upward force on the control rod at conditions simulating full flow of sodium coolant.

d. Fuel Element, Mark IB. The fuel-pin restrainers presently in use with the Mark-IB fuel elements create a problem during eddy-current measurements of the level of the sodium bond. Because of the large cross-section tip, or knob, the calculations of the displaced sodium become difficult and are often inaccurate. It would be desirable to redesign the fuel-pin restrainer to have a minimum, constant cross section, such as that of a small-diameter wire.

Destructive testing experiments were performed with two different models (see Figs. 1 and 2) to determine what axial load and deflection could be expected if a 0.040-in.-dia wire restrainer was used in this fuel element. A precision compressive testing machine measured the force exerted by a simulated fuel pin and the distance the pin traveled before a measureable (0.002-in.) distortion occurred at the fuel-element tube wall (see Fig. 1). Tables II and III show the data.

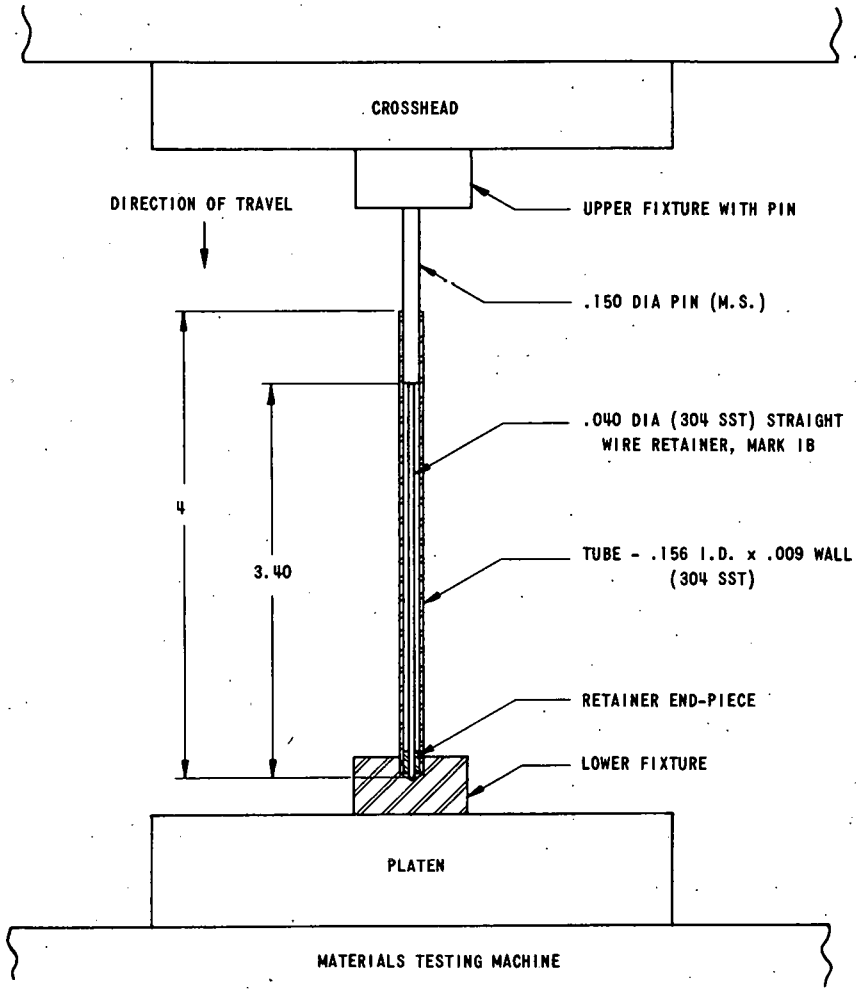

Fig. 1. EBR-II Fuel-pin Restrainer, Model #1 (Straight Wire) Compression Test Fixtures and Sample (Lengths in inches)

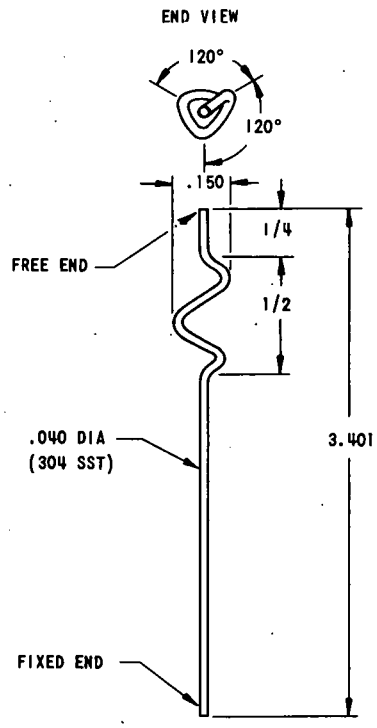

Fig. 2. EBR-II Fuel-pin Restrainer, Model #2 (Preformed Wire) (Lengths in inches)

TABLE II. Data for Model #1

Sample No.	Fuel-pin Travel (in.)	Force (lb)	Tube-wall Distortion (in.)
1	0.062	86	(Beginning)
1	0.125	93	0.010
2	0.062	81	0
2	0.072	81	0
2	0.082	67	0.002
3	0.062	68	0
3	0.072	70	0.004

TABLE III. Data for Model #2

Sample No.	Fuel-pin Travel (in.)	Force (lb)	Tube-wall Distortion (in.)
4	0.050	28	0
4	0.060	33	(Beginning)
4	0.070	41	0.004
5	0.080	31	0
5	0.090	34	0.004
6	0.050	27	0
6	0.060	29	0.003
7	0.050	22	0
7	0.060	28	0.001
7	0.070	31	0.004

These test results indicate that if a tube-wall distortion of approximately 0.002 in. is allowable, the following ranges of force and fuel-pin travel would be the limits for each model:

Model #1--(Straight wire) A load of 70 to 86 lb, and wire compression of between 0.062 and 0.082 in.;

Model #2--(Preformed wire) A load of 28 to 41 lb, and wire compression of between 0.06 to 0.080 in.

These results will be further analyzed before any decision is made to change the design of the fuel-pin restrainer.

3. Reactor Physics

SNARG calculations have been made for both Run 22 and the estimated 91-subassembly core. The SNARG calculations are in good agreement with the overall average of the fission rates as measured in Run 22, but did not very adequately predict the local perturbations of experiments. However, since the SNARG code did agree with the flux shape at the core-blanket interface, the calculations have been extended to the reference 91-subassembly core for estimation of fission rates at powers of 45 MW and above. Such calculations indicate that to maintain the same fission rate in Row 4 with the large, 91-subassembly core an increase in power to 48-50 MW will be needed and that some experiments now in Row 4 will have to be moved to Row 6 for power in the neighborhood of 62.5 MW.

A survey of the burnup data as calculated for reactor operation and measured in the subassemblies removed for Mark-IA surveillance show overall good agreement of about ±2%.

4. Fuel Cycle Facility (FCF)

Postirradiation measurements of sodium level are continuing to be made of subassemblies received from the reactor in an effort to isolate the causes of variations of up to 100% in swelling of fuel from various casting batches.

Data obtained from the examination of elements from subassembly C-199 (1.2 a/o maximum-0.95 a/o average burnup) indicated that several of the fuel rods had swelled axially to the degree that top ends of the fuel rods were in contact with the base of the restrainer (0.4-in. axial growth). The overall volume increase of these pins was about the same (12 v/o) as that in elements from other subassemblies that had received the same burnup. Confirmation of these data, obtained from bond-testing recordings, will be obtained by decanning these elements and measuring the actual length of these rods. In the postirradiation examination program, these are the first observations which indicated this degree of axial growth.

Production Summary for October 1966

Subassemblies received:	None	
Subassemblies dismantled:	14	
Subassemblies fabricated:	14	
Subassemblies transferred to reactor:	11	
Pins decanned:	1573	
Melt refining:	9 Irradiated	4 Recycle
Pour yield (average):	90.9	91.8
Injection-casting runs:	13	
Pin processing:		
Accepts:	1079	
Rejects:	68	
Pins welded:	1344	
Leak testing:		
Accepts:	1312	
Rejects:	51	
Bond testing (completed runs):		
Accepts:	1209	
Rejects:	62	
Surveillance: and product analysis:	C-218, C-161, C-199, B-320, B-323, C-216, C-231, C-213, B-318	

5. Surveillance

a. Examination of Irradiated EBR-II Fuel Jacketing. Five specimens prepared from a Type 304L stainless steel EBR-II fuel jacket were given a postirradiation anneal at 900°C for one hour, air cooled, and then burst-tested at 900°C. The results were compared with data from equivalent irradiated but not annealed specimens, and with data from unirradiated controls. The maximum fluence for the irradiated specimens was 1.2×10^{22} n/cm^2, and the maximum irradiation temperature was 517°C.

Two control-burst test specimens from unirradiated tubing, in the as-received annealed condition, but tested at 900°C, had tangential rupture strengths of 19,300 psi. The percent elongations based on diameter measurements ranged from 14.3 to 24.4% for the two, and the average was 18.7%.

Five specimens from each of two fuel jackets were burst-tested at 900°C in the as-received irradiated condition. The rupture strengths as well as those for the irradiated and annealed specimens are given in Table IV. Percent elongation values are shown in Table V.

TABLE IV. Rupture Strength at 900°C

Specimen Location	Tangential Rupture Strength (psi)		
	Irradiated		Irradiated and Annealed
	1	2	
1--Top	16,100	14,900	17,200
2	14,700	14,700	15,900
3	15,200	13,800	14,500
4	15,200	14,500	15,200
5--Bottom	14,900	14,500	15,600
Average	15,200	14,500	15,700

TABLE V. Percent Elongation from Burst Tests at 900°C

Specimen Location	Percent Circumferential Elongation					
	Irradiated				Irradiated and Annealed	
	1		2			
	Range	Avg	Range	Avg	Range	Avg
1--Top	2.6-14.7	6.9	3.5-5.7	4.6	4.9-6.6	5.7
2	3.4-7.1	4.8	1.0-2.9	2.2	1.3-4.7	3.1
3	4.6-12.9	7.1	0.5-7.3	2.9	0.3-1.3	0.9
4	1.3-3.4	2.6	1.8-5.6	3.2	0.0-7.5	3.2
5--Bottom	2.3-5.8	3.6	2.1-7.0	3.6	2.4-4.5	3.3

The rupture strengths of the irradiated samples were in every case lower than for the unirradiated in burst tests at 900°C. The ductilities of the irradiated and irradiated-and-annealed tube sections were about the same, but were much less than for the unirradiated tubes.

Previously irradiated specimens annealed at 900°C and tested at 500°C were shown to have recovered ductility (<1 to 12%) to the extent that it was again equal to that of unirradiated tubing at the 500°C test temperature. Different rupture mechanisms appear to be operating in the tests at 900 than at 500°C.

B. Physics Development

1. ZPR-3

Work is continuing on Assembly 48, the first in a series of plutonium assemblies in ZPR-3 with well-degraded spectra. Measurements with this assembly have been in progress since last June. A summary is presented herewith.

a. Core Composition. The "as-built" composition of Assembly 48 is given in Table VI. The differences between this composition and that specified for the International Comparison with calculations organized in connection with the ANL-sponsored Conference on Fast Critical Experiments, held in October 1966, are small. The drawer loadings are given in Fig. 3.

TABLE VI. Composition of Assembly 48
($\times 10^{22}$ atoms/cm^3)

Isotope	Core	Reflector		Isotope	Core	Reflector	
		Axial	Radial			Axial	Radial
Pu^{239}	0.1645			Na	0.6231		
Pu^{240}	0.0106			Fe	0.9985	0.5515	0.4444
Pu^{241}	0.0011			Cr	0.2681	0.1481	0.1193
Pu^{242}	0.00004			Ni	0.1330	0.0729	0.0587
U^{235}	0.0016	0.0082	0.0083	Mo	0.0206		
U^{238}	0.7427	3.8377	3.9798	Al	0.0109		
C	2.0767						

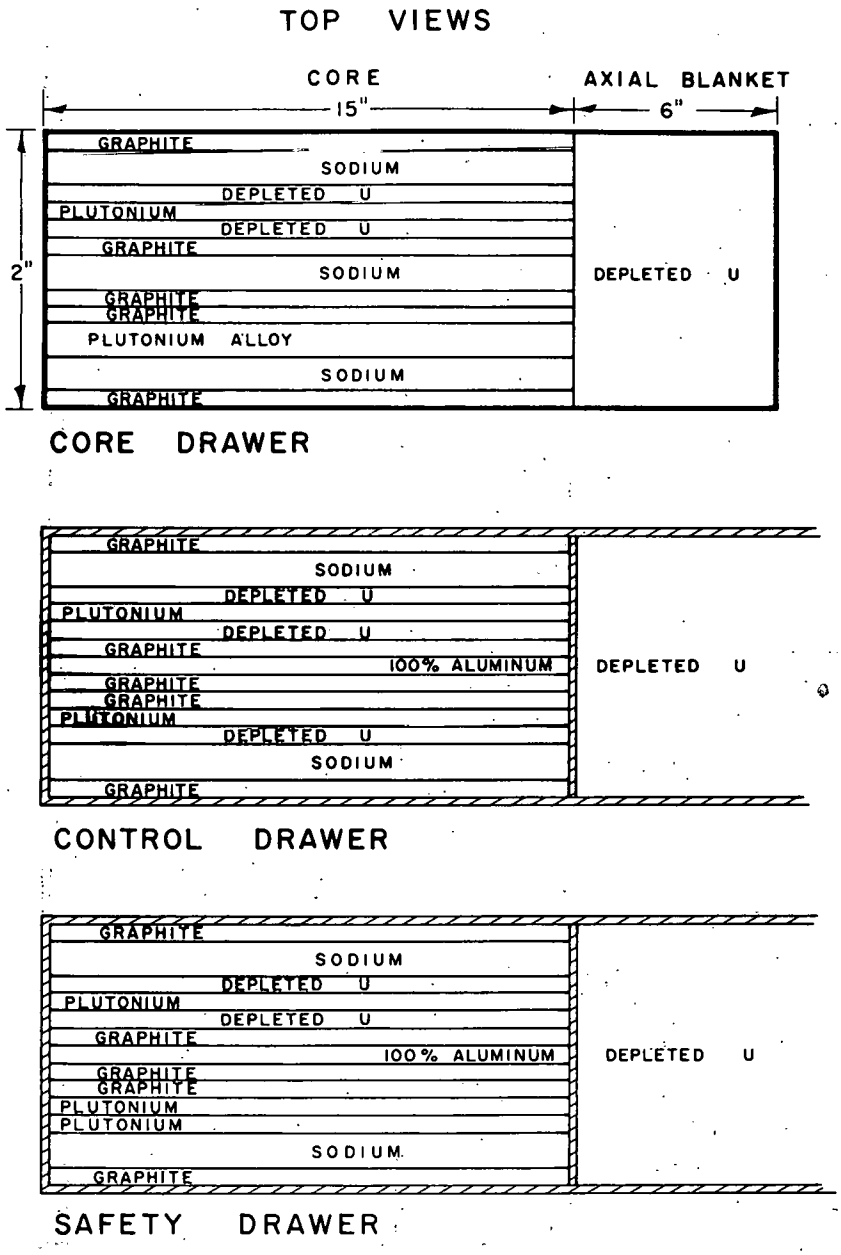

Fig. 3. Drawer Loadings for Assembly 48

b. The Critical Mass. To obtain the critical mass of the heterogeneous equivalent critical cylinder, a number of corrections must be applied to the loaded fuel mass of 260.78 kg Pu^{239}. In addition to the normal correction for the partial insertion of one control rod at the critical position, a correction must be applied for the fuel spikes in the control rod. These corrections are detailed in Table VII.

TABLE VII. A Summary of Critical Parameters for Assembly 48

Fuel Loading of Assembly as Built (324 Fuel Drawers, 8 Safety and 2 Control-rod Drawers)	260.78 kg of Pu^{239}
Corrections to the Loaded Mass for	
1. One control rod partly inserted	-0.64
2. Control-rod spiking	
(a) Replacement of safety and control drawers by fuel drawers	-5.61
(b) Fuel added at boundary to balance removal of spikes	+20.19
3. The irregular stepped outline of the core	-2.27
Mass Balance	272.45
Critical Mass of the Heterogeneous Cylinder	272 ± 1.5
Critical Dimensions	
Core Radius, cm	41.71
Core Height, cm	76.35
Core Volume, liters	417.2
Radial Blanket Thickness, cm	30
Axial Blanket Thickness, cm	30

A further correction to these figures is necessary for the effect of the interface gap between the two halves. This correction will be measured in a future experiment, but is estimated to reduce the quoted mass by about 2 kg. Calculations will also be made later to evaluate the correction for plate heterogeneity required to obtain the equivalent homogeneous critical mass. It is estimated provisionally that the critical mass of the truly homogeneous cylinder will be about 297 kg Pu^{239}.

c. Measurements of Fission Ratio. Measurements of fission ratios have been made at positions close to the core center using two sets of U^{233}, U^{234}, U^{235}, U^{236}, U^{238}, Pu^{239}, and Pu^{240} fission chambers. The Kirn chambers are sealed and have a relatively thick stainless steel wall. They have been used for the majority of measurements in past ZPR-3 assemblies. The new Davey spherical, thin-walled aluminum flow chambers each contain two foils in back-to-back geometry. Their mass calibrations have been determined from a knowledge of the plated mass and by using a thermal-flux-calibration technique.

Measurements were made in two positions close to the core center with the Kirn chambers placed back to back, at the front of the drawer pairs 1 O 14 - 2 O 14, and 1 Q 18 - 2 Q 18. The Davey chambers were placed at the front of drawers 1 O 14 and 1 Q 18.

The measured fission ratios obtained from the two sets of chambers are compared in Table VIII. Correction factors for the effect of

inelastic scattering in the Kirn chamber walls were determined experimentally in this assembly. The accuracy of the measured ratios is typically ±1.5%. The two sets of fission ratio results agree within the quoted errors. This agreement gives confidence to the independent mass calibrations of the two sets of chambers and in the wall-effect corrections applied to the Kirn chambers.

TABLE VIII. Measurements of Fission Ratio in Assembly 48

Ratio	Kirn Chambers Uncorrected	Kirn with Wall Correction	Davey Chambers	Corrected Kirn / Davey
U^{233}/U^{235}	1.454	1.454	1.480	0.98
Pu^{239}/U^{235}	0.995	0.995	0.976	1.02
Pu^{240}/U^{235}	0.231	0.241	0.243	0.99
U^{234}/U^{235}	0.193	0.201	0.204	0.99
U^{236}/U^{235}	0.0643	0.0679	0.0670	1.01
U^{238}/U^{235}	0.0284	0.0307	0.0307	1.00

The corrections applied to the measured fission ratios for the effect of inelastic scattering in the Kirn chamber walls are based on a small number of measurements with the same U^{235} and U^{238} foils used in both thin-walled and thick-walled stainless steel flow chambers. Davey used these results to deduce corrections to the other measured ratios. Since the foils in the Kirn chambers are sealed in, it was necessary to construct special fission chambers for this measurement. A pair of thick-walled stainless steel flow chambers was made, having the same dimensions as the Kirn chambers. A pair of thin-walled aluminum flow chambers with the same external dimensions as the flow chambers, but with walls about 0.010 in. thick, was also made. A set of U^{234}, U^{236}, U^{235}, and U^{238} foils were used. A U^{235} foil and one other foil were used for fission ratio measurements in both sets of chambers.

From a comparison of the measured ratios, the multipliers needed to correct the Kirn chamber results can be deduced, since the thin aluminum walls of the second set of chambers have a negligible effect on the measured ratios. The results of these measurements are compared with the values previously used in Table IX. The agreement is excellent, giving confidence in the previous evaluation of results from Kirn chambers.

d. Central Perturbation Measurements. Most of the central perturbation measurements in ZPR-3 assemblies were made with 2 x 2 x 2-in. samples of different materials. Also, a study of the effects of sample size and of the heterogeneity of the core on the measured reactivity worth per kg has been begun in Assembly 48.

TABLE IX. Measurements of the Change in Fission Ratios due to Scattering in the Kirn Chamber Walls

Fission Ratio	Thick-wall Chamber Ratio / Thin-wall Chamber Ratio	Multiplier to Correct Kirn Chamber Measurements	
		Measured	Estimated
U^{238}/U^{235}	0.918 ± 0.004	1.082	1.08
U^{236}/U^{235}	0.944 ± 0.004	1.055	1.06
U^{234}/U^{235}	0.959 ± 0.003	1.041	1.04
Pu^{240}/U^{235}	0.957 ± 0.003	1.042	1.04

The 2 x 2 x 2-in. sample changer consists of a modified core drawer with cutaway sides at the interface end to allow the insertion and removal of samples when the drawer is withdrawn from the reactor. There is a large reactivity change on removal of the drawer for the change-over of samples, which limits the rate of drawer motion. The separation in time of two measurements, one with the sample out and the other with the sample in, is typically about 30 min. During this time significant changes in the reactivity of the assembly can be produced by changes in temperature. The reference measurement with a central void was repeated numerous times to correct for this temperature drift, which is the prime factor in limiting the measurement accuracy to about 2×10^{-6} $\Delta k/k$.

In an attempt to diminish the importance of temperature drift on the measurements, and to permit the use of samples of a smaller size, an additional sample changer was designed for this assembly and permitted the insertion of small cylindrical perturbation samples at the core center by using a long steel rod, 0.45 in. in diameter, inserted in the radial traverse tube that passes close to the interfacial plane. The rod contained two carrier sections, with sample spaces 2 in. long x 0.42 in. in diameter, one of which was used for the sample and the other as a reference. The reference carrier position was either empty or contained a dummy can if a canned sample was in the sample carrier. By limiting the reactivity worth of the samples and moving no core material during the sample change, it was possible to compare sample and void with a time separation of about 4 min. Sample and void were interchanged several times to improve the accuracy and further reduce the importance of temperature drift. The accuracy of the measurements depends on the number of cycles made, and whether or not the normal control rods were moved. The limiting accuracy was about 10^{-7} $\Delta k/k$.

Measurements were made using both sample changers. The reactivity changes were determined from the movement of a calibrated autorod. For certain samples it was also necessary to adjust the position of the normal control rods. In this assembly 1% $\Delta k/k \equiv 1002$ Ih.

The first set of measurements was made using the 2 x 2 x 2-in. sample changer in the central drawer position 1 P 16. The reactivity worth of 2-in. cubes of iron, chromium, nickel, Type 304 stainless steel, graphite, aluminum, aluminum oxide, manganese, molybdenum, and depleted uranium, used in previous ZPR-3 assemblies, were measured. In addition, some measurements were made with small plate, foil, and cylindrical samples of smaller sizes by placing them in a thin-walled (0.015 in.), stainless steel box with outer dimensions 2 x 2 x 2 in. The errors for the measurements with small samples were too large to show any significant differences, due to size effects, from the results obtained with the cubes.

Two new 2-in.-cube sodium samples canned in stainless steel and two dummy cans were used to determine the sodium worth. The sample changer was modified so that the samples could be cycled without shutting down the reactor and reloading the changer. By waiting for good conditions of temperature stability within the assembly and by recycling the sodium samples and their dummy cans several times in succession, an accuracy of $\pm 3 \times 10^{-7}$ was achieved on the sodium measurement.

The measurements described below, made with the new cylindrical sample changer, are provisional. The samples included small cylinders and annular foil samples of the fissile and fertile materials, and tantalum. The cylinders range in diameter from 0.062 to 0.200 in., and the foils in thickness from 0.0012 to 0.040 in. Samples of boron enriched in the boron-10 isotope were also prepared in the same geometry, using boron powder canned in stainless steel. Two sets of plutonium samples were made with Pu^{240} content of 4.5 and 22%, respectively. Both sets were canned in stainless steel. The other materials used were either in the form of solid cylinders, 2 in. long x 0.42 in. in diameter, or were powders contained in stainless steel cans of the same outer dimensions.

The results of the measurements made in both sample changers are summarized in Tables X-XIII. Comparison of the measured inhours/kg obtained with the 2-in. cubes and the small cylinders for several materials shows clear evidence that the measured worth per unit mass is higher for the smaller sample. For the fissile samples the results show that the measured inhours/kg increase as the sample size increases, an effect which can be qualitatively attributed to internal multiplication with the sample. The results for boron and tantalum demonstrate the need for a careful understanding of the precise size of the sample used in any measurement when making a comparison with calculated values.

TABLE X. Central Perturbation Measurements with Enriched and Depleted Uranium Samples

Sample Type		Thickness, Diameter, or Cube Size (in.)	Measured Worth (1h/kg)
Enriched Uranium[a]			
Foils	Ann.	0.0014	315 ± 14
	Ann.	0.0034	314 ± 4
	Ann.	0.0052	312 ± 4
	Plate	0.0052	292 ± 38
	Ann.	0.0106	311 ± 3
	Plate	0.0106	321 ± 10
	Plate	0.02	316 ± 9
	Plate	0.04	319 ± 5
	Plate	0.062	322 ± 2
Cylinders		0.061	308 ± 5
		0.10	310 ± 2
		0.20	310 ± 2
Depleted Uranium[b]			
Foils	Ann.[c]	0.022	-23.3 ± 0.5
	Plate	0.125	-21.4 ± 1.6
Cylinders		0.20	-22.2 ± 0.5
		0.42	-20.8 ± 0.2
Cube		2 x 2 x 2	-19.2 ± 0.1

[a]Enrichment range 93.10 to 93.30% U^{235}.
[b]0.21% U^{235}.
[c]0.40% U^{235}.

TABLE XI. Central Perturbation Measurements with Plutonium Samples

Sample		Thickness or Diameter (in.)	Measured Worth (1h/kg)
Plutonium (4.5% Pu^{240})[a]			
Foils	Ann.	0.005	422 ± 5
	Ann.	0.010	427 ± 4
	Ann.	0.020	430 ± 4
	Plate[b]	0.086	468 ± 3
Cylinders		0.100	433 ± 5
		0.200	426 ± 4
Plutonium (22% Pu^{240})[c]			
Foils	Ann.	0.005	356 ± 6
	Ann.	0.010	366 ± 4
	Ann.	0.020	370 ± 3
Cylinders		0.062	356 ± 11
		0.100	371 ± 4
		0.200	381 ± 3

[a]Composition of 98.6 w/o Pu, 1.4 w/o Al, plus impurities. Plutonium mixture of 95.05 w/o Pu^{239}, 4.50 w/o Pu^{240}, and 0.45 w/o Pu^{241}.
[b]Measured in 2 x 2 x 2-in. sample changer.
[c]Composition of 98.8 w/o Pu, 1.2 w/o Al, plus impurities. Plutonium mixture of 72.24 w/o Pu^{239}, 22.28 w/o Pu^{240}, 4.63 w/o Pu^{241} and 0.79 w/o Pu^{242}.

TABLE XII. Central Perturbation Measurements with Boron and Tamtalum Samples

Sample		Thickness or Diameter (in.)	Measured Worth (1h/kg)
Boron[a] (Enriched in B^{10})			
Annular		0.010	7632 ± 40
		0.020	7523 ± 40
		0.040	5838 ± 30
Cylinders		0.060	7399 ± 80
		0.100	7307 ± 50
		0.200	6701 ± 30
Tantalum			
Foils	Ann.	0.005	-164 ± 5
	Plate	0.005	-169 ± 42
	Plate	0.010	-182 ± 21
	Plate	0.015	-167 ± 14
Cylinders		0.061	-142 ± 5
		0.100	-137 ± 2
		0.200	-125 ± 1
		0.200	-131 ± 14[b]

[a]Composition of 92.8 w/o B, 7.2 w/o impurities. Boron = 92.1 w/o B^{10}, 7.9 w/o B^{11}.
[b]Measured in 2 x 2 x 2-in. sample changer.

TABLE XIII. Central Perturbation Measurements for a Selection of Nonfissile Samples

Sample Type		Thickness, Diameter, or Cube Size (in.)	Measured Worth (1h/kg)
Fe	Cylinder	0.42	-12.3 ± 0.4
	Plate	0.25	-11.5 ± 2.0
	Cube	2.0	-11.3 ± 0.2
Cr	Cylinder	0.42	-9.4 ± 0.5
	Cube	2.0	-10.8 ± 0.6
Ni	Cylinder	0.42	-18.2 ± 0.2
	Plate	0.25	-18.7 ± 1.6
	Cube	2.0	-15.9 ± 0.2
SS 304	Cylinder	0.42	-14.1 ± 0.2
	Cube	2.0	-12.7 ± 0.2
Na	Cylinder	0.42	-5.6 ± 4.5
	Cube	2.0	-6.3 ± 0.3
C	Cylinder	0.42	-4.6 ± 1.2
	Cube	2.0	+1.3 ± 1.2
Al_2O_3	Cylinder	0.42	-11.5 ± 1.2
	Cube	2.0	-9.5 ± 0.1
Mo	Cylinder	0.42	-43.4 ± 0.4
		0.42	-45.4 ± 5.1[a]
	Plate	0.25	-46.6 ± 2.9
	Cube	2.0	-28.7 ± 0.3

[a]Measured in 2 x 2 x 2-in. sample changer.

Selected values from the measured results, generally from samples of the smallest size, have been used for comparison with the calculated values in a study of the assembly at the October Conference. The experimental results used for this purpose are given in Table XIV. One or two revisions of numbers made since the last information available was presented are noted.

TABLE XIV. Summary of Central Perturbation Measurements

Material or Isotope	Measured Worth (Ih/kg)	Sample Size Used to Derive Worth Value
U^{235}	+339 ± 4	Isotopic value derived from 3.4-mil enriched uranium and 22-mil depleted uranium annular samples.
U^{238}	-24.8 ± 0.5	Isotopic value derived from 3.4-mil enriched uranium and 22-mil depleted uranium annular samples.
Pu^{239}	+445 ± 4	Isotopic value derived from 5-mil annular samples of 4.5 and 22% plutonium.
Pu^{240}	+81 ± 20	Isotopic value derived from 5-mil annular samples of 4.5 and 22% plutonium.
B^{10}	-8926 ± 80	0.010-in. annular samples.
Steel (304)	-14.1 ± 0.2	0.42-in. cylinder.
Fe	-12.3 ± 0.4	0.42-in. cylinder.
Cr	-9.4 ± 0.4	0.42-in. cylinder.
Ni	-18.2 ± 0.2	0.42-in. cylinder.
Mn	-21.4 ± 0.4	0.42-in. cylinder.
Al	-15.7 ± 0.8	0.42-in. cylinder.
Na	-6.3 ± 0.3	2-in. cube.
C	-4.6 ± 1.2	0.42-in. cylinder.
O	-6.8 ± 0.9	Derived from values for 0.42-in. cylinders of Al and Al_2O_3.
Ta	-164 ± 5	0.005-in. annular sample.
Mo	-43.4 ± 0.4	0.42-in. cylinder.
CH_2	+1676 ± 70	0.42-in. cylinder.

e. Doppler-effect Measurements. The natural uranium and plutonium samples used consist of 70% theoretical density oxide pellets, contained in stainless steel elements. The compositions of the samples are given in Table XV. The pellet stack in each element was 1.27 cm in diameter by 15.28 cm long. Two elements of each type were used in any measurement. The samples were placed on the same axis and separated by a gap of 12.06 cm to form a single sample assembly. During the measurements the sample was placed parallel to the axis of the assembly, with the gap between the samples at the core midplane. The elements were fixed so that the axial expansion of one element was directed towards the core midplane while that of the other was away from the midplane. This resulted in a first-order correction for axial expansion effects.

TABLE XV. Masses and Compositions of the ZPR-3 Doppler Oxide Samples at 500°K

Isotope	Composition (10^{24} atoms/cm^3)	
	Natural Uranium	Pu^{239}
U^{238}	0.0156	
U^{235}	0.0001	
$Pu^{239\pm241}$		0.0147
Pu^{240}		0.0004
Oxygen	0.0314	0.0302
Total Mass (g)	274.4	263.8

The samples were oscillated at different temperatures and the reactivity changes measured relative to a reference material, by using a calibrated autorod.

The results of measurements made with high-purity Pu^{239} and natural uranium oxide samples are given in Table XVI.

TABLE XVI. Measurements of Reactivity Changes Produced by Heating Doppler Oxide Samples

T(°K)	Reactivity Change (10^{-6} dk/k)		
	Natural Uranium[a]	Pu^{239}[b]	Empty Can
300	0 ± 0.0		0 ± 0.046
355		0 ± 0.04	
500	-1.75 ± 0.09	-0.29 ± 0.05	+0.055 ± 0.052
650		-0.49 ± 0.06	
800	-3.76 ± 0.07	-0.87 ± 0.06	-0.023 ± 0.056
900		-1.01 ± 0.06	
1052		-1.25 ± 0.06	
1100	-4.89 ± 0.11	-1.16 ± 0.08	-0.015 ± 0.061

[a]Average of two sums.
[b]The lowest experimental temperature was 355°K due to the decay heat of the plutonium sample.

The natural uranium sample was measured twice to check the reproducibility of the technique. The average of the results is given in Table XVI. All but one of the results was within one standard deviation of

the average used. The plutonium results have not been corrected for expansion effects; thus the measured negative effect may not in fact be attributable to the Doppler effect. The natural uranium results showed a negative Doppler effect as expected. The expansion corrections for the natural uranium sample are believed to be negligible.

f. Neutron-spectrum Measurements. Measurements of the neutron spectrum at the center of the core were made using both proton-recoil counters and a Li^6 spectrometer. The proton-recoil measurements were made with both hydrogen- and methane-filled counters at a gas pressure of about 5 atm. The hydrogen-filled counter was used for the range from 1 to 150 keV, and the methane-filled counter was used above 150 keV. The measured spectrum is shown in Fig. 4. The fine structure can be attributed to scattering resonances in the light material present in the core.

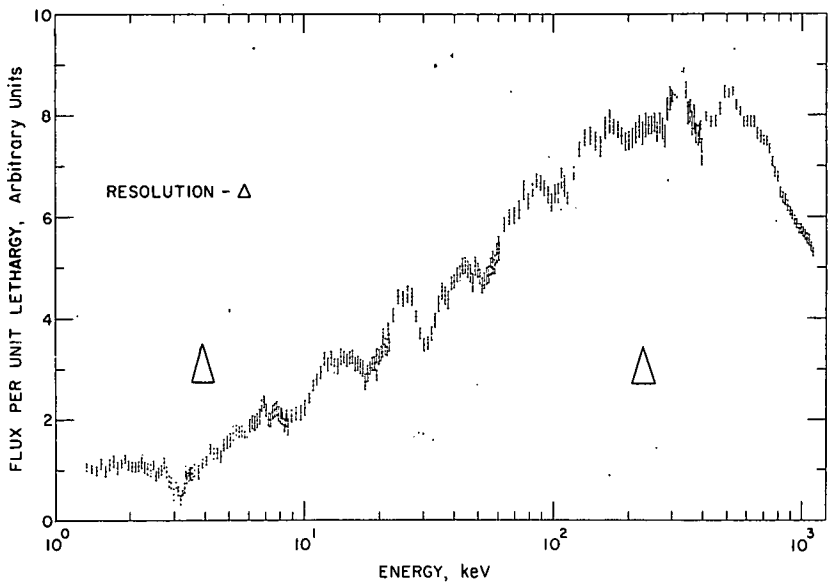

Fig. 4. Central Spectrum in Assembly 48 of ZPR-3

The Li^6 spectrometer consisted of a Li^6F layer on a thin organic film mounted centrally between the silicon surface-barrier detectors. The results from the Li^6 spectrometer were compared with those from the proton-recoil counters by calculating the pulse-height distribution for the Li^6 spectrometer using the measured gas-counter results. The agreement between the two is within counting statistics over the majority of the energy range.

g. Activation Doppler Measurements. Measurements of the change in the activation of a thin depleted uranium foil on heating have been made. The technique was basically that used for Assembly 47 (see Progress Report for May 1966, ANL-7219, p. 7). The results are being analyzed.

2. ZPR-6

A comparison has been made of measurements of central fission ratios obtained from the ZPR-6 Assemblies 4Z and 5, and ZPR-9 Assembly 11, which were expected to have similar neutron spectra at the center of the core. The measurements were made using 1/2-in.-dia solid-state counters placed at the center of the core of each assembly.

The results from a series of counter traverses taken along the radial (vertical) and/or axial center lines of the various cores are given in Table XVII. It is assumed that the orientation of the counter and the associated traverse mechanism would have little if any effect on the fission ratios measured at the center of the core. Since this seems to be borne out by the results from Assembly 5, the axial threshold data from Assembly 4Z are somewhat suspect. No suitable explanation for this discrepancy has been found to date, but investigations are continuing.

TABLE XVII. Central Fission Ratios Measured in ZPR-6 and -9 Assemblies

	ZPR-6 Assembly 4Z		ZPR-9 Assembly 11	ZPR-6 Assembly 5		
	with Spacer* Radial	Axial	without Spacer* Radial	without Spacer* Radial	Axial	with Spacer* Radial
U^{238}/U^{235}	0.0238 ± 0.0007	0.0267 ± 0.0008	0.0238 ± 0.0007	0.0238 ± 0.0008	0.0223 ± 0.009	0.0234 ± 0.007
U^{234}/U^{235}	0.172 ± 0.004	0.203 ± 0.005	0.175 ± 0.004	0.166 ± 0.004	0.159 ± 0.005	0.163 ± 0.004
Pu^{239}/U^{235}	0.967 ± 0.025	0.949 ± 0.025	0.986 ± 0.026	0.968 ± 0.025	0.949 ± 0.025	0.963 ± 0.024

*Spacer consists of 1/2-in.-thick U^{238} plate located in front drawers only when radial traverse measurements were made.

When the measurements were first made on Assembly 4Z, it was believed that there might be some spectral effect on the measurements due to the presence of a 1/2-in. spacer of depleted uranium which was present at the front of the drawers used in the radial traverse, but which was not present in the axial measurements. To explore this possibility, the radial measurements on Assembly 5 were made with and without the spacer. The results indicate that the counters are not overly sensitive to such an effect.

3. ZPR-9

ZPR-9 Assembly 11 was a zoned version of the full-size ZPR-6 Assembly-5 mockup. Comparison of the central worth measurements in the two assemblies has highlighted the fact that the small mismatch in the adjoint spectrum allowed in the design of Assembly 11 as compared to that of Assembly 5 was sufficient to cause easily observable mismatch in the central worths of sodium, and other scatterers. In order to test our ability to improve the matching, work on Assembly 11 was terminated and it was replaced with a redesigned zoned assembly where particular attention was paid to the adjoint spectrum in the design. The construction of the new assembly is presently under way.

Final measurements with Assembly 11 included fission-ratio and fission-rate traverses, a fission-spectrum adjoint measurement, and a high-temperature Doppler measurement on U^{238}. Data from these measurements are being processed.

The sodium-void coefficients in Assemblies 2 and 3 were calculated, using diffusion theory, one-dimensional perturbation, k-calculations, and two-dimensional perturbation calculations. The length-to-diameter ratio was approximately unity for Assembly 2 (L = D = 90 cm) and about 1/3 for Assembly 3 (L = 50.8 cm, D = 155 cm). Both reactors had uranium carbide cores of the same composition.

The cross-section set 244 was used and the ELMOE code corrected for composition, taking into account for U^{235} the measurements of P. White and for U^{238} the data reported by Columbia University.

The one-dimensional perturbation calculations were performed using the MACH 1 code and the perturbation subroutine DEL. Spectral variations were taken into account as accurately as possible by using slab geometry for regions near the axial blanket and cylindrical geometry for regions near the radial blanket.

The k-calculations were performed in two steps using the MACH 1 code; capture, spectral effect, and axial leakage were calculated in slab geometry, and the radial leakage was calculated in cylindrical geometry.

For the two-dimensional perturbation calculations, the real and adjoint fluxes were calculated by using the CANDID 2D code and the perturbations by using the PERC code.

Tables XVIII and XIX show the calculated and experimental results. The agreement between one- and two-dimensional perturbation calculations

TABLE XVIII. Calculated Sodium-void Coefficients in Assembly 2 (Ih/kg)

Type	Region Boundaries (cm)		Capture + Scatter		Leakage		Total			Total Expt
	Axial	Radial	DEL 1-dim	PERC 2-dim	DEL 1-dim	PERC 2-dim	DEL 1-dim	PERC 2-dim	k calc 1-dim	
Core Center	0- 7.62	0- 9.342	-2.45	-2.46	-0.44	-0.44	-2.89	-2.90	-2.71	-1.6
Slab	0-10.16	0-14.27	-2.32	-2.32	-0.92	-0.94	-3.24	-3.26	-3.07	-1.9
Slab	17.78-27.94	0-14.27	-1.52	-1.52	-3.16	-3.21	-4.68	-4.73	-4.63	-4.0
Slab	35.56-45.72	0-14.27	+0.58	+0.54	-6.38	-6.50	-5.80	-5.96	-5.91	-7.5
Ring	0-10.16*	14.27-25.11	-1.74	-1.72	-2.86	-2.84	-4.60	-4.56	-	-4.4
Ring	17.78-27.94	14.27-25.11	-1.19	-1.13	-3.96	-4.04	-5.15	-5.17	-5.14	-4.3
Ring	35.56-45.72	14.27-25.11	+0.45	+0.43	-5.56	-5.71	-5.11	-5.27	-5.22	-5.5
Ring	0-10.16*	25.11-35.37	-0.79	-0.81	-5.08	-5.07	-5.87	-5.89	-	-5.96
Ring	17.78-27.94*	25.11-35.37	-0.56	-0.52	-4.88	-4.93	-5.44	-5.44	-	-5.52
Ring	35.56-45.72	25.11-35.37	+0.29	+0.35	-4.43	-4.61	-4.14	-4.26	-4.22	-5.02
Ring	0-10.16*	35.37-46.50	+0.57	+0.53	-6.53	-6.54	-5.96	-6.01	-	-7.26
Ring	17.78-27.94*	35.37-46.50	+0.40	+0.40	-5.23	-5.27	-4.83	-4.87	-	-5.31
Ring	35.56-45.72*	35.37-46.50	+0.15	+0.38	-3.25	-3.39	-3.10	-3.01	-3.13	-3.39
Total Core	0-45.72*	0-46.50	-0.36	-0.20	-4.68	-4.71	-5.04	-4.91	-5.46	-5.15

*In these regions the one-dimensional perturbation calculations were made in cylindrical geometry.

TABLE XIX. Calculated Sodium-void Coefficients in Assembly 3 (Ih/kg)

Type	Region Boundaries (cm) Axial	Region Boundaries (cm) Radial	Capture + Scatter DEL 1-dim	Capture + Scatter PERC 2-dim	Leakage DEL 1-dim	Leakage PERC 2-dim	Total DEL 1-dim	Total PERC 2-dim	k calc 1-dim	Total Expt
Central Region	0- 7.62	0- 9.342	-1.45	-1.49	-0.44	-0.44	-1.89	-1.93	-1.72	-0.0
Central Region	0-15.24	0-14.27	-1.06	-1.10	-1.57	-1.57	-2.63	-2.67	-2.55	-1.23
Central Region	0-20.32	0-20.66	-0.73	-0.71	-2.54	-2.55	-3.27	-3.26	-3.21	-2.29
Central Region	0-25.4	0-24.91	-0.27	-0.28	-3.52	-3.54	-3.79	-3.82	-3.83	-3.23
Slab	0- 7.62	0-14.27	-1.42	-1.42	-0.49	-0.49	-1.91	-1.91	-1.77	-0.18
Slab	7.62-15.24	0-14.27	-0.77	-0.79	-2.64	-2.64	-3.41	-3.43	-3.34	-2.33
Slab	15.24-20.32	0-14.27	+0.30	+0.27	-5.48	-5.48	-5.18	-5.21	-5.15	-5.0
Slab	20.32-25.4	0-14.27	+1.54	+1.48	-7.88	-7.99	-6.34	-6.51	-6.40	-5.82
Ring	0- 7.62	25.87-36.45	-1.05	-1.13	-1.12	-1.21	-2.17	-2.34	-2.06	-1.06
Ring	0- 7.62	46.30-58.18	-0.53	-0.50	-1.85	-1.89	-2.38	-2.39	-2.33	-2.16
Ring	0- 7.62	65.10-69.98*	-0.07	-0.05	-2.05	-2.07	-2.12	-2.12	-	-2.25
Ring	0- 7.62	72.70-77.86*	+0.25	+0.24	-1.98	-2.05	-1.73	-1.81	-	-2.13
Total Core	0-25.4	0-77.86	-0.12	-0.06	-2.61	-2.64	-2.73	2.70	-2.83	-2.83

*In these regions the one-dimensional perturbation calculations were made in cylindrical geometry.

is very good in regions where the spectrum is influenced by both the axial and radial blanket and in the case that the total core was voided. These cases cannot be correctly described by one-dimensional theory.

The k and perturbation calculations agree within about 10%, the difference depending on the size and on the location of the region. A comparison of the calculated and experimental values shows that there is rather poor agreement at the center of the cores, where the spectral effect is strongly predominant. Corrections for heterogeneity effects and revisions to the cross-section sets are necessary to improve the situation. The leakage effect, which is the most important component in the outlying regions, is satisfactorily described by theory, but in general is underestimated by 10 to 20%. Transport effects at the core boundaries may be the cause of this difference. At the axial core boundary of Assembly 3, the calculated effect is somewhat larger than the measured value; however, due to the pancake shape of the core, this boundary is quite close to the core center and the analysis is obscured by the spectral effect.

The calculated results for voiding the total core are in good agreement with the measurements, in spite of the difficulties in calculating the spectral effect. This is in part due to the fact that in these cores the spectral effect is relatively small and the leakage effect, which is calculated with better accuracy, is strongly predominant.

4. ZPPR

a. Reactor Status. Construction is proceeding at the scheduled rate. Thirty-two piling foundation holes have been completed. The floor slab and foundation has been poured for the vault-workroom and the service floor of the support wing.

The present status of the reactor components is as follows:

(i) Bed and Tables: ANL representatives visited the Giddings and Lewis Machine Tool Co. Several minor adjustments were necessary on the machining of the tables. An interference between the movable tables and the bed was detected and corrected. Adjustments of machined surfaces in the order of 0.001 to 0.004 in. in distances up to 16 ft were necessary and are now being performed. The test procedure was reviewed with the vendor, and one additional test was proposed in which the coast of the movable table, freed from the ball screw drive, would be measured. Two 45-ton army tank trailers have been modified to haul and store the bed and tables upon arrival at the National Reactor Testing Station.

(ii) Matrix Drawers: ANL has received 1309 acceptable rear drawers and 1230 acceptable front drawers, for a total of 2539. At present the rejection rate of drawers received from the vendor, Mechanical Products Mfg., Seattle, Washington, is less than 1%. A total of 4148 drawers both front and rear are on order.

(iii) Nuclear Instrumentation: The nuclear instrumentation has been functionally checked out in the Juggernaut and Argonaut reactors at Argonne, Illinois. It is now being returned to Idaho.

(iv) Area Gamma Monitors: The area gamma monitors have been shipped to Idaho.

(v) Poison Safety Rod Drive: The vendor is fabricating the first drive, which will be checked for performance prior to fabricating the remaining 12 drives.

(vi) Reactor Knees: The castings have been completed by the vendor, Macauley Foundry Company of Berkeley, California. Due to war priorities, there is a delay of one month in machining the castings, which is now scheduled for November and December.

(vii) Personnel Shields: No bids were received for the personnel shields. The bids have been reissued and the bids are due on November 30.

(viii) Matrix Alignment: Information for the alignment plate has been received and the bid package is now being prepared.

(ix) Source Drives: The vendor, Teleflex, Inc., North Wales, Pennsylvania, is preparing drawings for submittal to ANL.

(x) Rod Drive Mounting Plates: ANL representatives visited the Greenlee Foundries, Inc., Chicago, Ill. One casting has been completed and is now being machined. This plate will be finished and checked before starting the second plate.

(xi) Fabrication is in progress on Matrix Tie-Down, Beta-Gamma Air Particulate Monitors, Particulate Stack Monitor, Loading Platform, and Drawer Springs.

(xii) Reactor Frame: The reactor frame has been fabricated, inspected, and received at Idaho.

(xiii) Reactor Plenum Assemblies: The outside structure of the plenums is being fabricated. The metal holders and tighteners for the neoprene plugs of the manifold have been received.

(xiv) Fuel Control and Safety Rod Drawers and Ball Joint Assemblies: These are being fabricated.

(xv) Poison Safety Blades and Sheaths: The order for the poison safety blades and sheaths has been placed with Van Vetter, Inc., Seattle, Washington.

(xvi) Control Consoles and Cabinets: The delivery of the consoles and cabinets from Amco Engineering Company, Chicago, has been delayed approximately 60 days.

(xvii) Boron Fabrication: Techniques of obtaining blades of high B^{10} content are being reviewed prior to soliciting bids.

(xviii) Matrix Tubes: These have been completed and received.

b. Flux Perturbation Specimens. Eleven flux-perturbation specimens were made during this reporting period. Each is a right cylindrical element, 0.420 in. in diameter and 2 in. long. The cores are plutonium-1 w/o aluminum alloy and the jackets stainless steel. Five specimens contain cylindrical cores, each with a different diameter of Pu^{240} content. The cores in the remaining six are annular "napkin" rings formed from sheet stock, either 0.020-, 0.010-, or 0.005-in. thick. The outside diameter of annular rings was 0.390 in. Each napkin ring differed in wall thickness or plutonium isotopic composition.

The solid cylindrical cores were made by machining. The annular rings were made by a process that includes rolling, shearing, and roll forming. The alloy was rolled at 375°C between rolls heated to 325°C. The stock was reduced bare to a thickness of 0.010 in. but was jacketed in stainless steel for further reduction. The rolled pieces were annealed at

485°C and were roll formed. The resulting napkin rings were loaded through a plastic membrane into stainless steel jacket cylinders. The assembled elements were welded, surveyed, decontaminated, and leak tested.

The loading of the 0.005-in.-thick napkin ring was extremely difficult. The thin metal oxidized rapidly. It was difficult to form to a precise cylinder. Under these conditions it was difficult to load and to avoid contaminating the exterior surfaces of the jackets.

C. Other Fast Reactor Physics

1. Nuclear Constants

Neutron radiative capture cross sections are being measured as a function of neutron energy between 5 keV and 3 MeV. Capture cross sections are needed to evaluate the behavior of materials proposed for structural or control use in reactors. The data are also useful in testing theories of nuclear reaction. The information gained by comparison of experimental data with theoretical values could allow the prediction of other neutron cross sections in the absence of experimental data.

The experimental method is that of neutron activation, in which a sample is irradiated in a monoenergetic neutron beam and counted with a beta- or gamma-ray counter. Monoenergetic neutrons are produced by bombarding lithium or tritium targets with protons from the Van de Graaff accelerator.

Measurements of the radiative capture cross sections of K^{41}, Mn^{55}, and Rb^{85} have been completed and are shown in Figs. 5 to 7, along with the results of other workers.[1-5] The experimental results have been compared with calculations using the statistical model of the compound nucleus, which gives compound nuclear cross sections averaged over resonances. The curves given in the figures were calculated using the model in the form given by Moldauer.[6-8] The calculations also include the variation of radiation width and level density with excitation energy and spin of the compound nucleus, and the variation of neutron widths from level to level.

The experimental data are accurately predicted by theory, at least up to neutron energies at which the energy levels of the target nucleus are known.

---

[1]Booth, R., Ball, W. P., and MacGregor, M. H., Phys. Rev. 112, 226 (1958).
[2]Hughes, D. J., Gorth, R. C., and Levin, J. S., Phys. Rev. 91, 1423 (1953).
[3]Stavissky, Yu. Ya., and Tolstikov, V. A., Atomnaya Energiya 10, 508 (1961).
[4]Johnsrud, A. E., Silbert, M. G., and Barschall, H. H., Phys. Rev. 116, 927 (1959).
[5]Macklin, R. L., Lazar, N. H., and Lyon, W. S., Phys. Rev. 107, 504 (1957).
[6]Moldauer, P. A., Engelbrecht, C. A., and Duffy, G. J., ANL-6978.
[7]Moldauer, P. A., Rev. Mod. Phys. 36, 1079 (1964).
[8]Moldauer, P. A., Phys. Rev. 135, B642 (1964).

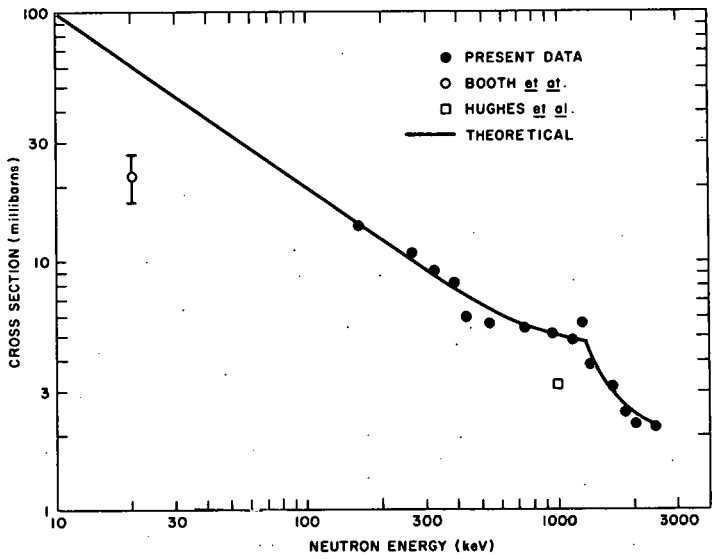

Fig. 5
Radiative Capture Cross Section of Potassium-41

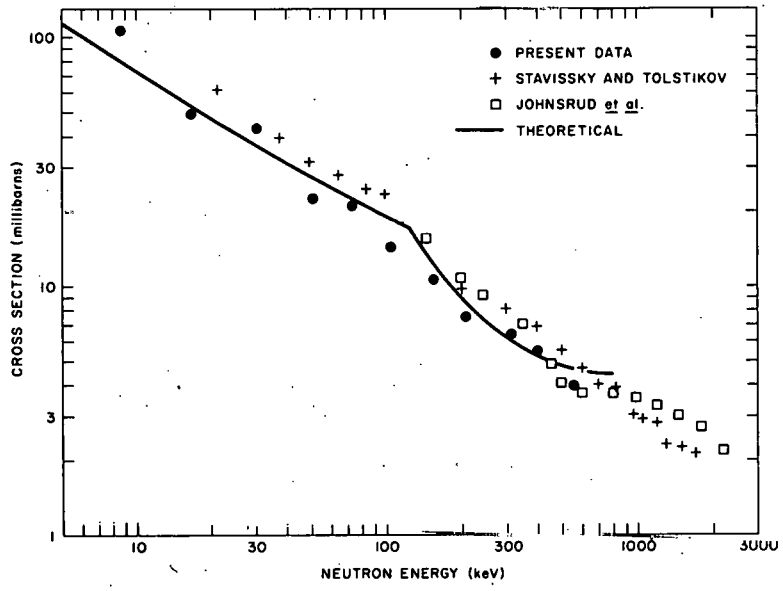

Fig. 6
Radiative Capture Cross Section of Manganese-55

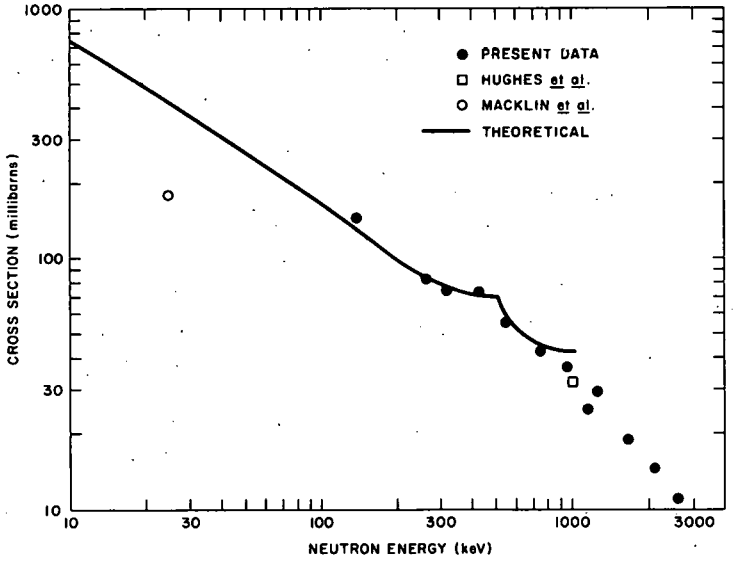

Fig. 7
Radiative Capture Cross Section of Rubidium-85

D. Component Development

1. Sodium Technology and Development

a. Effects of Sodium Impurities on Stainless Steel. When thin-walled 304 stainless steel tubing is soaked in sodium at high temperature, a brittleness develops, evidenced by snapping thin-walled tubes and by the higher electrical resistivities obtained after treating the 304 stainless steel with high-temperature sodium followed by the Strauss test.

Stainless steel (Type 304) capsules of 1/8-in. wall, with a capacity of 30 cc, were half filled, in an inert gas drybox, with sodium of 10 ppm or 100 ppm oxygen. To these capsules were added, singly, known weights of diamonds, reactor-grade graphite, and iron carbide to an extent that would (if soluble) thoroughly saturate the sodium. The capsules were then heated for 3 and 6 months, in a vertical position, in an argon atmosphere furnace (to prevent scaling) at 1100°F or at 1350°F. At the end of 3 months, half of the capsules were removed from the furnace and opened with a tubing cutter in an inert gas drybox. Sodium samples from each capsule were taken for carbon analyses, and an attempt was made to clean and weigh the residual carbides and carbon. The 304 SS capsules were subjected to metallographic examination after oxalic acid etching to reveal the carbides. Specific resistivities of sections of the tops and bottoms of the capsule representing vapor and liquid contacts were taken before and after subjecting the samples to the Strauss test.

One capsule containing iron carbide heated at 1350°F with oxygen concentration of 100 ppm, one capsule containing graphite heated at 1350°F with oxygen concentration of 100 ppm, one capsule containing diamonds heated at 1350°F with oxygen concentration of 100 ppm, and two capsules containing graphite heated at 1100°F with an oxygen concentration of 100 ppm and 10 ppm had large, well-defined crystals deposited on the inside of the capsules at the sodium level when the capsule was heated. The capsule containing graphite at 10 ppm O_2 heated to 1100°F contained a smaller amount of crystals than did the others. Chemical and X-ray analyses showed these crystals to be alpha iron. The condition common to four capsules exhibiting these crystals was the oxygen concentration of 100 ppm.

The problems of separating the excess materials in the bottoms of the capsules and obtaining proper sodium samples for carbon analyses were difficult. The diamonds were completely recovered from three capsules with either a diamond missing or the diamonds slightly attacked. The recovery of disintegrated graphite from the capsule sodium averaged about 90%, and the recovery of iron carbide granules averaged about 80%. It was assumed that the rest was in the sodium.

Micrographs (240X) of the inside walls of the capsules below the sodium level for capsules containing iron carbide, graphite, and diamond at 1350°F for 3 months at the two oxygen concentrations are shown in Fig. 8. The pictures indicate that the carbon from the iron carbide had

1350° F.

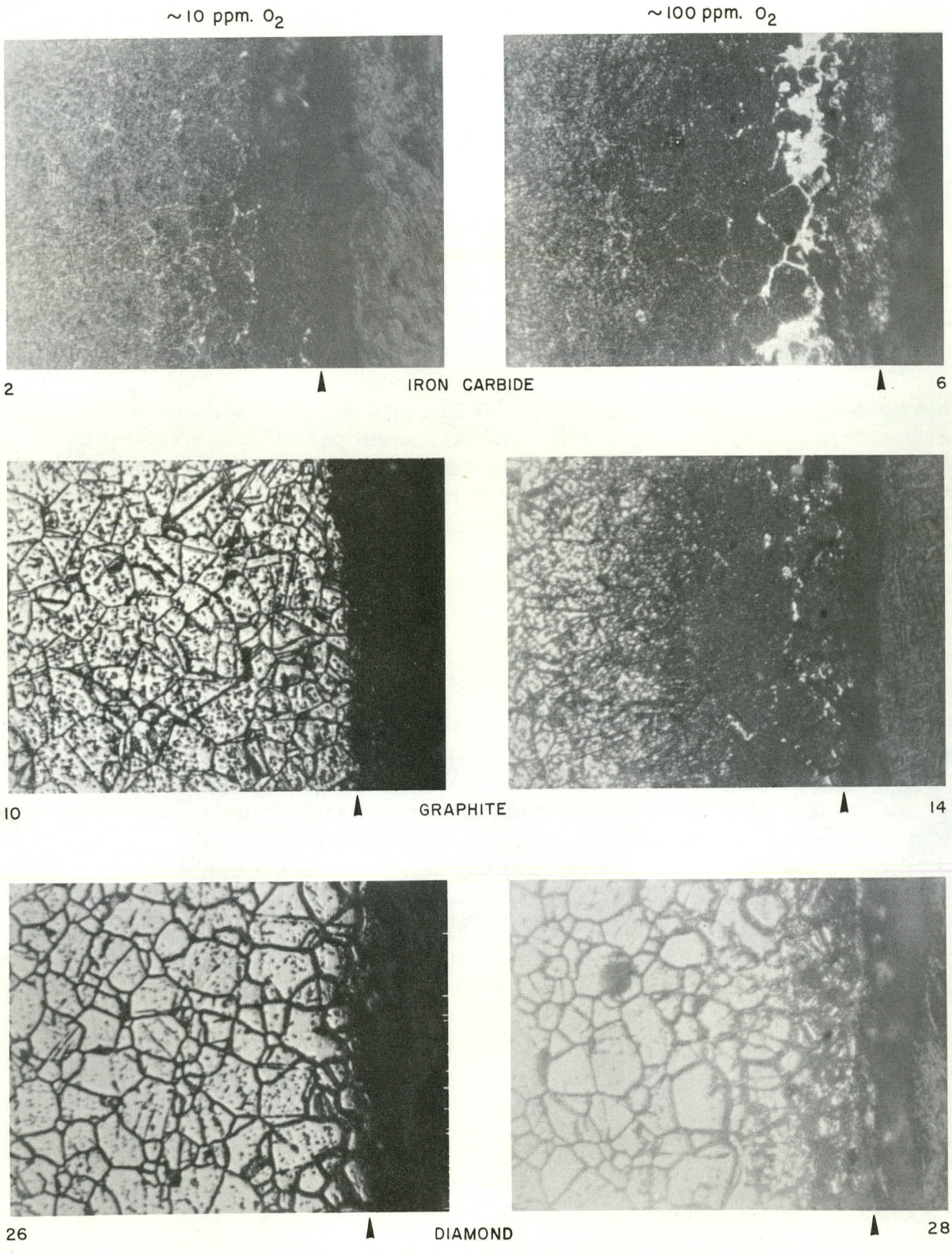

Fig. 8. Effects of Sodium Impurities on Stainless Steel

penetrated the surface to a greater depth than the carbon from the other two sources. Also, the carbon penetration is aided by the higher concentration of oxygen. In the cases of the capsules containing diamonds, no carbon penetration is shown. Subsequent microhardness determinations showed the dark areas of the micrograph to be harder, due to carburization which had taken place either by carbon solubility in the sodium or by the formation of minute quantities of carbon monoxide in the sodium containing a high oxygen content. The micrographic effects, while obtained in an unusual way, (soaked in sodium) do not greatly differ from the carburization obtained by soaking a steel in a commercial atmosphere at elevated temperature.

As expected, portions of the capsules exposed to the vapor phase only, showed no carbon penetration, nor was the crystal structure visibly different at the surface exposed to sodium vapor than in the center of the capsule wall.

The same observations applied to the capsules heated to 1100°F as to 1350°F, only to a lesser degree.

Specific electrical resistivities were taken of the bottom and top plugs of the capsules before and after Strauss testing. The resistivities before and after Strauss testing are shown in Table XX. The data do not reveal that any one set of condition is more deleterious than the other insofar as the resistivity is concerned.

TABLE XX. Resistivities[a] before and after Strauss Test

	Diamond		Reactor Carbon		Iron Carbide	
	Before	After	Before	After	Before	After
			1350°F			
10 ppm O_2 Vapor	74.4	89.2	84.3	84.8	76.4	89.2
Liquid	72.9	85.9	87.0	99.9	83.7	85.9
100 ppm O_2 Vapor	80.6	84.9	88.9	88.1	81.7	89.5
Liquid	75.0	83.4	75.3	92.8	87.3	90.0
			1100°F			
10 ppm O_2 Vapor	73.5	93.5	85.7	97.4	85.8	97.6
Liquid	79.1	93.5	69.2	83.3	82.8	94.8
100 ppm O_2 Vapor	78.8	88.4	86.8	95.3	87.8	96.7
Liquid	88.8	94.7	80.0	89.1	83.9	95.8

[a] x 10^{-6} ohm-cm.

After soaking the top and bottom plugs of the capsules, heated to 1350°F, in the standard Strauss solution for 60 min, it could be seen that the capsule bottom plugs, where the iron carbide had been resting, were badly chewed up and rough (due to carbide removal) while the top plugs in contact with the sodium vapor were unaffected. The bottom plugs of the capsules in contact with graphite had considerable pitted areas with the capsule top plugs unaffected. The bottom plug of one capsule containing diamonds was noticeably pitted while one other capsule showed a slight etch where the diamonds lay. The surfaces of these capsule top plugs exposed to vapor only were not visibly affected by the Strauss test.

On the capsules held at 1100°F, the Strauss solution showed heavy attack on the bottom plugs of the capsules containing iron carbide. The bottom plugs of the capsules containing graphite showed medium attack with oxygen concentration of 100 ppm. The bottom plug of one capsule containing diamonds with an oxygen concentration of 100 ppm showed slight attack where the diamonds were resting.

The data of Table XX show a wide scatter of values due to varying degrees of surface roughness. However, the comparison shows that the average increase in resistivity is about 9×10^{-6} ohm-cm, which is accountable by the normal carbide precipitation caused by heating the 304 SS to 1100-1350°F in any common heating medium. One reason that the sodium-soaked 304 SS capsule top and bottom plugs did not show marked increases in resistivities is the fact that the plugs were 1/4 in. thick and the surface change had not penetrated to sufficient depth to noticeably affect the overall resistivity readings.

All of the above are subject to confirmation of sodium analyses for carbon, stainless steel analyses for penetrated sodium, and the examination of the capsules held at temperatures for six months.

2. Materials Evaluation

a. Physicochemical Mechanics of Metals. Recent work is summarized in Fig. 9. The effects of pretreatment on four samples of Type 304 stainless steel and a control sample, which was given no pretreatment, are shown. The pretreatments are as follows:

Sample #1--Control Sample, no treatment given.

Sample #2--Solution Annealed, heated in an air furnace at 2000°F for one hour, then water quenched.

Sample #3--Sensitized, heated in vacuum for 15 hr at 1500°F, then furnace cooled.

Sample #4--Solution Annealed, heated in argon for one hour at 2150°F, then water quenched.

Sample #5--Sodium Exposed, treated for nearly 10,000 hr in sodium loop at temperatures between 1200°F and 1600°F.

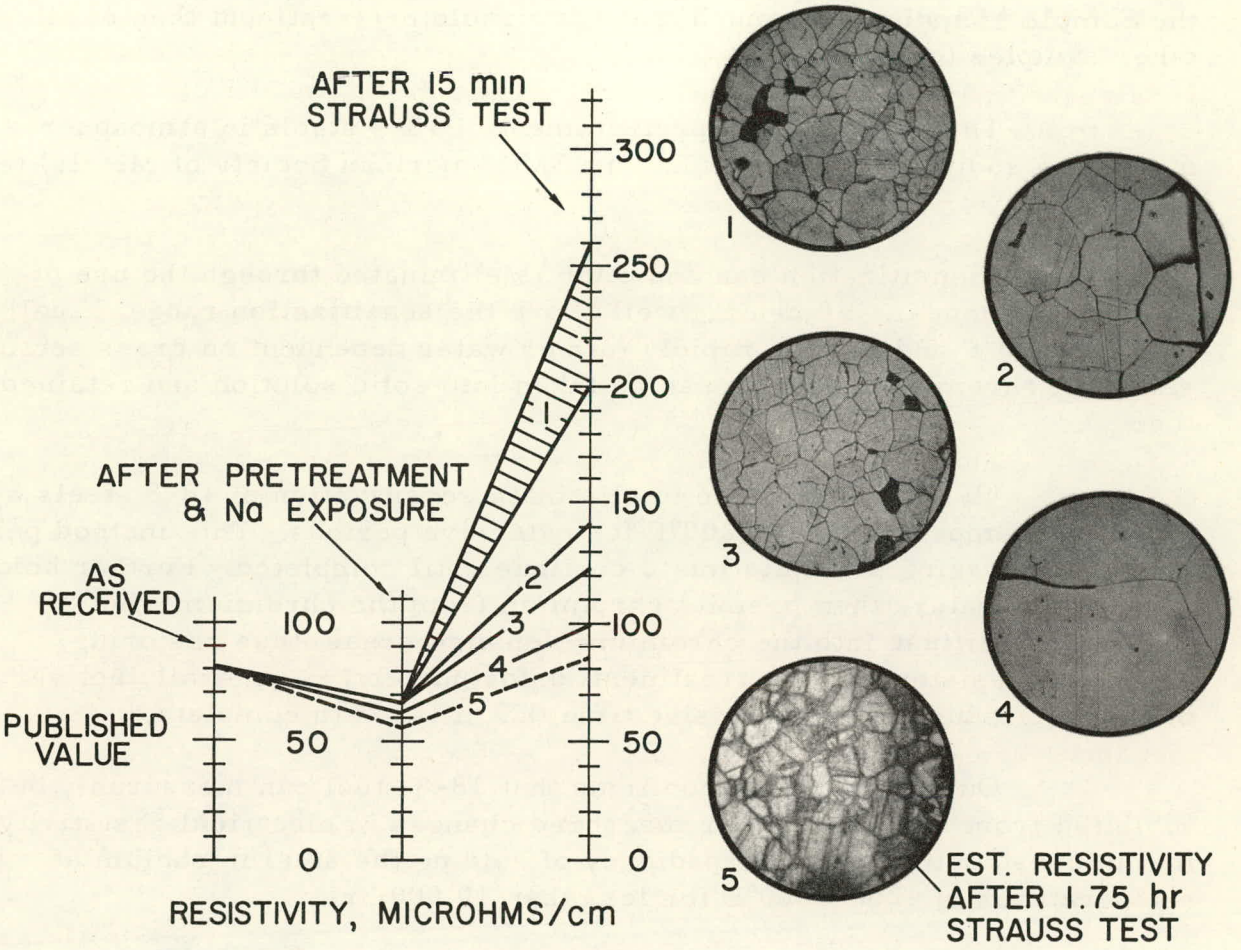

Fig. 9. Effects of Pretreatment of Resistivity of 304 SS

After these pretreatments, the samples were exposed to sodium for seven days at 1200°F. This was followed in each case by a 15-min Strauss solution test, except in the case of Sample #5, for which the test was carried on for 1.75 hr. The microstructures are shown in each case after the Strauss solution test.

Of special significance are the data and microstructure of Sample #5. This sample was taken from an engineering-size, forced-circulation, high-temperature loop and had a long history of nearly 10,000 hr of service in sodium at a temperature range of 1200 to 1600°F. The measured resistivity of this sample is the lowest of all pretreatment

specimens measured. In sharp contrast, Sample #1 of an "off the shelf" 304 SS specimen and exposed only to 1200°F had the highest resistivity value measured.

If one assumes that low-resistivity values, after Strauss test, are an indication of the integrity of the material, then the pretreatment of the Sample #5 indicates a much more favorable pretreatment than of all other samples tested.

The possibility of pretreatment of 18-8 steels in atmospheres other than sodium is discussed in an ASM (American Society of Metals) text as follows:

"Sensitization can and often is eliminated through the use of the solution anneal. By heating well above the sensitization range, usually 1850 to 2000°F and cooling rapidly (air or water dependent on cross section size), all chromium carbides can be taken into solid solution and retained there.

"It is also possible to eliminate sensitization of 18-8 steels by holding at temperatures of 1200°F for extensive periods. This method permits the damaging precipitation to continue until completed. Further holding at temperature then permits chromium from the chromium-rich austenite to diffuse into the chromium-depleted areas, thus restoring corrosion resistance. The treatment, unfortunately, is generally not very practical because of the extensive time that it takes to complete."

Our work to date confirms that 18-8 steel can measurably be inhibited from sensitization or measured changes in electrical resistivity and microstructure by the expediency of holding the steel in sodium at temperatures of 1200-1600°F for less than 10,000 hr.

The full impact of this work is emphasized further by calling attention to the fact that the system from which Sample #5 (least affected) has had a long and varied sodium oxide content since 1957 and has operated over that period of time without the benefit of a hot trap or a cold trap.

E. Fuel Development

1. Metallic Fuels

a. Irradiation of Uranium-Plutonium Alloys. A total of 20 full-length (14 in.) metal fuel rods are undergoing irradiation in the EBR-II reactor. Eighteen of these rods are U-Pu-Zr alloys severally jacketed in V-20 w/o Ti, Type 304 stainless steel, Type 316 stainless steel, Hastelloy-X and Hastelloy-X-280 tubing. These rods are operating at

maximum jacket temperatures of 630°C and at present have reached a calculated maximum 4.1 a/o burnup. Two additional rods are fueled with U-Pu-Ti alloy and are jacketed in V-20 w/o Ti tubing. The rods are being irradiated at maximum jacket temperatures of 540°C and have attained a maximum burnup of 4.2 a/o. Additional details on the design of the fuel rods and the irradiation conditions are summarized in Table XXI.

TABLE XXI. Status of Metal Fuel Irradiations in Progress

			Design Parameters					Operating Conditions			
										Burnup to Date	
Test Reactor	Capsule or S/A No.	Specimen Number	Fuel Composition (w/o)	Effective Density (%)	Cladding Composition	Cladding OD (in.)	Cladding Thickness (in.)	Power Density (kW/cc)[a]	Max Cladding Temp (°C)	a/o (U + Pu)	fiss/cc x 10^{-20}[a]
EBR-II	XG06	ND23	U-15 Pu-10 Zr	66	V-20 w/o Ti	0.209	0.016	1.7	540	4.1	9.8
EBR-II	XG05	ND24	U-15 Pu-10 Zr	66	V-20 w/o Ti	0.209	0.016	1.7	535	3.8	9.1
EBR-II	XA07	ND28	U-15 Pu-9 Zr	75	304 SS	0.208	0.021	2.0	630	4.0	11.2
EBR-II	XA07	ND41	U-15 Pu-9 Zr	75	304 SS	0.208	0.021	2.0	625	3.9	10.9
EBR-II	XA07	ND32	U-15 Pu-9 Zr	75	316 SS	0.196	0.015	2.0	605	3.7	10.3
EBR-II	XA07	ND43	U-15 Pu-9 Zr	75	Hastelloy-X	0.196	0.015	2.0	615	3.8	10.6
EBR-II	XA07	ND25	U-14 Pu-12 Zr	76	304 SS	0.208	0.021	1.9	600	3.4	8.8
EBR-II	XA07	ND27	U-14 Pu-12 Zr	76	304 SS	0.208	0.021	1.9	605	3.5	9.1
EBR-II	XA07	ND26	U-14 Pu-12 Zr	76	316 SS	0.196	0.015	1.8	590	3.3	8.5
EBR-II	XA07	ND29	U-14 Pu-12 Zr	76	316 SS	0.196	0.015	1.8	595	3.5	9.1
EBR-II	XA07	ND30	U-14 Pu-12 Zr	76	316 SS	0.196	0.015	1.9	615	3.8	9.8
EBR-II	XA07	ND31	U-14 Pu-12 Zr	76	316 SS	0.196	0.015	1.9	610	3.7	9.6
EBR-II	XA07	ND33	U-14 Pu-12 Zr	76	Hastelloy-X	0.196	0.015	1.9	605	3.6	9.4
EBR-II	XA07	ND34	U-14 Pu-12 Zr	76	Hastelloy-X	0.196	0.015	1.9	610	3.7	9.6
EBR-II	XA07	ND35	U-14 Pu-12 Zr	76	Hastelloy-X	0.196	0.015	1.9	615	3.8	9.8
EBR-II	XA07	ND37	U-14 Pu-12 Zr	66	Hastelloy-X-280	0.208	0.015	1.8	610	3.8	9.5
EBR-II	XA07	ND39	U-14 Pu-12 Zr	66	Hastelloy-X-280	0.208	0.015	1.8	610	3.8	9.5
EBR-II	XA07	ND44	U-14 Pu-12 Zr	66	Hastelloy-X-280	0.208	0.015	1.8	600	3.7	9.2
EBR-II	XG05	NC17	U-15 Pu-10 Ti	63	V-20 w/o Ti	0.209	0.016	1.6	540	3.9	8.6
EBR-II	XG06	NC23	U-15 Pu-10 Ti	63	V-20 w/o Ti	0.209	0.016	1.6	540	4.2	9.2
CP-5	CP-50	1N16	Th-20 U	75	V-20 w/o Ti	0.196	0.015	1.9	610	11.3	5.2
CP-5	CP-50	4N19	Th-20 U	75	V-20 w/o Ti	0.196	0.015	1.9	610	11.3	5.2
CP-5	CP-50	2N17	Th-10 Pu-10 U	75	V-20 w/o Ti	0.196	0.015	2.0	630	13.0	6.0
CP-5	CP-50	5N20	Th-10 Pu-10 U	75	V-20 w/o Ti	0.196	0.015	2.0	630	13.0	6.0
CP-5	CP-50	3N18	Th-10 Pu-20 U	75	V-20 w/o Ti	0.196	0.015	1.9	630	7.6	5.6
CP-5	CP-50	6N21	Th-10 Pu-20 U	75	V-20 w/o Ti	0.196	0.015	1.9	610	7.6	5.6

[a]Based on effective density.

The U-Pu-Zr and U-Pu-Ti alloy specimens being irradiated in the CP-5 reactor were removed and a postirradiation examination of the rods is in progress. Both rods are in excellent condition. The U-18.5 w/o Pu-14.1 w/o Zr jacketed in V-20 w/o Ti had reached a calculated 10.2 a/o burnup at maximum jacket temperature of 655°C. The U-15 w/o Pu-10 w/o Ti, which was also jacketed in V-20 w/o Ti, had reached a calculated 9.0 a/o burnup at maximum jacket temperature of 630°C.

Periodic nondestructive neutron radiographs of the capsules showed that the U-Pu-Zr alloy attained a maximum fuel elongation of 3% at 4.2 a/o burnup. This dimension did not change throughout the remainder of the irradiation.

The U-Pu-Ti reached a maximum elongation of 14% at 4.6 a/o burnup and conserved this dimension till the termination of the irradiation. It was anticipated that this would occur as sufficient radial volumetric

expansion had been provided between the fuel and the ID of the jacket to permit venting of the fission gases in the fuel (see Progress Report for April 1966, ANL-7204, p. 21).

Diameter changes in the jacketed rods were calculated from volume changes measured by immersion. On this basis, the U-Pu-Zr rod showed a 0.0002-in. dia increase and the U-Pu-Ti rod one of 0.0016 in. No measurable length change was noted for either rod. Prior to the actual sectioning of the rods, the sodium levels will be measured. The jackets will then be punctured for fission-gas recovery and analysis.

The six Th-10 w/o Pu-10 w/o U, Th-10 w/o Pu-20 w/o U, and Th-20 w/o U specimens that are being irradiated in capsule CP-50 were removed from the reactor and neutron-radiographed. Inspection showed the fuel pins to be intact and straight. The capsule will be returned to the reactor and the irradiation will be continued.

b. Fabrication of EBR-II Test Fuel Elements. Work was resumed on the preparation of uranium-plutonium-zirconium and uranium-zirconium alloy core fuel rods. Fifty-two rods loaded with U-15 w/o Pu-10 w/o Zr and U-15 w/o Pu-15 w/o Zr are scheduled to be tested in EBR-II. Fuel-pin diameter varies from 0.130 to 0.165 in. The rods are to be jacketed in stainless steel, vanadium-20 w/o titanium alloy, and vanadium-chromium-titanium alloy. All fuel rods will have rolled-in restrainers that will hold the fuel pin below the sodium bond. The restrainers are 0.25-in.-long plugs with four longitudinal grooves for sodium flow. They are held in position by rolling two circumferential beads in the jacket, one above and one below the restrainer body.

Previous attempts to alloy and cast uranium-zirconium, and uranium-plutonium-zirconium as a single-step operation were not very successful. The density of the zirconium is about one-third that of the uranium and plutonium, and the melting point is above that of either of the two metals. The bulky mass of zirconium tends to float to the top of the melt where the dissolution is extremely poor. Alloying temperatures above 1500°C were tried, but severe crucible reaction took place. The analytical results on the casting showed large zirconium variations below the desired compositional level.

It was found that 6 to 8 w/o of zirconium could be dissolved in the uranium in one operation and 15 w/o of zirconium in plutonium in a single alloying step at a temperature of 1400°C. Yttria-coated magnesia crucibles were used and were not attacked at 1400°C. The two billets were combined in the injection-casting melt and the small amount of zirconium was added to adjust the zirconium to 10 w/o. This alloy was successfully cast into 0.144-in.-dia Vycor molds at 1500°C.

The same technique has been used for preparing U-15 w/o Pu-15 w/o Zr and U-15 w/o Zr alloys. In this case the U-15 w/o Zr alloy must be prepared in two steps. The alloy has a liquidus temperature of about 1400°C, and it appears that it must be cast to above 1500°C. The first attempts to cast this material were not successful. Vycor molds softened and the crucibles were eroded at the casting temperature of 1500°C. High-purity fused-quartz molds had been obtained which have a softening point of over 1600°C. These will be tried in an early melt. Part of the problem appeared to be that the material solidified before it reached the top of the mold. New mold heating elements have been installed in the injection casting furnace to preheat the upper ends of the mold.

(i) Fuel Rods. The fuel rods were loaded and bonded in the normal way with the following exceptions. The bottom restrainer bead was rolled into the jackets before they were put into the hood line. After loading of the sodium and fuel pin, the rods were heated to 150°C and gently vibrated. The 0.25-in.-long restrainers were loaded and allowed to settle against the bead. The rods were cooled and the top restrainer beads were rolled into the jackets. The jackets and plugs were welded into place and the rods were decontaminated.

A tubing cutter with a blunt disc and nylon rolls was used to roll the beads into the jackets. A shoulder on the disc prevented grooving the jackets more than 0.005 in. deep. Previous work has indicated it would take approximately 175 lb to push the restrainer past the grooves. The jackets were scribed with narrow lines for proper groove location.

The rods were impact bonded 2000 times at 500°C. An extension on the bonder chamber was required for the 22- to 33-in.-long rods. The rods were sealed into the chamber under inert atmosphere to prevent oxidation of the vanadium-20 w/o titanium and uranium-chromium-titanium jackets.

Four modified EBR-II-type fuel rods were fabricated as eddy current standards. The rods were modified from Mark IA rod with 0.040-in.-dia restrainers without end knobs and adjusted sodium levels. These changes were made to increase the void volume and accuracy of the eddy current indications.

The fuel pins and jackets were obtained from production stock. The pins were normal U-5 w/o fissium alloy. The restrainers were made from Type 304 stainless steel by threading the 0.040-in.-dia wire into a simplified end plug.

The fuel rods were assembled and welded in the Building-350 hood lines. The impact bonder was used for bonding. The rods were impacted 2000 times at 450°C. Inspection for sodium level and

restrainer position was done by radiography. One rod had a high sodium level. The rods were sent to the Nondestructive Testing Group to determine the accuracy of new eddy current techniques for determination of sodium level.

2. Oxide and Carbide Fuels

a. Compatibility of (U,Pu)C with Potential Cladding Materials.

Testing of potential iron-, nickel-, and vanadium-base cladding materials with single-phase monocarbide and with two-phase hyperstoichiometric carbides continues. The single-phase monocarbide being used contains 4.83 w/o equivalent carbon; the hyperstoichiometric carbide contains 5.25 w/o equivalent carbon, resulting in a proportionate amount of $(U,Pu)_2C_3$ as a second phase.

Vanadium-15 w/o chromium-5 w/o titanium, after 42 days at 800°C, showed no metallographic evidence of reaction with either carbide composition. The test was conducted on discs of 30-mil sheet rolled from a small, arc-melted button. Further tests will be run when this material becomes available on a larger scale. The results, nevertheless, indicate a marked improvement in compatibility with (U,Pu) carbides when compared to vanadium-20 w/o titanium (TV-20), which, after heat-treatment at 800°C for 17 days, showed attack into grain boundaries for a distance of 95 μ with even further reaction along stringers.

Inconel-625 was tested with both carbide compositions at 700 and at 800°C. This material is of interest as a cladding material because of its greater strength at elevated temperatures as compared with Type 304 stainless steel or Hastelloy-X. The same type of reaction was noted in each of the compatibility couples. Three separate zones were observed metallographically in connection with this reaction. One of these was clearly in the direction of the fuel and appeared to be similar to the zone observed in Hastelloy-X (see Progress Report for April 1966, ANL-7204, p. 17). In addition, a dark, mottled zone started at approximately the original interface and extended in the direction of the cladding. Beyond this zone, fine precipitates, which, in the case of the 800°C tests, gradually became less frequent but larger in size as the distance from the interface increased, were observed in the Inconel-625. The average widths of the zones are shown in Table XXII along with the individual maximum widths observed at any point.

TABLE XXII. Extent of Reaction Observed Metallographically between (U,Pu) Carbides and Inconel-625 after 700 and 800°C Heat Treatments for 42 days

Type of (U,Pu) Carbide	Temp (°C)	Width of Reaction Zone in Direction of Fuel (μ)		Width of Mottled Reaction Zone in Direction of Cladding (μ)		Extent of Precipitates in Cladding beyond Reaction Zones (μ)	
		Avg	Max	Avg	Max	Avg	Max
Stoichiometric and Hyperstoichiometric[a]	700	18	30	20	25	25	35
Stoichiometric	800	25	37	23	30	105	135
Hyperstoichiometric	800	36	44	26	36	120	155

[a]Stoichiometric = 4.83 w/o equivalent carbon; Hyperstoichimetric = 5.25 w/o equivalent carbon.

Although the hyperstoichiometric carbide composition contained approximately 20% $(U,Pu)_2C_3$, there was no apparent difference in the extent of reaction, compared to single-phase monocarbide, with Inconel-625 at 700°C. At 800°C, however, a somewhat more extensive reaction was observed with the two-phase hyperstoichiometric carbide.

In comparison, reaction zones having an average width of 4 μ at 700°C and 8 μ at 800°C after 42 days were found for Hastelloy-X specimens in contact with the hyperstoichiometric carbide composition. Nominal compositions (w/o) of the two alloys are as follows:

	Ni	Fe	Cr	Mo	Co	W	Nb + Ta
Hastelloy-X	48	18	22	9	1.5	0.6	-
Inconel-625	61	3	22	9	-	-	4

b. Irradiations of Ceramic and Cermet Fuels. Mixed carbide, mixed oxide, and stainless steel-PuO_2 cermet elements received additional burnup as EBR-II went back into operation toward the end of October. The status of these elements is shown in Tables XXIII, XXIV, and XXV.

TABLE XXIII. Status of UC-20 w/o PuC Fuel Irradiations in EBR-II

		Design Parameters				Operating Conditions			
								Burnup to Date	
Capsule or S/A No.	Specimen Number	Effective Density (%)	Cladding Composition	Cladding OD (in.)	Cladding Thickness (in.)	Power Density (kW/cc)[a]	Max Cladding Temp (°C)	a/o (U + Pu)	fiss/cc x 10^{-20}[a]
XG05	SMV-2	84	304 SS	0.297	0.020	2.1	645	3.9	10.7
XG05	HMV-5	80	Hastelloy-X	0.297	0.015	2.2	670	4.0	10.5
XG05	NMV-11	84	Nb-1 w/o Zr	0.281	0.012	2.1	645	4.0	11.1
XO08	NMP-2	82	Nb-1 w/o Zr	0.281	0.012	1.6	545	2.2	6.0
XO08	NMV-4	80	Nb-1 w/o Zr	0.281	0.012	2.4	635	3.2	8.5
XO08	NMV-7	80	Nb-1 w/o Zr	0.281	0.012	2.1	605	2.9	7.7
XO08	NMV-12	86	Nb-1 w/o Zr	0.281	0.012	2.4	635	3.2	9.0
XO08	HMV-1	80	Hastelloy-X	0.297	0.015	2.1	640	2.9	7.6
XO08	HMV-4	80	Hastelloy-X	0.297	0.015	2.3	670	3.2	8.3
XO08	HWMP-1	82	Hastelloy-X + W	0.297	0.020	1.6	555	2.2	5.8
XO08	HWMV-1	83	Hastelloy-X + W	0.297	0.020	2.4	685	3.2	8.8
XO09	SMV-1	82	316 SS	0.306	0.024	1.6	570	2.4	6.5
XO09	SMP-1	80	316 SS	0.306	0.024	2.1	640	1.9	4.9
XO09	VMV-1	86	Vanadium	0.301	0.022	2.5	640	2.8	7.9

[a]Based on effective density.

TABLE XXIV. Status of UO_2-20 w/o PuO_2 Fuel Irradiations in EBR-II

		Design Parameters				Operating Conditions			
								Burnup to Date	
Capsule or S/A No.	Specimen Number	Effective Density (%)	Cladding Composition	Cladding OD (in.)	Cladding Thickness (in.)	Power Density (kW/cc)[a]	Max Cladding Temp (°C)	a/o (U + Pu)	fiss/cc x 10^{-20}[a]
XO09	SOV-5	82	304 SS	0.297	0.020	1.7	555	2.4	5.0
XO09	SOV-6	82	304 SS	0.297	0.020	1.7	565	2.6	5.3
XO11	SOV-3	83	304 SS	0.296	0.019	1.9	610	2.0	4.0
XO11	HOV-4	80	Hastelloy-X	0.295	0.014	1.8	600	1.9	3.8
XO11	TVOV-1	77	V-20 w/o Ti	0.297	0.020	1.7	575	1.9	3.6
XO11	SOV-7	85	304 SS	0.296	0.019	2.0	630	1.9	4.0
XO11	SOV-1	80	304 SS	0.296	0.019	1.7	590	1.9	3.7
XO11	HOV-10	86	Hastelloy-X	0.295	0.014	1.9	615	1.8	3.9
XO11	HOV-15	80	Hastelloy-X	0.295	0.014	1.7	590	1.8	3.6

[a]Based on effective density.

TABLE XXV. Status of Cermet Fuel Irradiations in EBR-II

Capsule or S/A No.	Specimen Number	Design Parameters: Fuel Composition (w/o)	Effective Density (%)	Cladding Composition	Cladding OD (in.)	Cladding Thickness (in.)	Operating Conditions: Power Density (kW/cc)[a]	Max Cladding Temp (°C)	Burnup to Date: a/o (U + Pu)	Burnup to Date: fiss/cc x 10^{-20}[a]
XO11	5P-9	SS-40 PuO_2	98	304 SS	0.301	0.015	0.88	495	2.6	2.0
XO11	5P-12	SS-27 PuO_2	99	304 SS	0.294	0.015	0.59	450	2.6	1.3
XO11	5U-14	SS-27 UO_2	98	304 SS	0.298	0.013	0.45	435	2.0	1.0

[a]Based on effective density.

c. Development of Process Equipment for Ceramic Fuels. An inert-atmosphere glovebox enclosing 480 ft^3 of space was installed and equipped for ceramic-fuel fabrication. Three double-module gloveboxes, 12 ft wide by 6 ft high, are used in an 18-ft-long train attached to the conveyor. The end box sets on a well 40 in. in depth to the floor, giving 9 ft of head room to the bottom of the craneway. The two other double-module boxes sit upon a cabinet base that encloses the vacuum pumping system.

The equipment installed in this glovebox line is a tungsten-element furnace and a plasma-reaction chamber. The tungsten furnace of a cold-wall design, has been tested at temperatures of 2700°C in a vacuum, and 2500°C with one atmosphere pressure of helium gas. Heat is supplied by four three-phase tungsten-wire-mesh heating elements within reflective heat shields. The heat shields are made of seven layers of thin tungsten sheet, and are supported in a water-cooled copper box within the vacuum chamber. The exterior shell of the furnace is a double-walled stainless steel tank with coolant water between the tank walls. The tank axis is horizontal and access to the furnace is by identical front and back doors, each of which carry a set of tungsten-mesh heating elements and heat shields. The doors must move outward along the furnace axis about 5 in. for the heater elements to clear. This is facilitated by drawing a door outward on two tracks to a position where it may be picked up and moved sideways in the hood by an electrically operated hoist. The furnace was designed so that all parts are accessible from the gloveports for maintenance and for changing the elements and heat shields. The heater box is cooled by four parallel water circuits, each of which is connected to its own flowmeter. A single water circuit is provided in each of the door panels. Electrical power is conducted to the heating element through water-cooled feed-throughs in the furnace shell and in the glovebox from a 100-kW saturable-reactance transformer.

The vibratory compaction of spherical powders has many advantages, if economical methods can be developed to produce the spherical powders. A reaction chamber was designed to develop a variety of arc-plasma and induction-coupled plasma devices for spheroidizing ceramic fuels, such as $(U,Pu)O_2$ and (U,Pu)C. This chamber consists of a spherical section, 28 in. in diameter mounted on top of a cylindroconical chamber that is 18 in. in diameter by 40 in. deep. The spherical section is equipped with five 10-in. flanges to which a variety of plasma-generating devices may be mounted. The unit has been initially equipped

as a high-intensity arc processor with a cavity-arc plasma torch. It also is planned to install an induction-coupled plasma torch upon the equipment in the future. The equipment will be tested for the semicontinuous fusion of granulated and powdered $(U,Pu)O_2$ and (U,Pu)C. Exploratory work is also being done on the synthesis of (U,Pu)C from $(U,Pu)O_2$ and carbon by the arc fusion methods.

Auxiliary equipment on this glovebox line consists of a dual 6-in. diffusion pumping system located in the cabinet beneath the gloveboxes, a 600-Amp welding generator and a closed coolant system for the furnace and reaction chamber. Each circuit of the cooling system is metered and full alarmed. The coolant system contains a maximum of about 20 gal with heat exchange to the Building 350 system of positive-pressure chilled water. Positive pressure is used instead of negative pressure to pump coolant through this system to provide an adequate flow to the high-temperature furnaces and plasma devices.

A second glovebox line was converted from air to argon atmosphere and equipped for carbide pellet making. This line encloses 190 ft^3 and is free standing. Conversion to argon atmosphere included a system for purifying and analyzing argon. The atmosphere is circulated through a platinum catalytic reactor, where the oxygen is combined with hydrogen, and through molecular sieves to remove the moisture. The analytic instruments are an electrolytic oxygen analyzer and a phosphorus pentoxide moisture analyzer. The line is equipped with blending and milling equipment, a 20-ton hydraulic press, a vacuum drying oven, and a carbon-tube resistance furnace capable of 2000°C operation.

d. Preparation of Ceramic Fuels for Fast Reactors. Synthesis of (U,15 w/o Pu)C by a fluidized process is being conducted on a scale of 300 g per batch (see Progress Reports for June 1966, ANL-7230, p. 45, and July 1966, ANL-7245, p. 10). Eight batches of material have been prepared to date. In these experiments, U-Pu alloy in the form of 3/8-in.-dia rods was hydrided to produce fine powder suitable for fluidizing. This powder was then carbided with a methane-hydrogen fluidizing gas at 550 to 800°C and 2 to 4 atm pressure.

The methane concentrations of the inlet gas stream (typically 2 to 10 v/o) and that of the outlet gas stream were determined by infrared analysis. The rate of carburization was determined from the difference between the inlet and outlet methane concentrations and from the gas flow rate. The extent of carbiding during the course of the run was obtained with an accuracy of ±5 to 10% by integrating the rate of carburization with respect to time. However, chemical analysis of the product yielded a more accurate value (±1%) for the final extent of carbiding, and the values obtained during the run were adjusted accordingly. The carbon content of the product, adjusted as noted above, is plotted as a function of time for two

typical runs in Fig. 10. In these two runs, carbiding was interrupted after 4 and 6.5 hr, respectively, to rehydride the residual metal in the particles and break up the carbide reaction layer which appeared to be inhibiting further carbiding. After a carbon content of about 4.0 to 4.2 w/o was reached (stoichiometric monocarbide contains 4.80 w/o carbon), the rate of reaction slowed down markedly as shown in Fig. 10. A rehydriding cycle at this composition permitted the completion of monocarbide formation in a few more hours. This rehydriding is not expected to be a major inconvenience to full-scale production of (U,Pu)C; in the most recent run, the entire cycle of hydriding-carbiding-rehydriding-carbiding was completed within 12 hr.

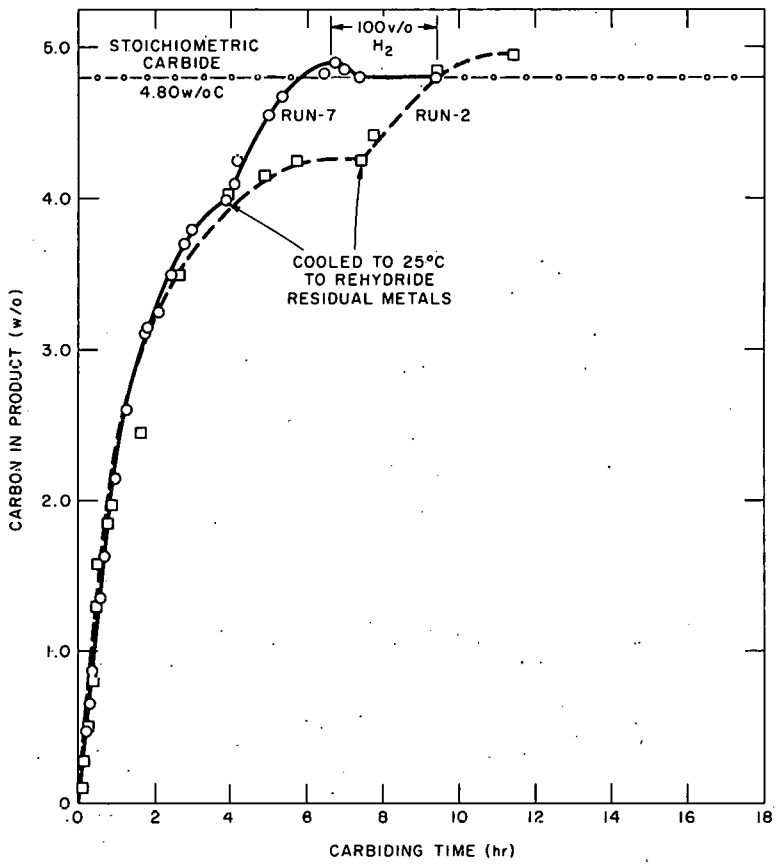

Fig. 10
(U,Pu)C Preparation in a Fluidized-bed Reactor. Run Conditions: 750-800°C; 60 psi; and 10 v/o CH_4-90 v/o H_2 (except in that portion of Run 7 where 100 v/o H_2 is indicated).

In the runs to date, the methane concentration in the CH_4-H_2 fluidizing gas has been such that U_2C_3 would be formed if the reaction was carried to completion. After the carbon concentration reaches the stoichiometric monocarbide level (4.80 w/o), the rate of carbiding is low, and excess carbon can be removed in the form of methane by subsequent use of pure hydrogen to reduce the sesquicarbide to monocarbide. This step in the process is illustrated in Fig. 10 in the plot for Run 7. The infrared analyzer monitoring the off-gas stream indicated the formation and release of a significant amount of methane (0.5 liter) during the period when the fluidizing gas was pure hydrogen.

The product analyses for the first eight runs are shown in Table XXVI. The oxygen contents for five of the runs were 0.058 w/o or lower, although the other three runs had oxygen contents of 0.10, 0.18, and 0.21 w/o. The increase in oxygen content above about 0.05 w/o is almost certainly caused by the introduction of oxygen during sampling and subsequent handling. Work is now proceeding on improving the sampling technique.

TABLE XXVI. Product Analyses of (U-15 w/o Pu)C Produced in a Fluidized-bed Reactor (300-g scale)

	Run Number							
	1	2	3	4	5	6	7	8
Total C (w/o)	4.11	4.96	4.89	4.92	4.78	4.89	4.80	4.92
Oxygen (w/o)	0.040	0.050	0.049	0.10	0.21	0.18	0.058	0.049
Nitrogen (w/o)	0.84	0.13	0.070	0.14	0.20	0.17	0.15	0.074
X Ray--Major	(U,Pu)C	(U,Pu)C	(U,Pu)C	(U,Pu)C	(U,Pu)C	(U,Pu)C	(U,Pu)C	a
Minor	βUH_3	None	None	$(U,Pu)_2C_3$	None	$(U,Pu)_2C_3$	None	a

[a]Not available.

Correction

In the Reactor Development Program Progress Report for September 1966, ANL-7255, the legend in Fig. 7, p. 28 should read: "Weight gain for formation of stoichiometric (U,Pu)C is 153 mg."

3. Fuel Cladding and Structure

a. Development of Refractory-metal Alloys for Service in Oxygen-contaminated Sodium. One of the two V-20 w/o Ti samples exposed to flowing sodium (6.1 m/sec, 650°C, 9 to 12 ppm oxygen by weight) for 139 days was sectioned and microscopically examined. A hardened zone, typical of those seen previously on exposed V-20 w/o Ti surfaces, was noted to a depth of about 50 μ. In all respects the sample was similar to those exposed much shorter times except for a deeper zone of oxygen penetration.

The surviving V-20 w/o Ti sample was replaced in the continuing test under the conditions described above. Other specimens in the same test are alloys of V-5 w/o Cr, V-15 w/o Ti-7.5 w/o Cr, and unalloyed vanadium. To date, the V-5 w/o Cr alloy has shown the lowest weight gain for comparable times, but this is for a relatively short time (~23 days).

A 70-day comparison test of six unalloyed metals in static oxygen refreshed sodium at 650°C (cold trapped to an oxygen content of 9 to 11 ppm) has been completed. The weight change data are summarized

in Table XXVII. It is clear that molybdenum and chromium are quite resistant under these conditions. The vanadium is probably next in resistance, with titanium, niobium, and tantalum quite poor. The samples are in process of metallurgical examination to determine depths of oxygen penetration.

TABLE XXVII. Behavior of Unalloyed Metals in Sodium at 650°C

	Weight Change (mg/cm^2) at Indicated Time (days)					
Metal	7.8	14.8	28.0	42.0	56.0	70.0
Chromium	-0.04	-0.04	-0.04	-0.04	-0.04	-0.08
Molybdenum	0	0	0	-0.03	-0.03	-0.03
Niobium	-0.11	-0.18	-0.63	-1.5	-2.1	-2.5
Tantalum	-1.5	-3.0	-7.6	-10.1	-11.8	-14.4
Titanium	+0.39	+0.33	-0.39	-0.99	-1.7	-2.3
Vanadium	+0.18	+0.15	-0.07	+0.11	+0.19	+0.22
Sodium Oxygen Content (Hg Amalgamation)	-	10.7 9.5	10.3	-	11.3	9.3

Two sets of V-20 w/o Ti tensile specimens and one set of V-20 w/o Ti tubes for tube-burst testing have been exposed to 650°C static sodium containing 8.5 ppm oxygen (by weight) as part of a cooperative program with the Applied Physical Metallurgy Group. A typical light-brown temper film was formed in all cases with corresponding small weight gains.

4. Fuel Reprocessing

The pyrochemical processing of fast reactor fuels of the ceramic type (e.g., oxide or carbide) clad with stainless steel is being investigated. A conceptual flowsheet currently under investigation has been previously described (see Progress Report for September 1966, ANL-7255, pp. 30-31). The process utilizes liquid metal-molten salt extractions and salt transport separations[9] for the separation of fissile and fertile constituents of the fuel from the fission products. Recent laboratory investigations of the current flowsheet are discussed below.

The first step after the decladding of oxide fuels (mixed oxides of plutonium and uranium) is the reduction of the oxide to metal (plutonium and uranium) by a Cu[33] w/o Mg alloy in contact with a molten salt (see ANL-7255, p. 30). The plutonium is soluble in the liquid alloy, whereas

[9]Salt transport separations are based upon the selective transfer of fissile and fertile materials from one liquid metal solution (donor) to another (acceptor) by cycling a molten salt phase which acts as a carrier between the two metal solutions. Noble and refractory metal fission products remain in the donor alloy.

the uranium is very insoluble. An experiment was carried out to determine if plutonium would coprecipitate with the uranium in the reduction step. In this experiment, which was conducted at 750°C (the temperature at which β-uranium precipitates) and at a mixing speed of 500 rpm, solid U_3O_8 suspended in 42.6 m/o NaCl-37.6 m/o $CaCl_2$-15 m/o $MgCl_2$-4.8 m/o CaF_2 was reduced by Cu^{33} w/o Mg alloy which contained about 0.6 w/o plutonium in solution. The U_3O_8 reduction amounted to 99.7% or greater. The results indicated that, within analytical uncertainty, all of the plutonium remained in solution in the alloy, that is, none of the plutonium had coprecipitated with the uranium.

In work related to the salt transport step, the distribution coefficients (K_d = w/o Pu in salt w/o Pu in metal) of plutonium between molten 50 m/o $MgCl_2$-30 m/o NaCl-20 m/o KCl and zinc-magnesium acceptor alloys saturated with plutonium at 600, 700, and 800°C were determined. The magnesium concentration in the Zn-Mg alloys ranged from 1 to 20 w/o. The distribution coefficient was found to reach a minimum value at about 5 w/o magnesium in the Zn-Mg alloy; the minimum values were 7.4×10^{-4}, 1.6×10^{-3}, and 7.6×10^{-3} at 600, 700, and 800°C, respectively.

These measurements also yielded data for the solubility of plutonium in liquid alloys at 600 and 700°C. The solubility of plutonium in the Zn-5 w/o Mg alloy is 0.31 w/o at 600°C and 2.4 w/o at 700°C; at 800°C the solubility was greater than the amount of plutonium used in the experiment. The combination of small values of K_d and solubilities indicates that the Zn-5 w/o Mg alloy would be an excellent acceptor alloy for plutonium when used at 600°C with the proposed Cu^{33} w/o Mg donor alloy. Satisfactory plutonium recoveries could also be achieved at a temperature up to about 700°C with the Zn-5 w/o Mg alloy.

F. Design Concept Analyses and Advanced Systems Evaluation

1. 1000-MWe Study

The AEC has approved the revised follow-on study proposals that were submitted by Atomics International, General Electric, Westinghouse, and Babcock Wilcox.

In order that these studies shall proceed on a comparable basis, ANL prepared a set of ground rules, a list of recommended parameters, and the ranges over which these parameters will be investigated. These items were discussed with the five participating contractors in a meeting on October 25, 1966 and general agreement was reached.

G. General Research and Development

1. Fast Reactor Core Parameter Study

The purpose of the fast reactor core parametric study is to determine, on a consistent design and analysis basis, the characteristics of oxide-, carbide-, and metal-fueled, sodium-cooled fast reactor cores in a "hot, dirty" midcycle equilibrium condition. Reactor-core characteristics will be determined for a wide range of core geometries. The core configurations to be studied will be selected via a preliminary analysis which will indicate the regions of mechanical and thermohydraulic practicality. Later the study may be extended beyond the uranium-plutonium cycle to include other fuel cycles or fuel-cycle variations.

Initial studies have been conducted for 1000-MW(e) oxide-fueled fast breeder reactors with core height-to-diameter ratios ranging from 0.1 to 1.0, and core power density in the range 300 to 700 kW/liter. Excessive coolant velocity and/or pressure drop through the core and axial blankets for coolant temperature rises of interest limit the region of design practicality to a fraction of that encompassed by the combination of parameters described above. The full-power fuel lifetime has been considered to be between 1.5 and 2.0 yr, with fuel burnup of 100,000 MWD/ton. A lower burnup level may also be considered in subsequent work.

For reference purposes, the initial reactors under study consisted of one core zone and one blanket zone. Heat-transfer and pressure-drop considerations were used to determine fuel, structure, and coolant volume fractions for given reactor dimensions. This information was then used to compute pertinent neutronic parameters, primarily via one-dimensional techniques (MACH I diffusion code; RE 224 cross-section set; equivalent bare core modeling). Upon completion of this initial work, consideration is to be given to radial zoning of core enrichment.

III. GENERAL REACTOR TECHNOLOGY

A. Applied and Reactor Physics Development

1. Half-lives for Spontaneous Fission of Cm^{242} and Cm^{244}

The standard method used to determine spontaneous-fission half-lives consists of fission fragment and alpha counting, which respectively yield fission rate and the number of atoms of the isotope present. In the method presented here the rate of alpha decay was determined, but instead of counting fission fragments, neutrons emitted in the fission process were detected. Consequently, alpha sources that are more intense than those which are utilized in fission-fragment counting may be used and whose applicability appears to be limited to alpha-to-fission ratios of the order of 10^6. This method also eliminates the problems of self-absorption of the fission fragments and alpha-pulse pileup, but introduces limitations of its own, such as uncertainties in neutron-detection efficiency and $\bar{\nu}$.

Samples were electroplated and flamed on platinum planchets 2.38 cm in diameter by 0.0127 cm thick. To prevent the spread of alpha contamination, the planchets were sealed in Lucite holders, and the detector assembly constructed to accept these holders. The detector was a lithium iodide crystal, enriched to 95.6% in Li^6, mounted on a photomultiplier tube (Dumont 6292). A sample of Cf^{252}, whose fission rate was known to $\pm 0.5\%$, was prepared and counted for calibration purposes.

In order to increase the sensitivity of the neutron detector and to make the detector response less sensitive to small changes in the fission-neutron spectrum that arise for different isotopes, the detector assembly was centered in a moderating system. For this purpose a stainless steel tank, 61 cm in diameter and 61 cm tall, was used. Two different neutron moderators were used, the first of which was heavy water (D_2O). The Cm^{242} and Cm^{244} samples were counted after the system was calibrated with the Cf^{252} neutron source. Upon completion of these measurements, the D_2O was replaced with ordinary water (H_2O). The measurements were repeated in the H_2O environment with the same samples used in the D_2O environment. The system was recalibrated using the same Cf^{252} neutron source.

The spontaneous-fission half-lives were calculated from the equation

$$T_f = A_\alpha T_\alpha \bar{\nu} \epsilon / R,$$

where T_f is the spontaneous-fission half-life, A_α is the alpha decay rate, T_α is the alpha half-life, $\bar{\nu}$ is the average number of neutrons emitted per fission, ϵ is the detector efficiency, and R is the neutron counting rate. As previously stated, ϵ was determined by counting a standard Cf^{252} neutron

source. Hence simply

$$\epsilon = m/\bar{\nu}S,$$

where m is the neutron counting rate due to a Cf^{252} sample of fission rate S, and $\bar{\nu}$ is taken as 3.78 ± 0.04.[10]

The experimental results in D_2O and H_2O are listed in Table XXVIII. The weighted averages of the results in the two environments are presented in Table XXIX together with previous results, which represent measurements made by counting fission fragments. There is good agreement between this and the previous work for Cm^{244}, but some disagreement in the case of Cm^{242}.

TABLE XXVIII. Experimental Results

Isotope	T_f (yr) D_2O Environment	T_f (yr) H_2O Environment
Cm^{242}	$(5.85 \pm 0.68)10^6$	$(6.16 \pm 0.20)10^6$
Cm^{244}	$(1.31 \pm 0.03)10^7$	$(1.34 \pm 0.04)10^7$

TABLE XXIX. Comparison of Results

Isotope	T_α (yr)	$\bar{\nu}$	T_f (yr) Present Work	T_f (yr) Previous Work
Cm^{242}	0.4452 ± 0.0055[11]	2.65 ± 0.09[13]	$(6.09 \pm 0.18)10^6$	$(7.2 \pm 0.2)10^6$[14]
Cm^{244}	18.11 ± 0.07[12]	2.810 ± 0.059[13]	$(1.33 \pm 0.03)10^7$	$(1.346 \pm 0.006)10^7$[12]

2. Control-rod Evaluation

The loss of reactivity caused by the insertion of a poison slab in a reactor may be determined from the perturbation-theory expression

$$-\delta\rho = \frac{\int_{slab} \phi^+ \delta\Sigma_a^p \phi dv}{\int_{core} \phi^+ \nu\Sigma_f \phi dv}, \qquad (1)$$

where adjoint fluxes are nonperturbed and real fluxes are perturbed values.

[10] Fueds, P. R., and Diamond, H., "Californium-252, A Primary Standard for Neutrons," Proc. Symp. Neutron Detection, Dosimetry and Standardization, IAEA, Harwell, England, Dec. 10-14, 1963, II, pp. 581-593.

[11] Hanna, G. C., Harvey, B. G., and Moss, N., Phys. Rev. 78, 617 (1950).

[12] Metta, D., et al., J. Inorg. Nucl. Chem. 27, 33 (1965).

[13] Soodak, H., (Ed.), Reactor Handbook, Vol. III, Pt. A, Chapt. I, p. 9, Interscience Publishers, John Wiley & Sons, New York (1962).

[14] Hanna, G. C., et al., Phys. Rev. 81, 81 (1951).

In a three-group representation, where $\Sigma_{a1} = 0$, Eq. (1) becomes

$$-\delta\rho \simeq \left(\frac{\overline{\phi_3^+(\text{slab})}}{\overline{\phi_1^+(\text{core})}}\right) \frac{\int \delta\Sigma_{a3}^{p}\phi_3 dv + \left(\frac{\overline{\phi_2^+}}{\overline{\phi_3^+}}\right)\int \delta\Sigma_{a2}^{p}\phi_2 dv}{\nu\int(\phi_3\Sigma_{f3} + \phi_2\Sigma_{f2})\,dv}. \qquad (2)$$

For most thermal and intermediate reactors $(\overline{\phi_2^+}/\overline{\phi_3^+})_{slab} \simeq 1$ when the slab is placed near the axis of the core. The numerator of the Eq. (2) may be represented by the absorption integral

$$A_t = N\int_0^{\infty}\int_0^{t}\int_0^{1} \sigma(E)\phi(E)e^{-N\sigma z/\mu} d\mu dz dE, \qquad (3)$$

where ϕ is the neutron flux incident to the surfaces of the absorber.

Evaluation of the absorption integral is simplified if we assume an isotropic distribution of incident neutrons. This assumption is justified on grounds that in a P_1 approximation, the isotropic P_0 and the P_1 components are almost equally attenuated by heavy absorbers encountered in control-rod work.

Another simplifying assumption made in the evaluation of Eq. (3) is that the reactor flux is assumed to have a hardened Maxwellian distribution at thermal energies, with a $1/E$ tail at epithermal energies.

It follows from Eqs. (2) and (3) that

$$A_t/\delta\rho \equiv Y$$

is nearly a constant for a given reactor and different poison slabs when these slabs have all the same dimensions and are placed in equivalent locations in the reactor core.

The evaluation of the fractions of thermal and epithermal neutrons absorbed by the slabs appears to be fairly accurate. Although the simplifying assumptions made in determining the reactivity losses due to the insertion of these slabs have the reduced accuracy of the calculation.

The averaged values of the ratios are given below for many samples tested in ZPR and FPR reactors,[15] where

$$\overline{A_t}/\delta\rho \equiv \overline{Y}.$$

[15] Bach, D. R., and Way, M. E., The Worth of Single Control Rods in Hydrogenous Reactors, KAPL-1961 (July 28, 1958).

Terms	Reactor			
	ZPR-1	FPR-13	FPR-11	FPR-12
Spectral Index C $= \frac{\Sigma_a(kTn)}{\xi \Sigma_s(0.625\ eV)}$	0.09	0.08	0.396	0.71
$\overline{Y}$	64.2	44.3	132.7	222.2
Avg Dev $\Delta\overline{Y}$(%)	4	3.8	6.7	6.6
No. of Samples	20	8	8	8

3. Use of Plutonium Fuel in Thermal Research and Test Reactors

Although plutonium fuel was used in MTR in 1958,[16] its use in research test reactors has not been widely considered. A survey of advanced research reactor types shows that when Pu^{239} is substituted for U^{235}, a considerable gain in useful thermal-neutron flux is obtainable. The reactor types and typical gains are summarized in Table XXX.

TABLE XXX. Typical Factors of Increase in Useful Flux when Pu^{239} replaces U^{235}

Reactor Description	Gain[a]
Spherical, Metal-fuelled Fast Core, D_2O Outer Reflector	1.75
Cylindrical Annulus, Metal-fuelled Fast Core, H_2O ITC	4
AARR Type	4.9

[a]Factor by which reaction rate is to be multiplied.

4. Evaluation of Cross Sections

The compilation of cross sections for molybdenum which are to be used in the ENDF/B library has been completed. A magnetic tape has been sent to Brookhaven National Laboratory containing the images of the ENDF/B cards for magnesium, titanium, and vanadium (see Progress Report for September 1966, ANL-7255, pp. 37-38).

Most of the data for molybdenum were obtained from the tables and graphs given by Schmidt.[17] However, a number of additions and changes in the data were made. The major changes are listed below.

[16]DeBoisblanc, D. R., and Marsden, R. S., Operation of the MTR on a Plutonium Loading, IDO-16508 (Dec. 22, 1958).

[17]Schmidt, J. J., Neutron Cross Sections for Fast Reactor Materials. Part II: Tables. Part III: Graphs, KFK-120 (Dec 1962).

Resonance parameters from Perzner et al.,[18] and some smooth capture cross sections were used over the energy range from 4 eV to 1 keV.

The energy range of the cross-section data given by Schmidt was extended from 10 up to 15 MeV.

Inelastic scattering cross sections from 200 keV to 1.5 MeV were used.[19]

Cross sections for n-2n and n-3n reactions[20] were used. These were calculated by the methods described in the reference.

Legendre coefficients for elastic scattering[21] were used up to 6 MeV. Coefficients derived from Abacus-2 optical-model calculations were used for energies above 6 MeV.

Values of $\bar{\mu}_L$, ξ, and γ were calculated from the Legendre expansion coefficients.

Parameters for the free-gas thermal scattering law were included.

Work is progressing on the compilation of cross sections for gadolinium, which is the last of the five materials in the ENDF/B library for which Argonne has responsibility.

5. The ARC System

Those aspects of the IBM Operating System and ARC concerned with module compilation and program linkages have been investigated using pseudomodules and data sets, and the results appear to be satisfactory. The main problems involve the ability to use generation data sets and the ability to label simply and to retrieve data sets generated in previous ARC runs. These problems are under current investigation.

Consideration is also being given to the question of appropriate size for a module and to the question of redundancy in the ARC System. Thus, for example, it may be reasonable from the standpoint of efficiency to include the criticality-search algorithms as subroutines in the one-dimensional diffusion-theory module and also have in the System a separate module for criticality search which would service the other neutronics modules.

---

[18] Pevzner, M. I., et al., "Investigation of Nuclear Levels by Neutron Spectroscopy. 1. Neutron Cross Sections of Molybdenum Isotopes in the 7-15000 eV Energy Range," Soviet Physics. JETP, 17, No. 4, 803-808 (Oct 1963).

[19] Smith, A. B., and Hayes, R., Fast Neutron Scattering from Elemental Mo, Sn, Sb, and Te, to be published.

[20] Pearlstein, S., "Analysis of (n, 2n) Cross Sections for Medium and Heavy Mass Nuclei," Nucl. Sci. Eng. 23, 238-250 (Nov 1965).

[21] NAA-SR-11980, Vol. IV: Compilation, Evaluation and Reduction of Neutron Differential Scattering Data, to be published.

The MC^2 code has been tested for the P1, consistent P1, and consistent B1 options, as well as for the treatment of hydrogen scattering and appears to be working satisfactorily.

A deficiency in MC^2 has been recognized in that the resonant scattering is not properly accounted for when calculating the fundamental-mode spectrum, so that the collapsed broad-group-resolved resonant cross sections are being overestimated in some cases. Resolution of this problem will be sought with the correct calculation of the Doppler effect as a goal.

a. Burnup Package Development. The Phase Zero package (see Progress Report for August 1966, ANL-7249, pp. 40-41) has been partially debugged. A straight depletion run can now be made with or without poison control, and with any number of subtime steps in the burn interval. The technique for searching to obtain consistent starting conditions in a fractional batch-loading scheme has been tested.

Current work is concentrated on developing new devices for accelerating the calculational time to do the work described above and to do the burn-time and equilibrium-cycle searches.

b. Correction of THERMØS Flux Normalization. A minor correction has been made to the transport-theory thermalization code THERMØS, which will eventually be represented by a module in ARC. The change involves proper normalization of the space- and energy-dependent fluxes in cell calculations. The changes in group cross sections as a result of this correction seem to be at most 0.3% for typical problems.

6. Quasistatic Excursion Code, QXI

Initial testing of the quasistatic excursion code QXI is now in progress. The formulation is basically similar to that published by Henry[22] in that the space-, energy-, and time-dependent flux is separated into a shape function and a purely time-dependent amplitude function. The amplitude function is obtained from the solution of a modified point kinetics equation set in which all coefficients are time-dependent. The shape function is obtained by solution of the quasistatic multigroup diffusion equation derived in the following way.

The full time-dependent solution may be written as

$$[M + \chi_p F_p(\vec{r}, t)]\, \Phi(\vec{r}, t) + \chi_d \lambda C(r, t) = V^{-1} \frac{\partial \Phi(\vec{r}, t)}{\partial t}, \qquad (1)$$

[22] Henry, A. F., "The Application of Reactor Kinetics to the Analysis of Experiments," Nucl. Sci. Eng. 3, 52 (Jan 1958).

where

M--diffusion operator without fission sources;

χ_p--prompt-neutron spectrum matrix;

$F_p(r, t)$--prompt fission source density;

$\Phi(\vec{r}, t)$--time-dependent total flux vector at $\vec{r}$;

χ_d--delayed-neutron spectrum matrix;

λ--delayed precursor decay matrix;

$C(\vec{r}, t)$--precursor concentrations at $\vec{r}$;

V^{-1}--inverse velocity.

The splitting of $\Phi(\vec{r}, t) = \psi(\vec{r}, t)\ \phi(t)$ is made unique by the conditions

$$\frac{\partial}{\partial t}\int_V\int_E V^{-1}\psi(\vec{r}, t)\ \psi^*(\vec{r}, o)\ dEdV = 0 \tag{2}$$

and

$$\phi(o) = 1.0, \tag{3}$$

where $\psi^*(\vec{r}, o)$ is the adjoint solution of Eq. (1) at $t = 0$. Now, define $\alpha(t)$ from

$$\phi(t) = e^{\int_0^t \alpha(\omega)\ d\omega}. \tag{4}$$

Substituting for $\Phi(\vec{r}, t)$ in Eq. (1), using Eq. (4), and dividing by $\phi(t)$, we obtain

$$[M + \chi_p F_p - \alpha(t)\ V^{-1}]\ \psi(\vec{r}, t) + \phi^{-1}\chi_d\lambda C(\vec{r}, t) = V^{-1}\frac{\partial\psi(\vec{r}, t)}{\partial t}. \tag{5}$$

The right-hand side of Eq. (5) is neglected, i.e., the quasistatic solution for $\psi(\vec{r}, t)$ is found.

Precursor concentrations $C(\vec{r}, t)$ are computed directly from the integral precursor equations.

Region material temperatures and volume fractions may be time-dependent, either through externally applied functions or as a result of internally computed feedbacks. Group-dependent capture and fission cross sections at any temperature are found from empirical expressions based on precomputed values at four temperatures.

B. Fuels and Cladding

1. Fabrication and Evaluation

a. Compatibility of Type 304 Stainless Steel with Intermediate Phases in the U-Pu-Ti System. Diffusion couple studies have recently been made to determine the compatibility of Type 304 stainless steel with intermediate phases having the C-32-type structure that occurs in the U-Pu-Ti system. During annealing for one week at 750°C, marked solid-state diffusion occurs between the binary phase U_2Ti and Type 304 stainless steel. The widths of diffusion bands formed in the U_2Ti phase and steel are 114 and 12 μ, respectively. On annealing at 800°C, liquid-phase formation occurs. Additions of plutonium to the intermediate phase decrease the temperature at which liquid-phase formation occurs in interdiffusion layers. For phases having the nominal compositions U-10.7 a/o Pu-35.6 a/o Ti and U-14.9 a/o Pu-40 a/o Ti, liquid phases occur in diffusion bands formed at 700 and 650°C, respectively.

From other work Type 304 stainless steel appears to be compatible with U-10 w/o Zr alloy at 800°C but incompatible, due to liquid-phase formation, with U-10 w/o Mo and U-10 w/o Zr-10 w/o Mo alloys at 750°C.

b. Irradiation of High-temperature Materials. A series of irradiations are in progress on ceramic fuel materials being developed under the high temperature materials program. The materials under irradiation include UC-20 w/o PuC, PuC, and US clad in Nb-1 w/o Zr. The irradiations are being made in instrumented capsules in the MTR. A summary of the irradiations is shown in Table XXXI.

TABLE XXXI. Status of Irradiations of Ceramic Fuel (Clad in Nb-1 w/o Zr) in MTR

		Design Parameters				Operating Conditions			
								Burnup to Date	
Capsule or S/A No.	Specimen Number	Fuel Composition (w/o)	Effective Density (%)	Cladding OD (in.)	Cladding Thickness (in.)	Power Density (kW/cc)[a]	Max Cladding Temp (°C)	a/o (U + Pu)	fiss/cc x 10^{-20}[a]
56-11	MV-2	UC-20 PuC	79	0.281	0.012	1.2	470	6.2	16.1
56-8	MV-3	UC-20 PuC	81	0.281	0.012	1.2	715	6.7	17.8
56-8	MV-5	UC-20 PuC	80	0.281	0.012	1.2	705	6.4	16.8
56-11	MV-6	UC-20 PuC	80	0.281	0.012	1.2	480	6.7	17.6
56-13	Z-4	UC-20 PuC	79	0.174	0.015	1.2	665	1.6	4.1
56-13	Z-5	UC-20 PuC	79	0.174	0.015	1.2	585	1.6	4.1
56-13	Z-7	UC-20 PuC	79	0.174	0.015	1.2	570	1.6	4.1
56-13	C-45	PuC	84	0.174	0.009	1.4	700	1.6	4.4
56-8	S-7	US	80	0.281	0.012	1.0	535	5.0	9.7
56-8	S-8	US	89	0.281	0.012	1.0	725	7.0	15.2
56-8	S-9	US	76	0.281	0.012	1.0	750	7.0	12.8
56-8	S-10	US	91	0.281	0.012	1.0	690	7.0	15.5
56-11	S-15	US	82	0.281	0.012	1.0	380	4.1	8.2
56-11	S-16	US	90	0.281	0.012	1.0	510	6.0	13.1
56-11	S-17	US	88	0.281	0.012	1.0	500	4.7	10.0
56-11	S-18	US	77	0.281	0.012	1.0	610	6.5	12.2

[a]Based on effective density.

An electron microscopic examination is in progress on specimens of vibratorily compacted powders of UC-20 w/o PuC irradiated to average burnups near 6.9 a/o. The UC fraction was not enriched, so virtually all fissions occurred in the PuC fraction. The burnup in the PuC, therefore, approached 35 a/o.

The specimens were ground and polished in the usual manner for optical metallography. Replication was done on chemically etched surfaces by using an acetyl cellulose film moistened in acetone. After decontamination, the plastic replicas were shadowed with carbon and Pt-20% Pd alloy. The plastic film was then dissolved away.

Numerous fission-gas bubbles were present in the PuC phase, with an average diameter near 2 μ. Spherically shaped second-phase particles with diameters generally less than one micron were also observed in the PuC. These particles are assumed to be associated with solid fission products. The original UC particles often contained a small amount of UC_2 platelets precipitated in a Widmanstätten structure in the UC matrix. In the irradiated specimens, the UC_2 platelets had disappeared in a zone approximately 6 μ wide in areas where the UC particles were adjacent to the PuC. The disappearance of the UC_2 platelets is believed to be due to either the effect of fission recoils from the adjoining PuC phase, or from diffusion of PuC into the UC and altered phase equilibria.

c. Dissolution Kinetics in Liquid-metal Systems. Internal-friction techniques for determination of interstitial element concentration in refractory metals are being developed as a possible method for measuring accurately the concentration of interstitial elements in sodium. A proposed method of analysis involves the equilibration, with respect to oxygen, of tantalum wires in liquid sodium. The high sensitivity of internal friction to low interstitial-impurity concentrations (i.e., a few ppm by weight) in body-centered cubic (bcc) metals permits accurate determination of these impurities in refractory metals. Internal friction peaks have been obtained for oxygen, nitrogen, and carbon in tantalum wires. At the present time emphasis is being placed on the study of oxygen.

The internal-friction samples being used are high-purity tantalum wires of 0.51-mm dia and 18.0-cm gauge length. This results in a frequency of oscillation of 0.27 cps. For this frequency the internal-friction peak occurs at 135°C for oxygen, 316°C for nitrogen, and 331°C for carbon. The close proximity of the nitrogen and carbon peaks makes their analysis slightly more difficult than that for oxygen.

The oxygen content of tantalum wire samples has been varied by out-gassing at 2400°C in a vacuum of $\sim 10^{-8}$ Torr and by heating in a low-pressure oxygen atmosphere. The peak heights for the internal friction of

oxygen obtained from these samples varied from $Q^{-1} = 0.159 \times 10^{-3}$ to $Q^{-1} = 17.2 \times 10^{-3}$. The lowest peaks are still well-defined and compare well with the higher peaks when normalized to the same height, thus indicating the high sensitivity of the method. A linear relationahip between peak height and oxygen content indicates that the peak of 0.159×10^{-3} corresponds to an oxygen content of 1.74 ppm by weight. The presence of oxygen at this concentration was not detectable by vacuum fusion analysis.

The oxygen partitioning between tantalum and sodium has been calculated from the best data available with the following result:

$$K = \frac{\text{ppm (by weight) } \underline{O} \text{ in Ta}}{\text{ppm (by weight) } \underline{O} \text{ in Na}} = 7.74 \exp\left(\frac{2194}{RT}\right).$$

This equation differs slightly from that used previously because of the use of more recent and reliable free-energy data. This equation gives a value of 21.6 ppm (by weight) oxygen in tantalum in equilibrium with sodium containing 1.0 ppm (by weight) oxygen. The potential for high sensitivity of this method for determining oxygen in sodium is thus illustrated, since it is possible to determine oxygen in tantalum accurately down to a few parts by weight per million.

Experimental tests are presently under way to verify the partitioning of oxygen between tantalum and sodium. Oxygen levels in the sodium are of the order of 8 to 12 ppm by weight. These concentrations can be accurately determined by vacuum distillation or mercury amalgamation techniques.

An apparatus in which the rotating-disc sample geometry can be used to investigate corrosion phenomena in a sodium system has been designed and is under construction. Provisions in the apparatus have been made to expose wire specimens simultaneously that will be used to determine the partitioning of interstitials such as oxygen, carbon, and nitrogen between the sodium and the bcc sample materials.

The final series of dissolution experiments at 1200°C in the Ta-Sn system have been completed. The data are in substantial agreement with predictions based upon a convective diffusion model for liquid diffusion-controlled dissolution. The final report on this work is in preparation.

d. Mechanical Properties of Uranium Compounds. Metallographic examinations of fractured UO_2 specimens shows distinct differences in the microstructures of the examined specimens. These differences, which involve a "mottled" appearance, were first thought to be caused by the transition from brittle to ductile fracture. Further examination, however, indicates that the "mottled" appearance is a function of the strain rate and the modulus of rupture, i.e., the mottled appearance is usually noted on the

specimens exhibiting a reasonably high modulus of rupture at a slow strain rate. The different forms in which the mottled areas occur depend on the test temperature.

e. Thermal Stability of Plutonium Ceramics. Measurements of the rate of evaporation of PuO_2 were continued. Since previous results had indicated that extensive reaction occurs between PuO_2 and both tungsten and molybdenum in vacuum, weight-loss measurements were attempted for a PuO_2 pellet suspended in a rhenium wire coil. The weight loss of the rhenium wire was about 3-4% of that of the pellet in vacuum evaporation runs at 1976 and 2011°K. Rhenium therefore appears to be more compatible with PuO_2 than tungsten or molybdenum. Failure of the furnace power supply has temporarily halted the evaporation experiments.

Work was started on the fabrication and analysis of mixed plutonium-uranium oxide pellets for use as specimens in future evaporation experiments. Pellets were sintered to 80% of theoretical density in an atmosphere of argon containing 6 v/o hydrogen at 1550°C.

Attempts were made to determine the oxygen contents of two mixed oxide pellets by the oxidation-reduction procedure described by Lyon.[23] Although Lyon reported that pellets oxidized in air at 750°C remained intact, we found that one of our pellets disintegrated on oxidation for 2 hr at 750°C in helium containing 1 v/o oxygen. A pellet heated at 1200°C in the helium-oxygen atmosphere also broke apart. The reason for the discrepancy in results may be that complete solid solution was not achieved by our sintering procedure.

f. Development of Thermal-diffusivity Equipment for Ceramic Materials. Two specimens of plutonium carbide were made by isostatic pressing and sintering of material prepared by arc melting. Initial measurements of thermal diffusivity and heat capacity resulted in considerable scatter of the calculated thermal conductivity values. Additional samples will have to be fabricated and investigated in order to clarify the data with the aid of metallographic and chemical analysis.

2. Radiation Damage to Structural Materials

a. Effect of Fast-neutron Irradiation on Jacket Materials. The effects of fast-neutron irradiation coupled with elevated temperature on the tensile, creep, creep-rupture, and tube-rupture properties of V-20 w/o Ti, V-15 w/o Ti-7.5 w/o Cr, AISI Type 304 stainless steel, Hastelloy-X, and Inconel-625 are being studied in the exposure range from 1×10^{21} to 1×10^{23} n/cm^2 and the temperature range from 500 to 750°C. Twenty-six capsules containing 60 tube-rupture specimens and 296 tensile-type specimens are being irradiated in EBR-II subassemblies XA07, XA08, XO09, and XO10 at temperatures between 500 and 670°C. The

[23] Lyon, W. L., The Measurement of Oxygen to Metal Ratio in Solid Solutions of Uranium and Plutonium Dioxides, GEAP-4271 (1963).

specimens have accumulated at the end of the report period total neutron exposures between 8.3×10^{21} and 3.2×10^{22} n/cm^2. The status and identification of the capsules are given in Table XXXII.

TABLE XXXII. Status of Irradiations of Cladding Materials in EBR-II

		Design Parameters				Operating Conditions	
S/A No.	Capsule Number	Cladding Composition	Type of Specimen	No. of Specimens	Specimen Environment	Max Specified Temp (°C)	Exposure to Date (n/cm^2)
XA07	AS-9	V-20w/o Ti	Tensile	16	Argon-helium	590	3.2×10^{22}
XA07	AS-10	Hastelloy-X	Tensile	16	Argon-helium	590	2.9×10^{22}
XA07	AS-11	304 SS	Tensile	16	Argon-helium	590	3.1×10^{22}
XA08	AS-1	V-20w/o Ti	Tube-burst	12	Argon-helium	540	2.6×10^{22}
XA08	AS-2	V-20w/o Ti	Tube-burst	12	Argon-helium	540	2.6×10^{22}
XA08	AS-3	Hastelloy-X	Tube-burst	12	Argon-helium	540	2.7×10^{22}
XA08	AS-4	Hastelloy-X	Tube-burst	12	Argon-helium	540	2.7×10^{22}
XA08	AS-5	304 SS	Tube-burst	12	Argon-helium	540	2.7×10^{22}
XA08	AS-6	V-20w/o Ti	Tensile	16	Argon-helium	580	2.8×10^{22}
XA08	AS-7	Hastelloy-X	Tensile	16	Argon-helium	580	2.6×10^{22}
XA08	AS-8	304 SS	Tensile	16	Argon-helium	580	2.6×10^{22}
XA08	AS-12	V-20w/o Ti	Tensile	16	Argon-helium	580	2.5×10^{22}
XO09	AS-14	V-20w/o Ti	Tensile	13	Argon-helium	670	2.3×10^{22}
XO09	AS-15	V-20w/o Ti	Tensile	13	Argon-helium	670	2.2×10^{22}
XO09	AS-27	304 SS Hastelloy-X	Tensile	13	Argon-helium	670	2.4×10^{22}
XO10	AS-16	V-20w/o Ti	Tensile	13	Argon-helium	500	8.8×10^{21}
XO10	AS-17	V-20w/o Ti	Tensile	13	Argon-helium	500	9.5×10^{21}
XO10	AS-18	V-20w/o Ti	Tensile	13	Argon-helium	500	8.3×10^{21}
XO10	AS-19	V-20w/o Ti	Tensile	13	Argon-helium	500	8.8×10^{21}
XO10	AS-20	V-20w/o Ti	Tensile	13	Argon-helium	500	9.7×10^{21}
XO10	AS-21	V-20w/o Ti	Tensile	13	Argon-helium	500	11.5×10^{21}
XO10	AS-22	Hastelloy-X	Tensile	13	Argon-helium	500	10.0×10^{21}
XO10	AS-23	304 SS	Tensile	13	Argon-helium	500	11.5×10^{21}
XO10	AS-24	304 SS	Tensile	13	Argon-helium	500	9.7×10^{21}
XO10	AS-25	304 SS	Tensile	13	Argon-helium	500	9.3×10^{21}
XO10	AS-26	304 SS	Tensile	15	Argon-helium	500	9.4×10^{21}

3. Techniques of Fabrication and Testing

a. Ultrasonic Instrument and Transducer Development. In order to complete our data on -325 and -500 mesh porous nickel, additional samples of various densities had been ordered. These samples were received and evaluated this month.

After the longitudinal velocities in the samples had been measured, acoustic-impedance (product of the density and longitudinal velocity) values were calculated. Graphs of acoustic impedance as a function of density (% theoretical) have been plotted. Such graphs will be useful in determining the densities of -325 and -500 mesh porous nickel that will be required to achieve a particular acoustic impedance.

For example, if an ultrasonic transducer probe is to be built with a lead zirconate-titanate transducer (Clevite's PZT-4), a porous backing whose impedance matches that of the transducer is desirable. The impedance of PZT-4 is 34×10^5 gm cm^{-2} sec^{-1}. From the graphs, it is found that a 79.1% dense backing of -500 mesh nickel would match this

value. Matched backings for other types of ceramic transducers could be derived in a similar fashion.

b. Development of a Neutron Image-intensification System. One advantage of using an image orthicon television camera to view the output screen of a neutron image-intensifier tube is that one can detect lower neutron intensities than can be detected with a simple vidicon television system. The improvement of neutron intensity one can achieve is about 100 times (see Progress Report for September 1966, ANL-7255, p. 48). An additional advantage for a dynamic neutron inspection system, is one of speed of response, for the vidicon camera tube will not follow motion so fast as that which an image orthicon camera tube can follow. The vidicon system has followed high-contrast object movement as fast as 5 m/min, as previously reported[24] for the neutron-beam facility at Juggernaut reactor. Recent tests with an image orthicon camera with the same equipment, indicate an improvement in speed of between two and three times. Object motion speeds faster than 15 m/min cannot readily be followed on the kinescope. Motion-picture records of the kinescope confirm that image blurring does occur for object motion faster than 15 m/min.

The effect of gamma radiation on an image orthicon television camera is being studied in a cooperative venture with D. C. Cutforth, Idaho Division. An image orthicon tube was subjected to a cobalt-60 gamma exposure of 10^6 R. The glass envelope of the tube was noticeably brown, but electrical operation of the tube remained unchanged. The loss in sensitivity due to the decreased transmission of light into the tube was estimated as less than a factor of two. Further gamma irradiation tests are in progress.

4. Engineering Properties of Reactor Materials

a. Sintering Studies on Powdered (U, Pu)C. Studies are being carried out with mixed, (U, Pu)C powders produced by the fluidized-bed techniques developed by the Chemical Engineering Division. The powders are produced from arc-melted alloys of U and Pu, which are hydrided (~250°C) and then dehydrided (~250 to 800°C) in one cycle. The dehydrided powder is then converted to carbide by flowing methane (~800 to 900°C) in a fluidized bed (batch operation). The object of these studies is to characterize the powders and evaluate their suitability for fabrication into fuel pellets.

A representative batch of powder, $(U_{0.85}Pu_{0.15})C_{1+x}$, with original analyses of 4.89 w/o C, 490 ppm O_2 by weight, and 700 ppm N_2 by weight, was received after being stored for approximately one month in the Chemical Engineering Division's glovebox. The atmosphere in this glovebox is high-purity He, with less than 10 ppm each of O_2 and H_2O by weight. Characterization of this material was carried out as rapidly as possible with the bulk of the powder not in use being stored in a vacuum desiccator.

[24]Berger, H., Kraska, I. R., Niklas, W. F., and Schmidt, A., "A Thermal Neutron Image Intensification System," IEEE Trans. on Nuclear Science 13, 79 (April 1966).

Susceptibility to contamination in a Metallurgy Division glovebox having an atmosphere of nitrogen containing ~50 ppm O_2 and ~100 ppm H_2O vapor was checked by exposing a powder sample (~5 gm) to the box atmosphere for approximately one month. A plot of the weight gain (see Fig. 11) indicated a relatively constant rate up to ~0.5% weight increase for the first 10 days; the sample continued to gain weight, but at a slower rate, to a cumulative weight increase of ~0.7%, after which the sample appeared to stop gaining weight. As indicated, the sample gained weight more rapidly when extensive work was carried out in the box, presumably due to greater diffusion of O_2 or H_2O vapor through the gloves. The exposed powder was subsequently used in fabrication tests, with some saved for potential analyses for oxygen and nitrogen.

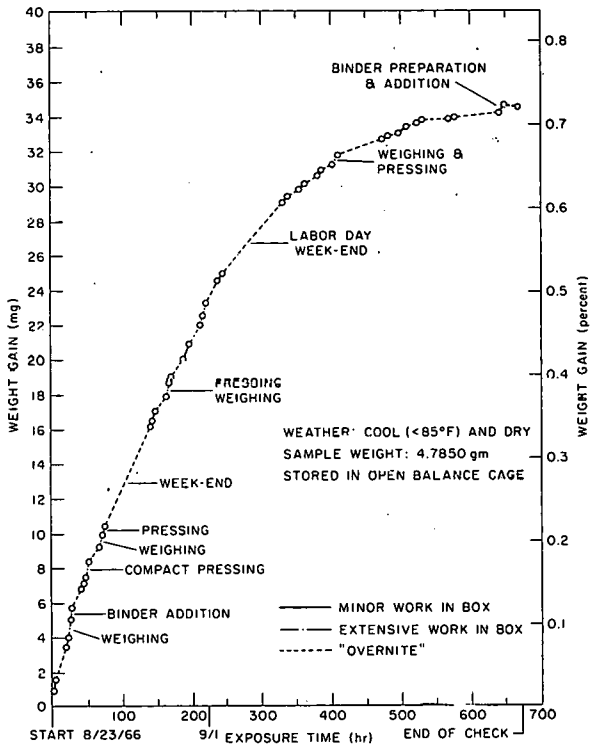

Fig. 11. Weight Gain of Mixed Carbide Powders, $(U_{0.85}Pu_{0.15})C_{1-x}$, Prepared by Hydride-Hydrocarbon Reaction in ANL Metallurgy Division Glovebox No. 141 (Once-through N_2)

Bulk density and screen analysis were determined with ~25 gm of powder. A loose, pour density of ~3.1 g/cc was obtained, and this density increased to a tap density of ~4.5 g/cc (after hand-tapping to minimum volume). The tap density is in reasonable agreement with values reported by the British for sinterable (ball-milled) carbide powders. Vibrating the powder through screens for a few minutes produced the following sieve analysis: 20.5% +200, 26.1% -200 +325, and 53.4% -325 mesh.

Pellet fabrication (~2 gm/compact for nominally 0.6-cm dia x 0.6-cm height) was carried out by standard techniques, i.e., intimate mixing of powder with binder (0.5% carbowax solution in alcohol), compacting the dried, binder-coated powders in a hardened steel die (of 0.711-cm dia) with a hand-operated hydraulic press and sintering in a tantalum resistance furnace under low-flow, high-purity argon (~2 cfh), at a slight positive pressure (~2 psig). Presintering (for binder removal) was carried out at increasing temperatures to ~900°C; the furnace was maintained at this temperature overnight and sintering was completed on the next day, using a 2-hr soak at the peak temperature. In early tests the effect of nickel powder additions was evaluated by adding 0.2 w/o Ni (-400 mesh) at the binder-addition stage. Typical fabrication results are tabulated in Table XXXIII for a series of tests investigating the effects of compaction pressure, nickel addition, and sintering temperature.

TABLE XXXIII. Fabrication of $(U_{0.85}Pu_{0.15})C_{1+x}$ Pellets from Mixed Carbide Powders Produced by Hydride Cycle on $(U_{0.85}Pu_{0.15})$ Metal Alloy, Followed by Hydrocarbon Synthesis

Compaction Pressure (tonne/cm²)	Nickel Added (%)	Green Density (g/cc)	Sinter Data				
			Temp (°C)	Wt Loss (%)	Volume Shrinkage (%)	Pellet Density	
						g/cc	% T.D.[a]
2.12	0	7.21	1550	0.87[b]	39.9	11.76	86.4
4.23	0	7.83	1550	0.57[b]	37.5	12.45	91.5
6.35	0	8.08	1550	0.57[b]	35.1	12.38	90.9
2.82	0	7.53	1650	0.60	37.9	12.01	88.3
4.23	0	7.90	1650	0.61	37.0	12.46	91.6
6.35	0	8.31	1650	0.50	34.3	12.58	92.4
2.82	0	7.47	1900	0.64	39.0	12.18	89.5
4.23	0	7.78	1900	0.57	37.0	12.27	90.1
6.35	0	8.21	1900	0.58	33.9	12.35	90.7
2.12	0.2	-	1550	- [b]	32.8	10.01	73.5
4.23	0.2	7.78	1550	0.79[b]	28.3	10.77	79.2
6.35	0.2	8.26	1550	0.72[b]	27.8	11.18	82.2
2.82	0.2	7.59	1650	0.83	33.1	11.24	82.6
4.23	0.2	7.87	1650	0.62	31.9	11.49	84.4
6.35	0.2	8.27	1650	0.59	30.6	11.83	86.9
2.82	0.2	7.40	1900	0.82	38.0	11.84	86.9
4.23	0.2	7.81	1900	0.73	34.9	12.02	88.3
6.35	0.2	8.23	1900	0.72	34.0	12.17	89.4

[a]Based upon 13.61 g/cc, a "weighted" average of the theoretical monocarbide densities of mixed carbides containing 15% plutonium.
[b]Questionable data due to poor quality of compacts, resulting in physical chipping, etc.

The data, obtained from the three sintering runs and based upon averages from two pellets, indicate the powder is moderately sinterable, achieving reasonable densities at temperatures as low as 1550°C; the optimum sintering temperature (for maximum density) appears to be 1650°C, with lower densities resulting at 1900°C (when no nickel is used). Conversely, when nickel was added, higher densities were achieved at increasing sintering temperatures. As indicated, the nickel powder has not behaved as a sintering aid, but actually hindered sintering action, since significantly lower densities were obtained in comparison to those from pellets prepared without nickel. The probable reason that nickel did not behave as a sintering aid is that it was not ball-milled with the carbide powders.

The results show that higher pellet densities are obtainable with increasing compaction pressures, within the pressure range investigated. The optimum compaction pressure appears to be ~4.23 tonne/cm², with insufficient green strengths evident in compacts pressed at 2.12 tonne/cm² and pressing becoming somewhat difficult at pressures above 6.35 tonne/cm². Compacts pressed for the first run (1550°C sinter) were made by a

single pressing action and were relatively weak. In subsequent compact fabrication it was found that a double pressing action, with release of entrapped gas between pressings, produced sounder compacts of slightly higher green density.

Weight losses were reasonable considering the 0.5% addition of Carbowax (and 0.2% nickel in some of the compacts), especially when one realizes a finite (unknown, but readily visible) amount of stearic acid, die lubricant (applied to the die cavity as a solution in CCl_4), adheres to the pressed compact. Neglecting the data on nickel-containing compacts, the results suggest minor, if any, differences in CO removal (or plutonium losses) at sintering temperatures of 1550, 1650, or 1900°C. These conclusions are essentially borne out by the few analytical results, shown in Table XXXIV. The other important fact from the analyses is that nitrogen contamination of the powders occurs as readily as does "O_2 pickup," since the pellets were ~1000 ppm higher in each of O_2 and N_2, in comparison to the original powders. These impurities are about one-half to one-third greater than the amount typically obtained in carbide products (i.e., ~700 ppm O_2 and ~500 ppm N_2). The analyses, indicating 5.13 to 5.14% equivalent carbon, appear to agree with metallographic examination indicating appreciable second-phase sesquicarbide.

TABLE XXXIV. Typical Analyses of Sintered Mixed Carbides Prepared from Hydride-derived Carbides

Original Powder Analyses			Fabrication Conditions			Analyses from Sintered Pellets		
C (%)	O_2 (ppm)	N_2 (ppm)	Pressure (tonne/cm^2)	Sintering Temp (°C)	Density (% T.D.)	C (%)	O_2 (ppm)	N_2 (ppm)
4.89	490	700	4.23	1550	90.8	4.88	1700	1600
4.89	490	700	423	1900	89.9	4.86	1600	1700

b. Tensile Properties of the V-15 w/o Ti-7.5 w/o Cr Alloy. Tensile properties were determined for V-15 w/o Ti-7.5 w/o Cr as a function of temperature and at a constant strain rate of 2×10^{-4} sec^{-1}. From the load-elongation data obtained at the various test temperatures, the following properties were determined: Young's modulus, yield stress, ultimate tensile strength, true stress-strain curves, reduction in area, total elongation, uniform elongation, strain-hardening exponent, and the strength coefficient.

The effect of test temperature on the ultimate tensile strength, yield stress and Young's modulus is shown in Fig. 12. The largest decrease in these values occurs between 600 and 800°C ($\approx$0.4 to 0.5 T_m), which is within the recovery range for this alloy.

The true stress-strain curves for the various test temperatures are shown on logarithmic coordinates in Fig. 13. In the range of uniform plastic deformation prior to necking (i.e., when $\epsilon^n = \sigma/K$, where n is strain-hardening exponent and K is the strength coefficient), the curve at 400°C

was erratic at strains above 3×10^{-2}. The autographic load-elongation curves at 200 and 400°C exhibited a "saw-tooth" shape, which is typical of strain aging behavior but not easily resolved in the logarithmic curves of Fig. 13. This behavior is more pronounced at 400°C. Similar peaks have been observed in unalloyed vanadium from 200 to 450°C.[25] The slightly higher ultimate stress at 400°C as compared to 200°C in the uniform plastic deformation region can be due to strengthening by strain aging.

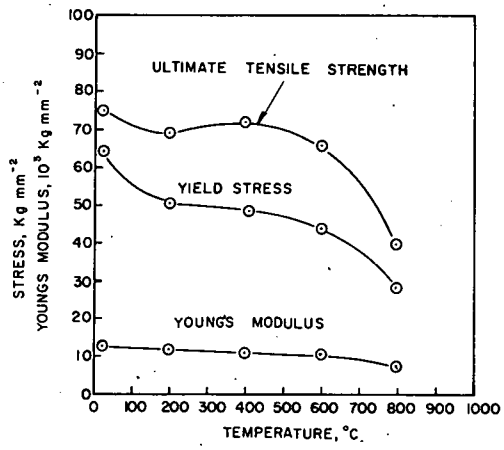

Fig. 12. Short-time Tensile Properties of V-15 w/o Ti-7.5 w/o Cr Annealed at 850°C for 1 hr (Strain rate--2×10^{-4} sec^{-1})

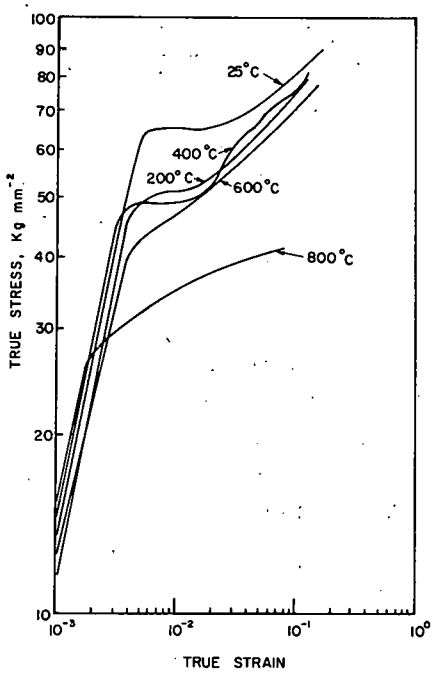

Fig. 13. True Stress vs. True Strain for V-15 w/o Ti-7.5 w/o Cr Annealed at 850°C for 1 hr (Strain rate--2×10^{-4} sec^{-1})

Tensile parameters not included in Figs. 12 and 13 are listed in Table XXXV. Again, the 800°C test produced the greatest variation of these

TABLE XXXV. Mechanical Property Parameters for the V-15 w/o Ti-7.5 w/o Cr Alloy at Various Temperatures

Test Temp (°C)	Reduction in area (%)	Elongation (%)	Uniform Elongation (%)	Strain Hardening Exponent n	Strength Coefficient K(kg mm^{-2})
Room	56	29	17.7	0.18	123
200	60	15.5	13	0.21	123
400	35	28	12.6	0.19	116
600	52	28	15.5	0.165	102
800	99	50	7	0.07	49

[25]Thompson, R. W., and Carlson, O. N., The Effect of Nitrogen on the Strain Aging and Brittle-Ductile Transition of Vanadium, IS-994 (Aug 1964).

parameters. Except for the two temperatures where strain seemed to occur, i.e., at 200 and 400°C, the agreement between uniform elongation and the strain-hardening exponent n was very good as predicted by theory.

C. Engineering Development

1. Heat Transfer, Fluid Flow, and Mechanics of Materials

a. Niobium-1% Zirconium Loop. This facility is designed to investigate the heat transfer and two-phase flow characteristics of boiling sodium to a temperature of 2100°F and a pressure of approximately 8 atm. Among the variables to be investigated are boiling heat flux and temperature difference up to the critical flux occurrence, boiling and adiabatic two-phase pressure losses, vapor volume fraction, boiling stability parameters, and ultimately the transient behavior of some of these same quantities.

Modifications to the loop are still underway and additional equipment for the loop facility is being installed. The last eleven thermocouple assemblies are in place. Supports have been installed to prevent the electromagnetic pump from rotating or moving axially because of the torque and thrust forces exerted by the induction field required for pumping fluid through the Nb-1% Zr helix. Final alignment and calibration of the tantalum shutters are complete. Several repairs and calibrations of instrumentation have been completed in preparation for higher temperature operation.

b. Electron-bombardment Heater Experiment. Approximately 500 hr of testing with the 0.030-in.-dia uncarburized, thoriated-tungsten filament and 300 hr with the 0.030-in.-dia tungsten filament have been achieved. Heat fluxes ranging up to 350,000 Btu/hr-ft^2 have been supplied to the anode during these tests. This experiment is approaching limiting design conditions, and modifications are underway to provide for higher heat fluxes for short periods of time.

These tests and an evaluation of the electron-bombardment heater (EBH) study by Eimac Corporation will provide the basis of the final EBH design for use in the 2100°F Nb-1% Zr loop.

c. Countercurrent Turbulent Liquid Metal Flow. Experiments with the first mercury-to-mercury concentric tube heat exchanger have been terminated. The measured Nusselt Numbers and efficiencies showed a strong dependence on the fluid inlet temperature difference (see Progress Report for September 1966, ANL-7255, p. 55), indicating that an extraneous mode of heat transfer between the fluids was present. The cause of this discrepancy is still not known. The second test section which was designed to limit further possible heat transfer between the fluids at the ends of the heat exchanger is nearing completion and will be installed in the loop as soon as it is completed.

After termination of the tests with the first test section, a leak was detected in the seals in the mercury pump. This mechanically sealed pump was replaced with an available canned-rotor type. When the canned-rotor pump was run with mercury, however, it appeared to develop too large a head and overload the motor. Discussions with the manufacturer's representative revealed that although the impeller and motor supplied with the pump were supposedly chosen for operation with mercury, the most probable explanation for the difficulty was that the impeller was actually too large. Consequently, the loop will be down until the seal in the mechanically sealed pump is replaced or a new impeller is obtained for the canned rotor pump.

Smaller valves, 1/2 and 1/4 in., were installed in parallel with the original control valve assembly to provide better control for low flow rates.

2. Instrumentation and Control

a. Effects of Interfacial Transport Processes on Film Condensation. In preparation for the final design of the condensing test section, the air-water test section has been installed. Loop and test-section instrumentation is almost complete. The loop should be ready to run by the week of October 24, 1966.

In its initial runs the flow pattern in the liquid film will be observed by dye injection. This will allow a determination to be made of the effectiveness of the injector design in eliminating secondary flows. In the next series of runs the entrance effects resulting from the method of injection of the liquid film will be determined. This will also allow the instrumentation for measuring film thickness to be tested.

Analysis of the entrance effects for two-component flow has utilized momentum integral techniques. The equations have been programmed and preliminary results from the CDC 3600 computer are encouraging.

b. Condensing Injector Studies. In the past, data were obtained for condensing injector operation with steam and water. Steam velocities up to 2500 fps ($M_1 \approx 1.5$) at the entrance to the mixing section of the injector and discharge pressures greater than the upstream pressure of either steam or water were also readily obtained. The measured discharge pressure was, when averaged over all runs, about 40-50% of calculated discharge pressure, assuming no losses. Also, axial pressure profiles indicate that mixing in the injector does take place at constant pressure, even when the inlet vapor flow is supersonic. Void measurements were taken at various axial positions in the mixing section during several runs. These measurements indicate a great amount of interaction between the liquid and vapor streams. The results of a typical run are shown in Fig. 14. The void measurements shown are taken from a cross-channel trace at the

center position and indicate a dispersion of the central liquid jet. The upstream flows are unaffected by an increase in back pressure up to the point of choking. More data will be taken in the immediate future.

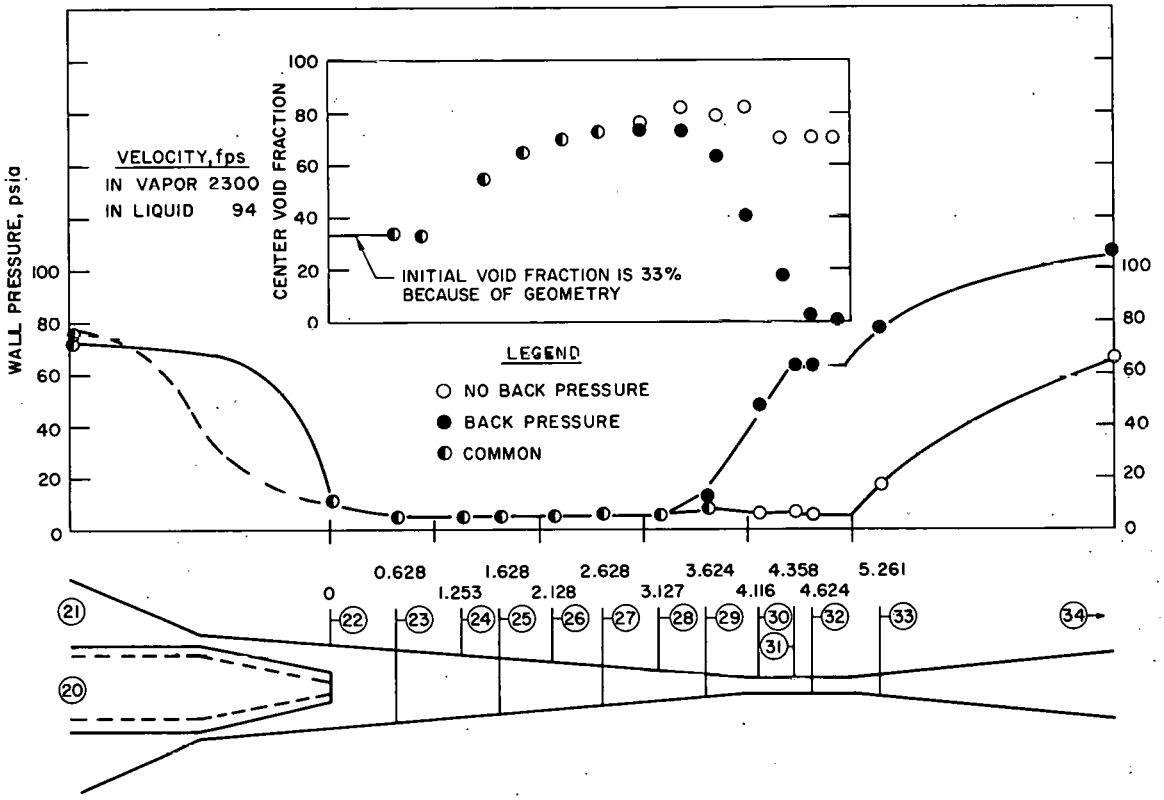

Fig. 14. Axial Pressure Distribution and Central Void Fraction in Mixing Region with and without Imposed Back Pressure

D. Chemistry and Chemical Separations

1. Fluoride Volatility Processes

a. Recovery of Uranium and Plutonium from Low-enrichment Fuels: Laboratory Support Work

(i) Fluorination of UO_2-PuO_2-Fission Product Pellets. Development studies are being performed in a 2-in.-dia fluid-bed reactor to determine optimum conditions for fluorinating UO_2-PuO_2 pellets containing fission products. The process is based on the selective volatilization of uranium as UF_6 by reaction with bromine pentafluoride followed by volatilization of plutonium as PuF_6 by reaction with fluorine. Previous work (see Progress Report for September 1966, ANL-7255, p. 57) has shown that with a single use of the alumina bed, plutonium removal from the alumina bed is less than 99%. A series of three experiments (runs Purse-10, -11, -12) were performed to evaluate the reuse of the alumina bed and to determine if it is possible to reduce the plutonium concentration in the final alumina bed to less than one percent of the total quantity of plutonium charged to the system.

The processing sequence for the three runs involved in the following steps: (1) charging of the oxide fuel pellets, (2) oxidation of the pellets to U_3O_8 and PuO_2 fines for 4 hr at 450°C with 20 v/o oxygen in nitrogen, and (3) fluorination with 10 v/o BrF_5 in nitrogen for 2 hr at 300°C to form volatile UF_6 and nonvolatile PuF_4. Three processing cycles were performed during the three runs; the nonvolatile PuF_4, which remained in the bed after each cycle, was allowed to accumulate in the system. Fluorination of the plutonium to volatile PuF_6 was accomplished after the third cycle (run Purse-12) using 90 v/o fluorine. The fluorination step was carried out as follows: 10 hr at 300°C, 5 hr while the temperature of the reactor was increased from 300 to 550°C, and 3 hr at 550°C.

The charge for each run was 650 g of UO_2-PuO_2-fission product pellets and 0.6 g CsF and 0.16 g RbF. For runs Purse-11 and -12, the cesium fluoride and rubidium fluoride were mixed with 50 g alumina prior to being charged to the fluid-bed reactor. Thus, the total weight of alumina in the fluid bed in the three runs was 1200 g, consisting of 1100 g of alumina in the starting bed for run Purse-10 and 100 g added in the subsequent runs.

The concentrations of uranium and plutonium in the final alumina bed after fluorination with fluorine were 0.003 w/o and 0.009 w/o, respectively. These values correspond to a removal of 99.9% of the uranium charged to the reactor and a removal of 99% of the plutonium charged in the three runs. The amount of plutonium remaining on the alumina after three uses of the same bed was less than two-thirds of the amount which would have remained if three separate beds had been used for the processing of three separate charges of fuel.

Analyses of bed samples taken during the course of the plutonium fluorination step indicated that after 5 hr of fluorination at 300°C very little plutonium had volatilized at that temperature. Similarly, no further reduction in plutonium concentration was observed after 1 hr fluorination at 550°C. Thus, it appears that a shorter fluorination period could be employed for plutonium removal: 5 hr at 300°C, 5 hr from 300 to 550°C, and 1 hr at 550°C. This is a reduction in fluorination time of seven hours.

The fluoride content of the final alumina bed was 3.5 w/o, indicating that only a small fraction of the alumina was fluorinated to aluminum fluoride during the alumina-bed-reuse experiments. It appears that deterioration of the bed material by exposure to fluorine will not be a process problem.

(ii) Neptunium Fluoride Chemistry. Laboratory-scale studies of the reaction of neptunium tetrafluoride (NpF_4) and bromine pentafluoride (BrF_5) are being carried out to determine the behavior of neptunium when oxidized nuclear fuel is contacted with BrF_5. The reaction between NpF_4

and BrF_5 at 300 to 400°C volatilizes neptunium, presumably in the form of neptunium hexafluoride (NpF_6). Chemical analyses of solid residues remaining after partial conversion of NpF_4 to NpF_6 show no evidence of formation of neptunium fluorides intermediate between NpF_4 and NpF_6 in the reaction of NpF_4 with BrF_5.

Two experiments were performed to investigate the reaction between bromine trifluoride (BrF_3) and NpF_4. At 400°C, the reaction proceeds with the formation of a volatile neptunium compound (presumably NpF_6). The color of the condensed reaction products was similar to the color of bromine.

IV. ADVANCED SYSTEMS RESEARCH AND DEVELOPMENT

A. Argonne Advanced Research Reactor (AARR)

1. General

The architect-engineer, Burns and Roe, Inc., completed the Title I report which was submitted to the AEC for approval on October 7, 1966. Because of the large amount of material being presented, the report was divided into five (5) volumes as follows:

Volumes 1A and 1B-Design Description
Volume 2--Drawings
Volume 3--Schedule and Cost Estimate
Volume 4--PERT Networks
Volume 5--Calculations

At present the key personnel at Burns and Roe are evaluating the ramification of the change to a HFIR-type core on the facility design as indicated in Title I. They will continue on a minimal effort basis until the Laboratory receives approval of the Title I report from the AEC.

Because of the decision to change to an HFIR core in AARR, a number of development activities, related to the core structure or stainless steel cermet fuel development, have been dropped.

All development work on the control-rod-drive mechanisms has been terminated. The top drive mechanism had been completed in the shop and will be placed in storage. The design of the bottom drive mechanism had been completed.

The material compatibility studies are completed and a final report will be issued in the near future.

Fuel-materials-development subcontractors have been ordered to cease all work and prepare reports on the work performed to date. The cessation of work occurs at a disadvantageous point in some activities as full benefit of information will not be derived from the irradiation specimens and the samples that have already been prepared.

The fuel-assembly development work was completed in October on a reduced scope of work for the contractor. The final report should be issued in November.

Core-structure design on the rhomboid AARR stainless steel core was terminated and work has been started on modifying the vessel internals to accept the HFIR core. Drawings and specifications on components for the HFIR facility have been received from Oak Ridge.

2. Nondestructive Testing of AARR Components

The flash method of determining thermal diffusivity α and thermal conductivity K has been utilized to measure the thermal properties of AARR fuel plates. Measurements with the unirradiated material were made from ambient temperature to 800°C with intermediate measurements at 100°C. The twenty samples included five specimens from each of the following plates:

(a) BMI sample plate #50;

(b) Martin Co. sample plate #48;

(c) Sylcor full-length plate #4;

(d) BMI full-length plate #57.

For the specimens cut from the first three of the above makes of fuel plates, α and K were found to be increasing functions of temperature. The five samples from any one fuel plate gave measured values agreeing to ±5%, but differences between the average values of the fuel plates were about 10-15%. At room temperature, α varied from 0.0245 to 0.0316 cm^2/sec, and K varied from 0.0255 to 0.0326 cal-cm/cm^2-sec-°C. At 800°C, α varied from 0.0300 to 0.0367 cm^2/sec, and K varied from 0.0335 to 0.0395 cal-cm/cm^2-sec-°C.

Plate BMI-57 exhibited thermal properties that decreased with increasing temperature. Measured values were also relatively low, e.g.,

$$\alpha = 0.0145 \text{ cm}^2/\text{sec}; \quad K = 0.0160 \text{ cal-cm/cm}^2\text{-sec-°C}$$

at room temperature, and

$$\alpha = 0.0115 \text{ cm}^2/\text{sec}; \quad K = 0.0123 \text{ cal-cm/cm}^2\text{-sec-°C}$$

at 800°C. The thermal properties, as measured here, depend not only on the fuel-plate composition, but, also, on the quality of the bonds between the core and the jacket. As the highest measured value for K at room temperature is less than that for UO_2, it is believed that the thermal properties of plate BMI-57 are indicative of poor bonding.

3. Reactor Physics Experiments

A phasing-out program of experiments has been planned for the stainless steel-U^{235} reactor core loadings in the Criticality Facility. In view of the anticipated shift to an HFIR-type reactor core, the detailed experiments scheduled for the SS core will be severely curtailed.

The enlarged ITC system has been modified to reflect the planned use of an aluminum ITC shroud instead of a SS shroud. Replacement of SS by aluminum increased reactivity slightly, and increased the peak flux per unit reactor power by approximately 5%, as measured with bare U^{235}-fission detectors.

Planned experiments were completed to measure certain effects of beryllium liners at the edge of the enlarged internal thermal column. Three rings of beryllium were available, as shown in Fig. 15. The reactor was made critical on water level, with control rods fully withdrawn. Replacement of water by beryllium increased reactivity, as evidenced by the drop in the water level at reactor criticality. The results are shown in Table XXXVI.

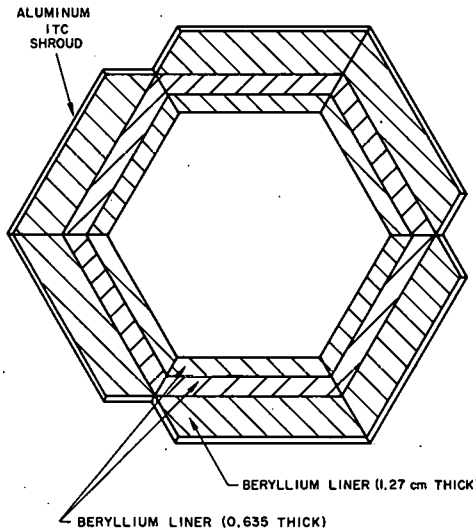

Fig. 15. Enlarged Internal Thermal Column (7.2-cm Equivalent Radius) with Beryllium Liners

TABLE XXXVI. Water Levels at Criticality for Various ITC Conditions

Condition of the ITC[a]	Water Level at Criticality[b] (cm)
Stainless Steel ITC Shroud;	
100% H_2O	120.7
Aluminum ITC Shroud;	
100% H_2O	119.3
1.27-cm-thick Be liner	115.2
1.90-cm-thick Be liner	113.7
2.54-cm-thick Be liner	112.6

[a] For full-length hexagonal beryllium rings.

[b] The top of the active fuel zone nominally is at 132.4 cm. Thus, in each of these experiments, part of the fuel was uncovered. The level of the foils was at 106.3 cm, for the radial traverses shown in Fig. 17.

Relative radial distributions of U^{235}-fission activity were measured with bare U^{235}-Al foils, as a function of the total thickness of the beryllium liners. These measurements, summarized in Fig. 16, are normalized to unit activity at the vertical axis of the ITC. The peak flux per unit power decreases monotonically as the thickness of the liner is increased. There is an increase in the peak-to-average power density in the reactor core as the beryllium thickness is increased.

4. Theoretical Reactor Physics

The programs of theoretical reactor physics analysis have been redirected to studies with the HFIR-type reactor core.

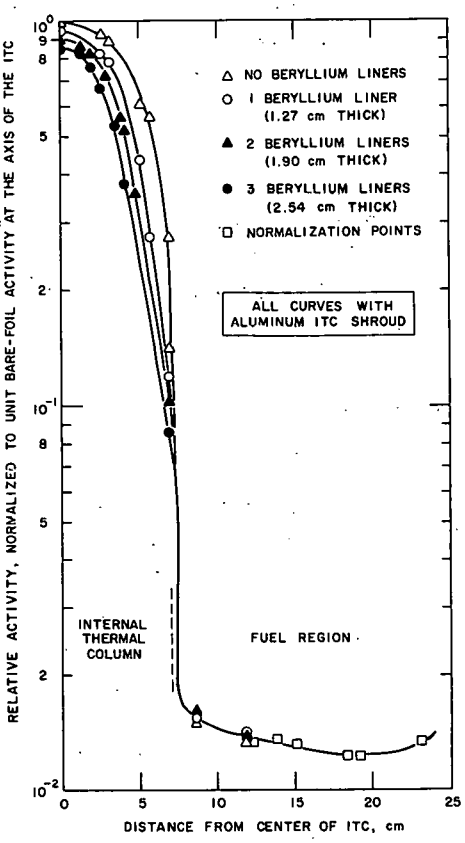

Fig. 16

Radial Distributions of U^{235} with Beryllium Liners in the Internal Thermal Column

The response of the reactor core to hypothetical rapid insertions of reactivity beyond prompt criticality is being studied. Two models have been formulated for these preliminary analyses:

1. the entire additional thermal energy of the reactivity excursion is stored uniformly in the fuel plates; the core volume remains constant; and the entire equilibrium volumetric thermal expansion of the fuel plates is compensated by the ejection of coolant fluid from the reactor core;

2. the additional energy is stored in the fuel plates; one-third of the volumetric expansion is directed along the length of the plate, thereby increasing the height of the active fuel zone; the remaining two-thirds of the volumetric expansion is compensated by ejection of coolant.

Of the two models, the first is considered to be the more nearly realistic, because the involute fuel plates are welded to strong circular rings which would remain relatively cool during the excursion. The calculated reactivity effects of fuel-plate expansions are given in Table XXXVII.

TABLE XXXVII. Reactivity Effects of Fuel-plate Expansion[a]

Percentage Expansion	Model 1	Model 2
30	- 8.0%	- 3.6%
60	-21.6%	- 8.2%
80	-37.6%	-12.1%

[a]Model 1: constant core volume; Model 2: constant core lateral area, expanding length.

V. NUCLEAR SAFETY

A. Coolant Dynamics

1. Coolant (Water) Expulsion Studies

Work is continuing on the computation of expulsion velocities.

Several simplified models of sodium expulsion are continually being evolved.

2. Superheat Experiments

This experiment is designed to measure the degree of liquid superheat required to initiate nucleate boiling in sodium under various conditions simulating a reactor environment. Typical parameters will be systematically varied to determine their independent and combined effects upon the liquid superheat necessary to initiate nucleation. The parameters to be examined are: (a) pressure, (b) dissolved gas content, (c) heat flux, (d) surface characteristics, and (e) the pressure-temperature history of the system.

The system is being evacuated and degassed in preparation to filling with sodium. The initial fill should be made this coming month.

One of the desired measurements is the location of the liquid-vapor interface within the test section. This interface within a steel container can be measured directly by passing X rays through the container to impinge on a detector, producing either a visual image or an electrical signal. For fast response of the detector, power-line ripple in the X rays should be minimal. Hence, the power supplied to the X ray tube should be relatively ripple-free both in filament current and in high-tension voltage, for the effect on X-ray intensity is magnified greatly.

To reduce line ripple economically, two 150-kV capacitor banks of 0.016 microfarad each were ordered and installed. Bleeder resistors across each bank eliminated shock and radiation hazards from stored charge. For portability, the power supply and capacitor banks are mounted on a wheeled cradle.

The intensity of X rays from the unmodified generator goes from zero to maximum value with line frequency. With the installed capacitors, a typical intensity variation is 15% peak-to-peak, far less than before the change. Calculations give an estimate for peak ripple in the high voltage as 1.1%, which increases to 9.5% at the detector after passage through 5.7 g/cm^2 of copper. From unpublished tests at Oak Ridge, it appears

likely that the remainder of the ripple is due to alternating current in the filament of the X-ray tube.[26]

In addition to beam ripple, fluctuations in line voltage can affect X-ray intensity adversely. A voltage regulator is on order to hold line fluctuations to ±0.1%, with an anticipated October delivery. These additions to the system will provide a more constant source of X rays for studies of transient heat transfer.

3. Sodium Expulsion Experiment.

In this experiment, it is planned to investigate the mechanism of coolant expulsion in a simulated reactor environment. Hence, this experiment includes the measurement of the void distribution, expulsion velocities, pressure transients, and liquid superheats during coolant expulsion.

The high-speed vacuum pumping station has arrived and is being checked out.

A bid has been accepted for the programmed electron-beam heater. The purchase is awaiting approval by AEC.

4. Critical Flow Studies.

Calculations of the progression of accidents in sodium-cooled reactors reveal that critical flow may exist in the core, leading to detrimental effects such as voidage of the coolant channel, shock phenomena, and pressure buildup.

The construction of experiments to study critical flow of different fluids is continuing. The major portion of the sodium loop is nearing completion. By the next reporting period, the first test section is expected to be installed, and shakedown tests of the instrumentation for measuring pressure and flow rate should be completed.

A relatively simple combined pressure-control and flow-rate device has been developed and successfully tested on the subatmospheric water loop. Only minor modifications appear necessary in order to apply the same package to the sodium loop.

5. Effects of Rapid Heating of Reactor Components.

A phase of the Reactor Safety Program consists of the study of the influence of rapid insertion of energy into a cooled system, observed predominantly in the form of temperature, pressure, and coolant-flow

[26]Reynolds, J. W., ORNL, personal communication, March 29, 1966.

modifications. In order to estimate these effects in a complex set of reactor internal structures, certain simplified system analyses and experiments are performed.

One item of interest is to relate the structural response to the assumed thermodynamic behavior of the system. "System size," which in this context reflects the dominant mode of transmission, storage, and dissipation of energy, may have an important influence. For example, a small, low-energy system would have the acoustic traversal time as a significant characteristic. In this case a locally induced distrubance is effectively observed everywhere at once. Should the containing structure be soft, i.e., possess a large free vibration period, the system response to a given energy insertion could be radically different from that of a system contained within a stiff structure.

Tentatively, the following classification has been devised:

a. Small, low-energy, stiff structure;

b. Small, low-energy, soft structure;

c. Large, low-energy, stiff structure;
d. Large, low-energy, soft structure;
} wave models

e. High-energy, shock-wave model.

Note that in systems a and b only the pressure is time dependent. In systems c, d, and e the disturbance is both time- and space-dependent. System e poses additional problems, among them being the dependence of transmission velocity upon the magnitude of the disturbance.

For the initial investigation a small, structurally flexible system is assumed. Although no totally acceptable heat-transfer or pressure-generation models currently exist, a simplified fluid and heat-transfer model was assumed but which introduced volume-change terms to correspond with structural deflections. Again, for the sake of simplicity a structure model of rectangular cross section with flat plate walls was used, so that structural-deformation expressions could be written immediately. Much of this preliminary analysis can be changed to basically cylindrical geometry with the additional assumption of initial deformations; however, at the very first stages the additional complexities are unwarranted.

The equations to describe the momentum model, thermodynamic assumptions, structural-component deformation and dynamics, and energy-partition assumptions have been written. In general, the resulting set of differential equations is nonlinear and coupled, thus precluding an exact analytical solution. The use of a digital computer is being considered for solution, as well as a further attempt to introduce linearizing approximations.

B. Fuel Meltdown Studies with TREAT

1. Transient In-pile Tests of W-UO_2 Cermets

A summary report[27] has been prepared of the transient experiments conducted in TREAT with fuel specimens for the ANL W-UO_2 fast rocket reactor to test the behavior of the fuel under rapid temperature excursions. Samples of standard configuration and composition were made at Argonne according to fabrication specifications that were established at the time of manufacture. Uranium enrichment was specified to provide an adequate ratio of sample power to reactor power, consistent with acceptable internal flux depressions. Each sample was contained inside a standard TREAT transparent meltdown capsule assembly,[28] using a specimen load frame adapted to the needs of the experiments. Instrumentation consisted of four surface-mounted, fast-response W-5% Re vs W-26% Re thermocouples, and high-speed color photography (camera speed was 2000 frames per second).

Eight specimens were run, in two groups of four (see Table XXXVIII). The first sample was given two low-energy reactor excursions as check transients. The next two were subjected to single transients of increasing severity, and the final specimen of the first group was heated in a slower, "flattened" power transient.

TABLE XXXVIII. Summary of TREAT Tests

Sample No.	Transient Duration (sec)	Reactor Integrated Power (MW-sec)	Maximum Recorded Surface Heating Rate (°C/sec)	Maximum Recorded Surface Temperature (°C)
1	0.43	164	1,700	800
1	0.3	284	3,900	1,460
2	0.3	377	5,600	1,790
3	0.2	487	8,000	2,200
4	2.1[a]	332	800	1,460
5	0.2	540	12,000	2,600
6	3.0[a]	495	1,400	2,050
7[b]	0.2	523	14,500	2,750
8[c]	0.2	532	16,000	2,750

[a] "Flattened" transient.
[b] Sample given two additional transients of same severity.
[c] Sample given five additional transients of same severity.

After review of results from the first group, final specifications were made for the last group of samples. Samples 5 and 6 were given short and "flattened" power excursions, respectively, of greater severity than in the first group. Sample 7 was given three high-energy short excursions, and sample 8 was subjected to six successive high-energy transients.

[27] Marchaterre, J. F., Dickson, J. J., Hoglund, B. M., and Kalba, V. M., "Refractory Metal Fast Reactor for Nuclear Rocket Propulsion," AIAA Bulletin 2, 207 (May 1956).

[28] Golden, G. H., Dickerman, C. E., and Robinson, L. E., ANL-6457 (Jan 1962).

2. Calculations of Transient Temperature by Use of the Hybrid Computer

The equations prepared for use in analog computer calculations of transient temperature for fast reactor safety experiments (see Progress Report for April 1966, ANL-7204, p. 77) have proven to be unsuitable, and have been rewritten using a modification of the equations used in the ARGUS code. The calculation is now stable, but incorporates an advance over the general-purpose ARGUS code in that the diffusion equation describing the thermal behavior of the fuel treats the thermal conductivity as temperature-dependent. Cylindrical geometry is used.

This technique is a general tool using the Reeves analog machine linked to the PDP6 digital computer. The analog computer solves the ordinary differential equations arising from a finite-difference approximation of the heat-transfer equations for a single pin surrounded by flowing coolant. The pin can be either a solid cylinder or of annular form. Duties of the digital computer can be summarized as follows: (1) accept input data, (2) calculate coefficients for the system, (3) set analog potentiometers, (4) check system, (5) control calculation, (6) store results. The hybrid program has been checked, using constant material properties, against ARGUS for a case with a power excursion with constant coolant flow, and for another case with constant power during a flow decay.

3. Strain-hardening Analysis of a Pulsed EBR-II Fuel Tube

Because of the rapid nature of pressure pulses which can be generated in fuel pins exposed to transient irradiation in TREAT, strain hardening can be considered an important factor in reducing the integrity of the fuel tube, whereas a static analysis would predict ductile yield and containment.

The behavior of an EBR-II fuel pin under an internal pressure in the form of a step pulse of 1000 psi, decaying linearly in 40 ms, was analyzed using the results of Constantino[29] for the Ludwik strain-hardening law:

$$\sigma = \sigma_0 \epsilon^n,$$

where

σ = the effective stress, psi;

σ_0 = constant in the Ludwik law;

ϵ = effective strain, in./in.;

n = strain-hardening exponent.

[29] Constantino, C. A., J. Appl. Mech., 32, 104 (1965).

The properties used in the analysis were taken from a compilation by Cottrell and Savolainen.[30]

The critical static pressure for damage was found to be 2560 psi. The pulse described was found equivalent to a step pulse of 2120 psi, which does not decay. In static loading, the clad, which has an initial outer diameter of 0.174 in., will fail when stretched to 0.265 in. In dynamic loading failure will take place when the diameter is 0.197 in. This agrees with Constantino's conclusion that the dynamic strength may be much less than its static strength for a large strain-hardening exponent.

C. TREAT

1. Operations

A cluster of Zircaloy-clad UO_2 fuel rods (metal-water reaction sample CEN-223) was irradiated in a steam environment above a water-filled crucible. A flat-top transient was used to maintain a relatively constant power level for approximately 40 sec to simulate conditions that might exist following a reactor loss-of-flow accident. The sample was returned to Argonne, Ill., for analysis to determine the extent of the metal-water reaction.

2. Large TREAT Loop

The out-of-pile system was heated to operating temperature without sodium, leak tested, and returned to room temperature. Prior to installing a test section in the reactor, the loop will be filled with sodium and tested at design flow and temperature conditions.

D. Chemical and Associated Energy-transfer Problems

1. Calculation of the Extent of Metal-Water Reaction and Core Heating during a Loss-of-coolant Accident (CHEMLOC-I Program)

Analysis of the effect of the reaction of steam with fuel cladding metal in a loss-of-coolant accident in a water-cooled reactor has continued. The loss-of-coolant accident resulting from a break in a primary-system water pipe has been taken to be the "maximum credible accident" for most of the power reactors built to date. Water loss following the pipe break brings the core into contact with steam. The decay energy in the core is sufficient to cause the fuel cladding to be heated rapidly to temperatures at which metal-steam reaction can occur.

In previous analyses using the proposed LOFT (Loss of Fluid Test) reactor as a model, calculations were made for 25-mil-thick Zircaloy-clad

[30] Cottrell, W. B., and Savolainen, A. W., ORNL-NSIC-5, U. S. Reactor Containment Technology, Vol. I.

and 15-mil-thick stainless steel-clad, UO_2-core fuel (see Progress Reports for April 1965, ANL-7045, p. 67 and March 1966, ANL-7193, p. 94). In these analyses the core was divided into 156 equal-volume segments, each of which was assigned to one of 10 groups according to its rate of decay heating. The effects of heat transfer in the core by conduction, radiation, and convection, and the effects of unequal steam distribution to the various segments due to hydrogen formation were neglected in the analyses.

The recently developed Fortran computer program (designated CHEMLOC-I), which describes the core heating and chemical reaction up to the time of fuel melting, takes into consideration the effects of evaluating the temperatures of the gas, cladding, and fuel separately; the effects of transfer of heat by axial conduction in the cladding and fuel, by radial conduction between cladding and fuel, by radial radiation from cladding to cladding, and by convection between the cladding and the flowing gas; and the effects of changing hydrogen concentration in the steam.

For the analysis, the core is divided into a number of radial zones, each having the same number of fuel rods, as shown in Fig. 17. The center zone, No. 1, is a cylinder; the remaining zones are annuli. The decay heating varies axially within each zone as well as radially from zone to zone. Steam enters the bottom of the core at a rate which may be constant or may vary with time.

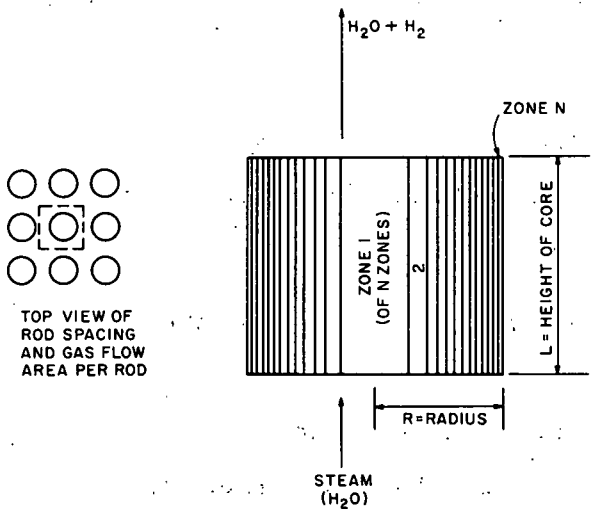

Fig. 17. Reactor Core as Zoned for CHEMLOC-I Calculations

As the steam flows upward through the core, the concentration of hydrogen increases due to chemical reaction of the steam with the cladding; thus, the cladding in the lower sections of the core tends to be contacted by gas having a higher steam concentration. Since on reaction with the cladding, one mole of water vapor forms one mole of hydrogen, the molar flow rate of gas does not vary with vertical (axial) core position.

A heat and mass balance was made on an elemental section of a fuel rod together with the associated gas flow area, in zone i, of length $\Delta\ell$, and at distance ℓ from the bottom of the core, as shown in Fig. 18.

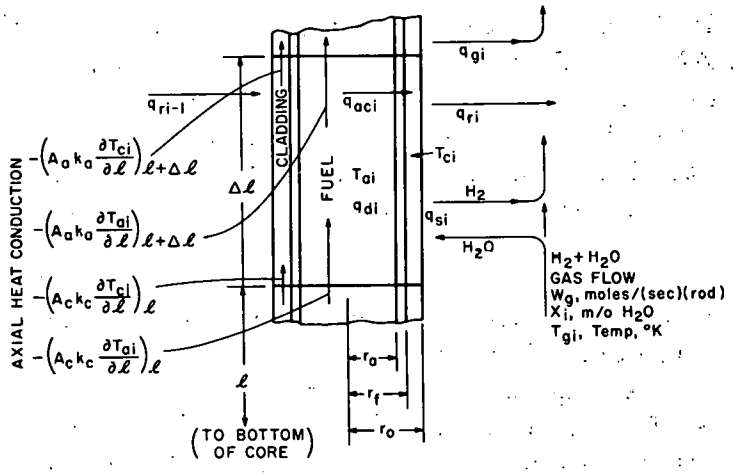

Fig. 18. Section of a Reactor Core Fuel Rod (Zone i) Showing Heat and Mass Transfer

The heat gain of the fuel per unit length of rod is the sum of the following terms:

q_{di} = decay heat per cm of rod, cal/(sec)(cm);

$-q_{aci}$ = heat transferred from cladding, cal/(sec)(cm);

$A_a k_a \frac{\partial^2 T_{ai}}{\partial \ell^2}$ = net heat gained by axial conduction, cal/(sec)(cm),

where

A_a = cross-sectional area of fuel, cm^2;

k_a = thermal conductivity of fuel, cal/(sec)(cm)(°K);

T_{ai} = temperature of the fuel, °K.

The heat gain of the cladding per unit length of rod is the sum of the following terms:

q_{aci} = heat transferred from fuel, cal/(sec)(cm);

$-q_{ri}$ = heat radiated to zones i + 1 and i - 1, cal/(sec)(cm);

q_{ri+1} = heat received by radiation from zone i + 1, cal/(sec)(cm);

q_{ri-1} = heat received by radiation from zone i - 1, cal/(sec)(cm);

q_{si} = heat produced by chemical reaction, cal/(sec)(cm), which may be limited by the chemical reaction rate (kinetic), the diffusion of steam to the reacting surface (diffusion), or by the complete reaction of the cladding;

$-q_{gi}$ = heat transferred from gas, cal/(sec)(cm);

$k_c \frac{\partial}{\partial \ell}\left(A_c \frac{\partial T_{ci}}{\partial \ell}\right)$ = net heat gained by axial conduction, cal/(sec)(cm),

where

A_c = cross-sectional area of the cladding per rod;

k_c = heat conductivity of the cladding, cal/(sec)(cm)(°K);

T_{ci} = temperature of the cladding, °K.

The heat gain of the gas as it flows past a unit length of rod is

q_{gi} = heat transferred from the cladding, cal/(sec)(cm).

The rate of oxidation of the cladding is:

q_{si}/Q_c, g/(sec)(cm),

where

Q_c = the heat of reaction of the cladding, cal/g.

The rate of steam consumption and hydrogen formation in the oxidation of the cladding is

$q_{si}/Q_c M_c$, moles/(sec)(cm),

where

M_c = grams of cladding reacted per mole of steam, g/mole.

The temperature increase of the fuel is equal to the heat received by the fuel (in time dt) divided by the heat capacity of the fuel, or

$$dT_{ai} = \frac{q_{di} - q_{aci} + A_a k_a \frac{\partial^2 T_{ai}}{\partial \ell^2}}{C_{p_a} W_a} dt, \text{ °K,} \qquad (1)$$

where

C_{p_a} = specific heat of fuel, cal/(g)(°K);

W_a = weight of fuel per length of rod, g/cm of rod;

t = time, sec.

The temperature increase of the cladding is equal to the heat received by the cladding (in time dt) divided by the heat capacity of the cladding, or

$$dT_{ci} = \frac{q_{aci} - q_{ri} + q_{ri+1} + q_{ri-1} + q_{si} - q_{gi} + k_c \frac{\partial}{\partial \ell}\left(A_c \frac{\partial T_{ci}}{\partial \ell}\right)}{C_{p_c} W_c} dt, \ ^\circ K, \quad (2)$$

where

C_{p_c} = specific heat of the cladding, cal/(g)(°K);

W_c = weight of cladding per length of rod, g/cm of rod.

The temperature increase of the gas flowing along the cladding is equal to the heat received by the gas (in distance $d\ell$) divided by the heat capacity of the gas flowing past the rod in unit time, or

$$dT_{gi} = \frac{q_{gi}}{W_g C_{p_g}} d\ell, \ ^\circ K, \quad (3)$$

where

C_{p_g} = specific heat of the gas, cal/(mole)(°K);

W_g = gas flowing past one rod, moles/(sec)(rod).

The reduction in cladding-metal radius due to oxidation is equal to the weight of metal oxidized divided by the weight of cladding metal per unit of radius, or

$$d(r_0 - r_i) = \frac{q_{si}}{2\Pi r_i \rho_c Q_c} dt, \ cm, \quad (4)$$

where

r_0 = initial radius of cladding, cm;

r_i = radius of unreacted cladding, cm;

ρ_c = density of cladding, g/cm^3.

The change in steam concentration in the gas as it flows along the cladding is equal to the steam consumption divided by the rate of gas flow past the rod in unit time, or

$$dX_i = \frac{q_{si}}{W_g Q_c M_c} dl \ moles/mole, \quad (5)$$

where

X_i = steam concentration, moles/mole in the gas;

$1 - X_i$ = hydrogen concentration, moles/mole in the gas.

The heat-generation and heat-transfer terms, q_{di}, q_{aci}, q_{ri}, q_{ri+1}, q_{ri-1}, q_{si}, and q_{gi}, were expressed in terms of (a) dimensions of core, fuel, cladding, and fuel rod; (b) densities, specific heats, thermal conductivities, diffusivities, and other physical properties of the fuel, cladding, steam, and hydrogen as functions of temperature; (c) chemical reaction rate constants; (d) reactor power and its variation over the core, and decay in fission product heating; (e) radiation emissivity; (f) initial temperatures for use in differential equations 1 to 5.

Chemical reaction rate constants for the zirconium-steam reaction, reactor power distribution in the core and fission product decay heat generation, and initial core temperatures have been previously discussed.[31,32]

Chemical reaction rate constants for stainless steel-steam reactions and heat and mass transfer coefficients for gas in laminar flow along reactor fuel rods have been also discussed (see Progress Report for March 1966, ANL-7193, pp. 94 and 96).

In the computer program, provisions are made to include other oxidizible surfaces, such as cans around subassemblies, and to include the heat capacity effects of materials, such as control rods, in addition to the fuel, fuel cladding, and cans.

The CHEMLOC-I program was developed for integrating differential equations 1 to 5 to solve for T_{ai}, T_{ci}, T_{gi}, $r_0 - r_i$, and X_i as a function of zone i, distance ℓ from the bottom of the core, and time t, for steam flow rates which are constant or which vary with time.

The LOFT core was used as a model for the CHEMLOC-I calculations. The LOFT core consists of 3328 UO_2 fuel rods each 0.39 in. in dia by 3 ft long, with 0.025-in.-thick Zircaloy-2 cladding. The rods are spaced on a square lattice with 0.58 in. between centers. The core was divided into 13 radial zones. Previously reported values[31] were used for the power distribution as a function of core location and the decay heating as a function of time.

Computer calculations were made for an initial core temperature of 285°C and for an initial core temperature distribution corresponding to the equilibrium temperature at operating power.[32] Calculations were made

[31]Chemical Engineering Division Semiannual Report, July-December 1964, ANL-6925, p. 215.
[32]Chemical Engineering Division Semiannual Report, January-June 1965, ANL-7055, p. 192.

Percent Hydrogen in Steam Leaving Top of Core

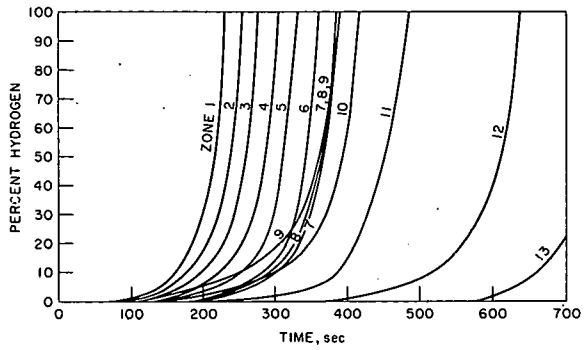

a

Temperature Profile Map (Approx. 10% of core at or above 2800°C)

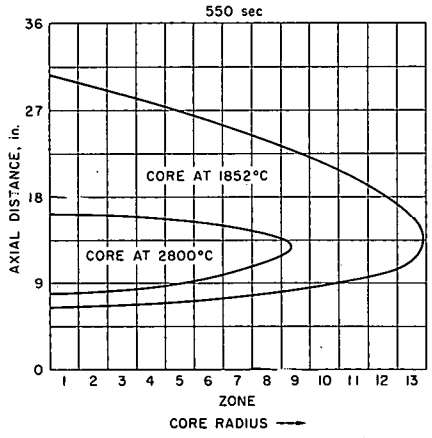

d

Initial Core Temperature 285°C; Steam Flowrate 1000 lb/hr

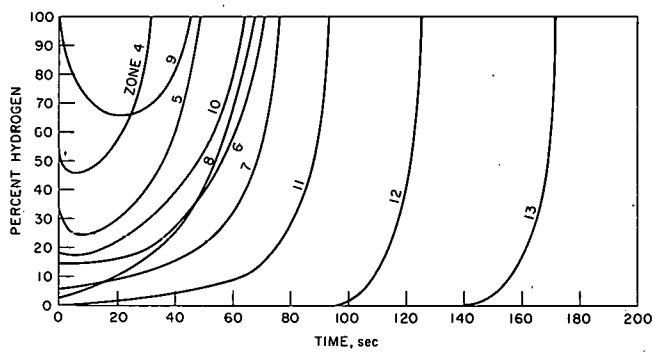

b

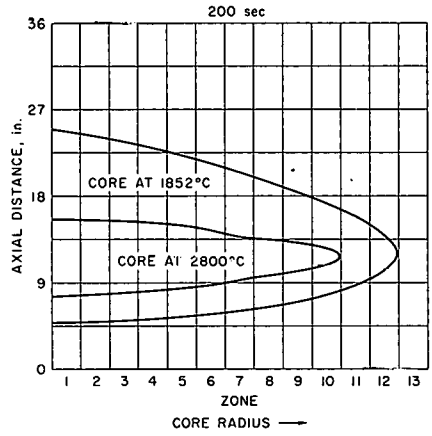

e

Initial Core Temperature--That Corresponding to Operating Power; Steam Flowrate 1000 lb/hr

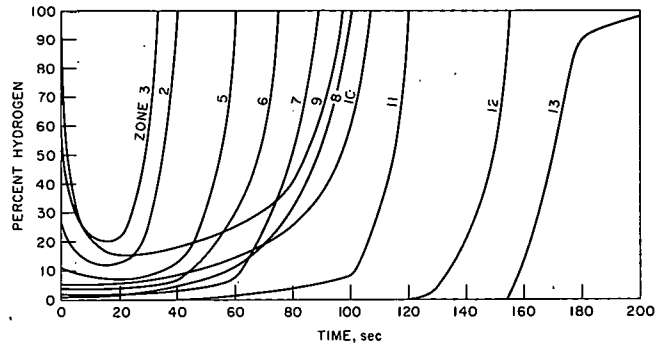

c

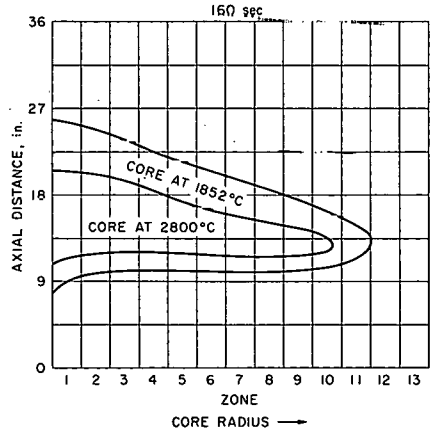

f

Initial Core Temperature--That Corresponding to Operating Power; Steam Flowrate Initially 3600 lb/hr (Decreasing exponentially)

Fig. 19. Typical Data Excerpts from CHEMLOC-I Computations for a Loss-of-coolant Incident

for constant steam flow rates of 100, 1000, 5000, 7500, and 10,000 lb/hr, and for variable steam flow rates starting at 3600 lb/hr and decreasing exponentially with time.

Figure 19 (a, b, and c) shows typical computed results for the concentration of hydrogen in the gas leaving the top of the core from the various zones as a function of time. The data are for initial core temperatures and steam flow rates as indicated. The crossing of the lines at zone 9 is caused by the increase in enrichment at zone 9. When the core is initially at a temperature corresponding to operating power, the core is sufficiently hot for considerable steam-zirconium reaction to take place immediately. The reaction rate is sufficient to give 100% hydrogen from zones 1, 2, and 3 initially. The cladding is assumed to have an initial oxide film corresponding to 10^{-4} cm of metal; this causes an initial rapid oxidation since the chemical reaction rate is inversely proportional to the oxide thickness. As the oxide film increases, the oxidation rate decreases and then increases as the temperature increases.

Figure 19 (d, e, and f) shows temperature profile maps of the core for the conditions of Fig. 19 (a, b, and c, respectively). Contour lines are shown for 1852°C (m.p. of zirconium) and 2800°C (m.p. of UO_2) at the time when approximately 10% of the core volume is at or above 2800°C.

Figure 20 shows the percent of cladding reacted as a function of time for various initial core temperatures and steam flow rates.

The computer calculations indicate that for an initial core temperature of 285°C, constant steam flow rates of 7500 and 10,000 lb/hr are sufficient to avoid extensive heating of the core.

Extension of the calculations to longer periods of time requires assumptions regarding the mechanism of core meltdown. Development of a meltdown model (CHEMLOC-II) is in progress.

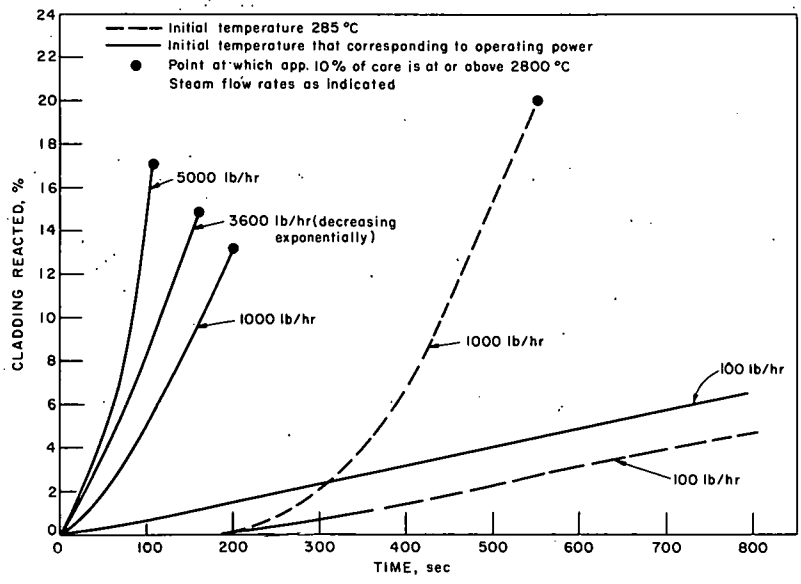

Fig. 20

Cladding Reacted as a Function of Time for Various Temperature and Steam Conditions

VI. PUBLICATIONS

Papers

Preparation of Mg^{24} from $Mg^{24}O$
N. R. Chellew, R. K. Steunenberg, and J. D. Schilb
Nucl. Instr. Methods 44(1), 149-150 (September 1966) Letter

Axial Solids Mixing in Fluidized-Packed Beds
J. D. Gabor
Chem. Eng. Progr. Symp. Ser. 62(67), 35 (1966)

Fluidized-bed Technology
J. B. Buckham and N. M. Levitz (ed.)
Chem. Eng. Progr. Symp. Ser. 62(67) (1966)

Thermodynamics of Dilute Solutions of Plutonium in Liquid Magnesium
I. Johnson, J. B. Knighton, and R. K. Steunenberg
Trans. Met. Soc. AIME 236, 1242-1246 (September 1966)

Statistical Models for Surface Renewal in Heat and Mass Transfer. Part I. Dependence of Average Transport Coefficients on Age Distribution
L. B. Koppel, R. D. Patel, and J. T. Holmes
AIChE Journal 12(5), 941-946 (September 1966)

Statistical Models for Surface Renewal in Heat and Mass Transfer. Part II. Techniques for Measurement of Age Distribution at Transport Surfaces
L. B. Koppel, R. D. Patel, and J. T. Holmes
AIChE Journal 12(5), 947-955 (September 1966)

The Synthesis of Stoichiometric Uranium Monocarbide in a Fluidized Bed by the Uranium Metal-Hydrocarbon Gas Reaction
E. J. Petkus, A. D. Tevebaugh, C. C. Payne, and J. P. Bartos
Chem. Eng. Progr. Symp. Ser. 62(67), 76 (1966)

High Temperature Thermometry--Service and Related Experience
C. F. Reinke, L. E. Robinson, and R. O. Ivins
Proc. High Temperature Thermometry Seminar, Washington, February 24-26, 1965. USAEC Report WASH-1067 (March 1966), pp. 22.1-22.2

Dose Distribution in the Argonne High-Level Gamma Irradiation Facility
H. G. Swope
Atompraxis 12(8), 398-401 (August 1966)

An Analysis of the Fission Cross Sections of Th^{232}, U^{233}, U^{234}, U^{235}, U^{236}, Np^{237}, U^{238}, Pu^{239}, Pu^{240}, Pu^{241}, and Pu^{242} from 1 keV to 10 MeV
W. G. Davey
Nucl. Sci. Eng. 26, 149-169 (October 1966)

Thermal Properties of Compositions in the System UO_2-ZrO_2-CaO
R. S. Kern and R. J. Beals
Bull. Am. Cer. Soc. 45, 821 (September 1966) Abstract

High Temperature Creep of Tantalum
J. E. Flinn and E. R. Gilbert
Trans. Met. Soc. AIME 236, 1512 (October 1966)

Discussion: Effects of Grain Size on Tensile and Creep Properties of Arc-Melted and Electron-Beam-Melted Tungsten at 2250 to 4140°F
E. R. Gilbert
Trans. Met. Soc. AIME 236, 1511-1512 (October 1966)

Corrosion of Refractory Metal Alloys in Oxygen-Contaminated Sodium
H. A. Levin, W. E. Ruther, and Sherman Greenberg
Proc. AEC-NASA Liquid Metals Information Mtg., Gatlinburg, April 21-23, 1965. U. S. Atomic Energy Commission Publication CONF-650411, p. 63. Abstract

Compatibility of U-Pu-Fz Fuel Alloys with Potential Cladding Materials
C. M. Walter and J. A. Lahti
Nucl. Appl. 2, 308-319 (August 1966)

Lithium Corrosion Studies at Elevated Temperatures
J. Y. N. Wang
Proc. AEC-NASA Liquid Metals Information Mtg., Gatlinburg, April 21-23, 1965. U. S. Atomic Energy Commission Publication CONF-650411, p. 137. Abstract

Corrosion Test Coupons--Mechanical Cleaning
C. A. Youngdahl
Materials Protection 5, 53-54 (October 1966)

Polarization Studies in Oxygen-Contaminated Sodium
C. A. Youngdahl and Sherman Greenberg
Proc. AEC-NASA Liquid Metals Information Mtg., Gatlinburg, April 21-23, 1965. U. S. Atomic Energy Commission Publication CONF-650411, p. 74. Abstract

Nuclear Hospital of the Year 2000 May Rest on Ocean Floor or Ice Floe
David H. Lennox
Hospital Life, Sept/Oct 1966, Vol. I, No. 3, p. 5 (Presented at the American Association of Hospital Consultants, Chicago, August 27, 1966)

Refractory Oxide Insulated Thermocouple Analysis and Design
G. F. Popper and T. Z. Zeren
Proc. High Temperature Thermometry Seminar, Washington, February 24-26, 1965. USAEC Report WASH-1067 (March 1966), pp. 21.1-21.26

The (d,n) Reaction on Mg^{24} and Si^{28}
S. G. Buccino, D. S. Gemmell, L. L. Lee, J. P. Schiffer, and A. B. Smith
Nucl. Phys. 86(2), 353-362 (October 1966)

Calculating Space-Dependent Reactor Transfer Functions Using Static Techniques
C. E. Cohn, R. J. Johnson, and R. N. MacDonald
Nucl. Sci. Eng. 26, 198-206 (October 1966)

Fast Reactor Meltdown Program
C. E. Dickerman
Nucl. Safety 7(4), 424-434 (Summer 1966)

Activation of Gold Spheres and Foils in Nonisotropic Neutron Incidence
F. H. Helm
Nucl. Appl. 2, 325-334 (August 1966)

A Method of Calculating Resonance Absorption in Circularized Cell
P. H. Kier
Nucl. Sci. Eng. 26, 230-236 (October 1966)

The following appeared as Abstracts in Trans. Am. Nucl. Soc. 9(2) (1966):

Hydrogen in Irradiated Pressure Vessel Steel
A. D. Rossin
p. 389

Transient Irradiations of Vibrationally Compacted UO_2 Fuel in TREAT
R. C. Liimatainen, M. D. Freshley, and F. J. Testa
p. 395

Design of a Shielding Window for a Nuclear Reactor Containment Cell
T. W. Eckels and Abraham Smaardyk
p. 618
Also, Proc. 14th Conf. on Remote Systems Technology, Pittsburgh, October-November 1966. Am. Nucl. Soc., Hinsdale, Ill., 1966, pp. 107-114

ANL-Mark-E4A Electric Master-Slave Manipulator
R. C. Goertz, J. H. Grimson, C. W. Potts, D. P. Mingesz, and G. A. Forster
p. 618
Also, Proc. 14th Conf. on Remote Systems Technology, Pittsburgh, October-November 1966. Am. Nucl. Soc., Hinsdale, Ill., 1966, pp. 115-123

The ANL Mark-TV2--An Experimental Five-Motion Heat-Controlled TV System
R. C. Goertz, J. F. Lindberg, D. P. Mingesz, C. W. Potts, and D. E. Kuehn
p. 619
Also, Proc. 14th Conf. on Remote Systems Technology, Pittsburgh, October-November 1966. Am. Nucl. Soc., Hinsdale, Ill., 1966, pp. 124-128

Maintenance and Repair of Contaiminated Equipment for the EBR-II Fuel Cycle Facility
C. E. Stevenson, M. J. Feldman, D. C. Hampson, and D. M. Paige
p. 621
Also, Proc. 14th Conf. on Remote Systems Technology, Pittsburgh, October-November 1966. Am. Nucl. Soc., Hinsdale, Ill., 1966, pp. 149-155

Fusible Metal Seals in Process Equipment
W. E. Miller, G. J. Bernstein, D. C. Hampson, R. F. Malecha, and M. A. Slawecki
p. 626
Also, Proc. 14th Conf. on Remote Systems Technology, Pittsburgh, October-November 1966. Am. Nucl. Soc., Hinsdale, Ill., 1966, pp. 213-218

ANL Reports

ANL-6621 PROCUREMENT AND PROCESSING OF EBR-I CORE IV URANIUM AND HARDWARE
R. A. Beatty, F. D. McCuaig, and C. H. Bean

ANL-7145 DEFORMATION ANALYSIS OF A CIRCULAR COUPLED-PLATE STRUCTURE
H. Halle

ANL-7148 CHANNEL-WALL LIMITATIONS IN THE MHD INDUCTION GENERATOR
Edward S. Pierson and William D. Jackson

ANL-7168 (Volume I) FAST REACTOR TEST FACILITY (FARET) Volume I. Description and Program
J. D. Geier, Ed.

ANL-7189 THE ROLE OF THE ADJOINT FLUX IN DETERMINING REACTOR STABILITY
Richard Harry Jason

ANL-7194 GENERAL INPUT SPECIFICATIONS FOR ANL REACTOR PROGRAMS
M. Butler and H. Greenspan